Nuclear Magnetic Resonance and Rheological Studies of Carbohydrate-1-Ethyl-3-Methyl-Imidazolium Acetate Solutions

Wafa Mosbah Ezzawam

School of Physics and Astronomy

University of Leeds

A thesis submitted for the degree of

Doctor of Philosophy

June 2018

The candidate confirms that the work submitted is her own and that appropriate credit has been given where reference has been made to the work of others.

To My Daddy

Thank you for the best life you gave to me

Acknowledgements

I would like to thank my supervisors at University of Leeds and Libyan Embassy London-Cultural Affairs, Dr. Michael Ries and Mr Housam Ounalla for all their support, guidance and patience. I would also thank Dr. Robin Damion and Dr. Dan Baker and Mrs Amanda. Especial thankful to my best friends (Safa, Maruwa, Afanan, Abeer, Shoug, Amy, Sinead and Fatama) for their existence in my life. Especial thankful to my lovely family for their support and encouragement.

Abstract

The dissolution of carbohydrates in Ionic liquids has received attention for many decades and still is to this day. Solutions of xylan and xylose in 1-ethyl-3-methylimidazolium acetate [C2mim] [OAc] were individually examined at various temperatures (20 °C-70 °C) using NMR spectroscopy, diffusion and the low field spin-lattice and spin-spin relaxation times (T_1 and T_2) as well as rheology measurements. The ratio of the diffusion coefficients for the anion to the cation remained constant upon the addition of xylan and xylose, showing that the anion and cation were equally affected by the presence of the carbohydrate. The activation energies for translational diffusion motion of both ions in the xylose solutions were similar to these found in published cellobiose. The addition of xylose and xylan individually have affected the mobility of the protons, with a decrease occurring with increasing carbohydrate concentrations. We are looking at the interactions between plant polymers, such as xylan with cellulose, with the aim to form biomimetic materials. A solution of cellulose and xylan in the ionic liquid 1-ethyl-3-methylimidazolium acetate [C2mim] [OAc] was examined using NMR diffusion, low field relaxometry and rheology measurements at various temperatures (20 °C-60 °C). We observed that the dissolving mechanism of xylan in the IL [C2mim] [OAc] is close to that for cellulose. The diffusion coefficient of the anion is preferentially more reduced by cellulose than by xylan. It is generally agreed that the anion is more active in the dissolution of carbohydrates than the cation. The dissolution mechanism of cellulose and xylan in the IL [C2mim] [OAc] can be examined via the mobility of the ions. We proposed that the number of accessible OH groups belonging to the carbohydrates are reduced at certain xylan-cellulose blend compositions, showing that at these concentrations there are significant interactions between the two biopolymers.

Abbreviations

ILS	Ionic Liquids
NMR	Nuclear Magnetic Resonance
BPP	Bloembergen, Purcell and Pound
C2mim	1-Ethyl-3-Methylimidazolium
OAc	Acetate
PFG	Pulse Field Gradient
OH	Hydroxyl Group

Nomenclature

D_i	Self-diffusion coefficient
$R_{H,i}$	Hydrodynamic radius
T_1, T_2	Relaxation times
τ_{rot}	Rotational correlation time
μ	Zero shear rate viscosity
η	Viscosity of polymer solution
$[\eta]$	Intrinsic viscosity
α	Associated fraction
f	Micro-viscosity per-factor Or Correction term
E_A	Activation energy

Contents

List of Figures

List of Tables

Chapter 1

Introduction

1.1 A Brief History of Ionic Liquids

Ionic liquid (ILS) are organic salts that have a melting point below 100°C with some being liquids even below room temperature [1, 2]. ILs can be formed from numerous different anions combined with many different cations [3, 4]. The most common cations used are imidazolium, pyridinium, ammonium and phosphonium derivatives [5]. The one most frequently used for biomass processing, including cellulose itself, is imidazolium[6]. Ionic liquids have been employed in many fields, such as solvents, in catalysis, separation technology and electrically conducting fluids [7, 8]. In 1934, Graenacher proposed the use of molten N-methylpyridinium chloride as a solvent to dissolve cellulose, and observed that this salt has a relatively low melting point at just 118°C [9]. Ionic liquids were employed for dissolution, homogeneous derivatization and biomass general processing. Swatloski originally reported on 1-butyl-3-methylimidazolium chloride [BMIM] [Cl] being the first use of an ionic liquid in the field of cellulose technology [10, 11]. The most important reasons to select ILs to process biomass are their ‘‘green’’ credentials (low vapour pressure) potential variety (‘‘designer’’ solvents), as well as the advanced understanding of the solvents’ properties that have developed. Moreover, the use of ILs will allow an increase in solution efficiency and reduction of undesirable solvents, coupled with control and flexibility in the processing methodology [12-14].

Over the last two decades, ionic liquid 1-ethyl-3-methylimidazolium acetate [C2mim] [OAc] has received much attention as an excellent solvent to dissolve green material such as cellulose and also non-green like carbon dioxide [7, 15, 16]. This because the IL [C2mim] [OAc] has useful properties, such as a lower melting point, vapour pressure and viscosity than most ILs, in addition to its good thermal stability and suitable for biodegradability [17, 18]. Therefore, IL [C2mim] [OAc] is utilized as the solvent to dissolve carbohydrates, such as glucose, cellobiose and xylan. The chemical structure with spectrum of the IL [C2mim] [OAc] solvent is shown in Figure 1.1. This solvent consists of the imidazolium cation [C2mim] and the acetate, anion [OAc] [5, 18].

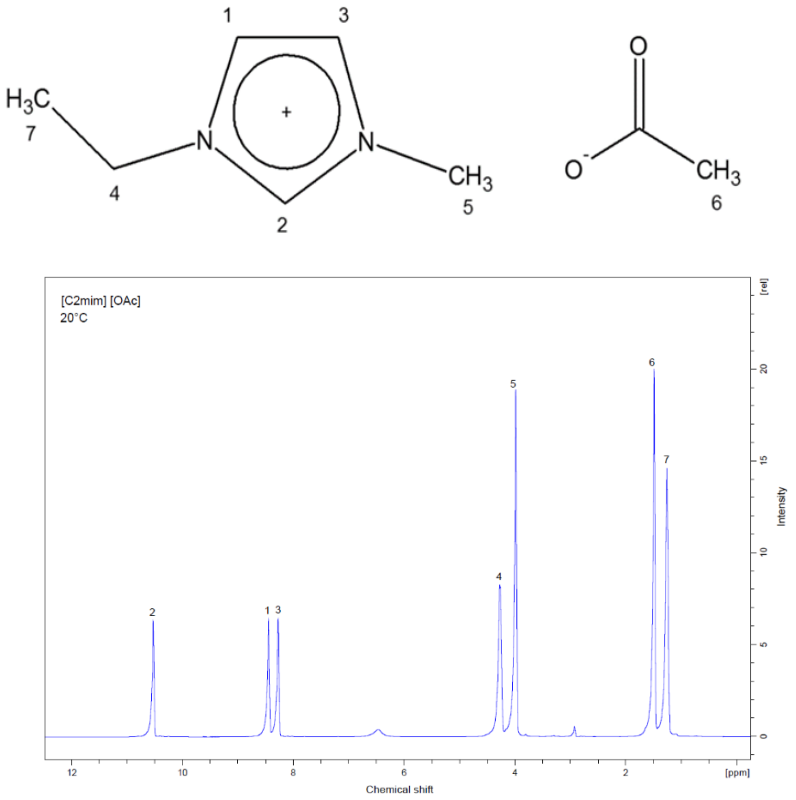

Figure 1.1: The chemical Structure and spectrum of 1-ethyl-3-methylimidazolium acetate, cations $[C2mim]^+$ and anion $[OAc]^-$ with the labelling of NMR resonance peaks (1-7).

1.2 Carbohydrates

Biopolymer carbohydrates are renewable sources for a wide variety of biomass-based products and applications, such as food, materials and energy supplies [19, 20]. Carbohydrate is a molecular compound made from the elements: hydrogen, oxygen, and carbon [21]. Examples are cellulose, xylan (polysaccharides) and xylose (monosaccharide). Carbohydrate monosaccharide consists of one sugar unit, while a polysaccharide is more than three sugar units bonded together [22, 23]. Recently, the dissolution of carbohydrates (polysaccharides and monosaccharides) in ionic liquids has attracted much attention, to develop sustainable materials with excellent physical and chemical properties [24].

In 1838, the first research on cellulose was carried out by Anselme [25]. Cellulose is the world's most abundant naturally occurring biopolymer, found in plants, bacteria and fungi and is predicted to become the largest source of renewable materials. Cellulose has numerous significant applications in the fibres, paper and paint industries [26, 27]. It has a hydrogen-bonded supramolecular structure, containing D-anhydroglucopyranose units connected by β (1→4) glyosidic bonds [28, 29]. Hydrogen bonds form between the hydroxyl group of neighbouring chains and give toughness and strength to the cellulose structure [30]. Figure 1.2 present the monomer of cellulose, two glucose units. Cellulose is insoluble in most organic solvents and water. Therefore, there has been significant effort to find ways to process cellulose using different solvents and reagents [31], such as the viscose method that uses carbon disulphide [32]. The procedure of viscose was developed by scientists Charles Frederick Cross and Edward John Bevan. In 1892, they obtained British Patent no. 8,700 for ‘‘Improvements in Dissolving Cellulose and Allied Compounds’’ [33].

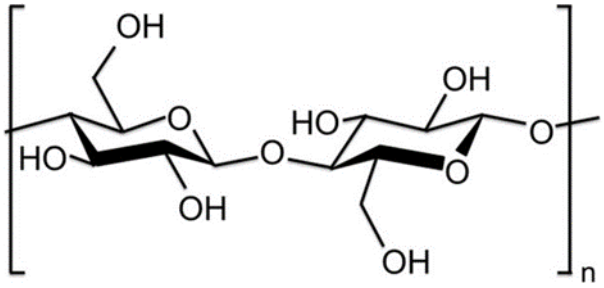

Figure 1.2: The molecular structure of cellulose(taken from ref [34]).

Xylan is the second most abundant carbohydrate (polysaccharide), on earth after cellulose [35]. Xylan is found in the cell walls of plants and comes in a wide range of structures, where this diversity in structures is correlated with their functions in plants. Figure 1.3: The molecular structure of xylan. shows the structure of xylan. This a polysaccharide and consists predominantly of $\beta-(1\rightarrow4)$ – linked xylose residues [36]. The differences in the xylan backbone structure depend on the extraction procedure and the botanical source.

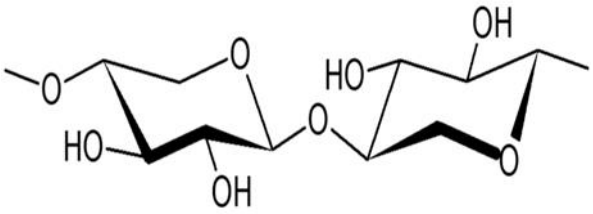

Figure 1.3: The molecular structure of xylan.

The composition of the xylan backbone commonly contains a galactose, xylose, arabinose and mannose, as well as an esterases group (acetyl and ferulic acid). Like cellulose, xylan is insoluble in water [36]. Recent studies are interested in employing xylan in numerous applications, such as paper, food industry, biofuel, as well as, in pharmaceutical as a prodrug. Xylan ester has been employed as a carrier a drug and also sulphate derivatives to use as antiviral drugs [37, 38]

The structures of three carbohydrates monosaccharides so far described are shown in Figure 1.4. Xylose can be derived from hemicellulose such as xylan [39]. Glucose and xylose have a variety of industrial applications such as pharmaceutical [40] and food production, and in food supplements. Glucose is classified as a simple carbohydrate, a monosaccharide, having five OH groups [41]. Glucose is found in plants and in the bloodstream of humans. Cellobiose is classified as a disaccharide and consists of two $D-$ glucopyranose units connected by a β (1→4) glyosidic bond [39, 41]. These carbohydrates are soluble in most organic solvents and water.

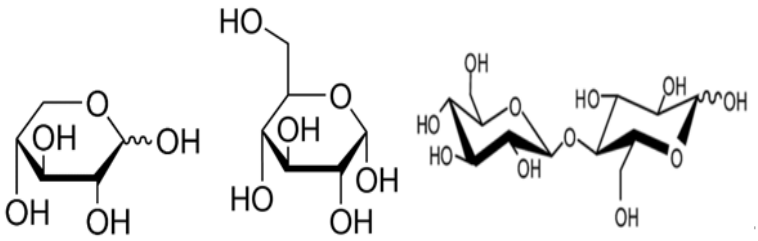

(a) (b) (c)

Figure 1.4: The chemical structure of D-xylose(a), glucose (b) and cellobiose (c) (taken from refs [42, 43]).

1.3 Mixture of Carbohydrates Dissolved in Ionic Liquids

The blends of two or more carbohydrates, by using ionic liquids, are considered as promising materials for applications in biotechnology and medicine [7, 44]. Cellulose and xylan are the most abundant natural polymers; therefore they are a desirable target for sustainable materials. Ionic liquids have utilisation into biopolymers applications, such as to extract, dissolve and mix. For example, ionic liquid N, N‑diethyl‑N‑(2‑methoxyethyl)‑N‑methylammonium alanine [N221ME][Ala] was utilised to obtain cellulose II from cellulose type I [45].

These polymers can be dissolved in solvents such as 1-ethyl-3-methylimidazolium acetate [C2mim] [OAc], 1 − butyl − 3-methylimidazolium chloride [BMIM] [Cl] and N−methylmorpholine-N-oxide [NMMO] [46, 47]. Ionic liquids can be used to extract polysaccharides from a plant, by using 1,3 − Dimethylimidazolium methyl methylphosphonate [C1mim][(MeO)(Me)PO2] solvent [48]. A natural interaction occurs between cellulose and xylan throughout the cell wall assembly in a plant. This interaction is one of the primary concerns in this work, and it is relevant to numerous industrial techniques [49-52]. The bacterial non-cellulose (this known as cellulosic material) was used as a support with Arabinoxylan to produce uniform transparent films, and absence of one of these polymers may cause weak mechanical properties of the film [53]. Xylan was employed to reinforce a cellulose structure and control the morphology to produce new fibres [8]. This is because the hydroxyl groups, OH of xylan have a significant impact on the solubility of cellulose [51, 54]. It also is possible to make a hydrophobic film[55] with good mechanical properties and thermal stability, from blending xylan and cellulose with glycerol as a plasticiser [56]. Paananen et al., studied interaction between xylan and cellulose fibres, using the atomic force microscopic technique to measure elastic module of these fibres, they found that the addition of xylan can influence cellulose, making the fibres have a higher strength [57, 58].

Recently studies focused on a mixture of carbohydrates in IL[C2mim] [OAc]. An interaction happens between OH group of polymers and diffusing particles of solvent, at specific stoichiometric ratios [35, 56, 59]. Gordobil et al. found that an interaction between the ions of IL [C2mim] [OAc] and molecules of xylan and cellulose system, and these gave non-linear behaviours between mechanical property and mixture polymers weight fraction (w/w) [56]. Sundberg et al., also reported that the correlation between the mixture carbohydrates concentrations and the mechanical properties of the blended films, showing this to be not linearly dependent on concentration, which may be due to the interaction between cellulose and xylan. These polymers give tensile and stiffness to film when they are together [35].

Nuclear Magnetic Resonance (NMR) is employed to determine both molecular structure and dynamics in a wide range of scientific disciplines. NMR can study the chemical and physical properties of molecules in solution and solid state; it can determine crystallinity, solubility of a solution [60], phase changes, conformational exchange, diffusion and rotational motion [61]. Simmons et al. studied the influence of xylan on cellulose fibres by following the chemical shift of molecules using ^{13}C NMR spectroscopy [62]. In this study we will explore the interactions between xylan/xylose and IL [C2mim] [OAc], as well as between cellulose and xylan in solution, using liquid-state NMR techniques.

1.4 Thesis Overview

This thesis presents an investigation into a number of carbohydrates dissolved into the IL [C2mim] [OAc] and how they can influence the diffusivity of ions, using primarily NMR diffusion, and low and high field relaxation times, as well as rheology across arrange of temperatures 20 ℃ -70℃. The viscosity measurements used a dynamic stress-controlled rheometer. An investigation process started with several steps: first of all, Arrhenius equation was modelled and applied to data each of diffusion and relaxation times and rheology, to calculate the activation energy of ions in a viscous medium. Secondly, The Bloembergen, Purcell and Pound (BPP) theory and Stokes-Einstein- Debye equations are applied to the experimental data, to understand the relationship between microscopic diffusion, relaxation times and macroscopic viscosity. By determining the correction term, or also known as the micro-viscosity per-factor, and the size of hydrodynamic radii of the ions. Chapter 2 begins with an introduction of the laboratory techniques and the basis of nuclear magnetic resonance, NMR and the Bloembergen, Purcell and Pound, BPP theories used in following chapters. Chapters 3, 4 and 6 are results based, each consisting of experimental results and analysis of data. Chapter 5 is an investigation of the influence of different carbohydrates on the diffusivity of ions of IL [C2mim] [OAc].

Chapter 3 studies xylose dissolved in ionic liquid [C2mim] [OAc] using NMR and rheology methods and are compared to the cellobiose system. Chapter 4 employs a similar approach with xylan dissolved in IL [C2mim] [OAc] using NMR and rheology techniques and are compared to a cellulose system. Chapter 5 presents the in-depth analysis of NMR and rheology data of five carbohydrates which are glucose, cellobiose, xylose, cellulose and xylan each individually dissolved in IL [C2mim] [OAc] and these systems are compared to each other. Chapter 6 uses IL [C2mim] [OAc] to dissolve two polymers together which are cellulose and xylan and then measured using NMR and rheological techniques. This thesis attempts to understand the distinction of the influence of different carbohydrates on the ions of ionic liquid [C2mim] [OAc], and an investigation of the interaction between blended carbohydrate polymers on the diffusivity of ions in solution.

Chapter 2

Background Theory and Experimental Method

2.1 Introduction

Chapter Two begins by laying out the theoretical background for the research, and looks at the principles of Nuclear Magnetic Resonance (NMR), including diffusion and relaxation times. Experimental techniques were used to investigate transitional diffusion and rheological properties of carbohydrate solutions. Nuclear Magnetic Resonance (NMR) and rheology measurements will form the experimental data. The carbohydrates used were xylose, xylan and cellulose, and the solvent was 1-Ethyl-3-Methylimidazolium Acetate [C2mim] [OAc].

2.2 Nuclear Magnetic resonances (NMR) Theory

NMR exploits the spin and magnetic properties of certain NMR active nuclei. Classically, the motion of the internal electrical charge (e.g. nucleus of hydrogen) produces a small magnetic field [63]. Hence, this nucleus (proton) possesses a magnetic moment μ that is related to its spin I of a nucleus:

$$\mu = \gamma \hbar I \tag{2.1}$$

with γ the magnetogyric ratio, this is a fundamental nuclear constant and $\hbar$ is the reduced Planks constant. Each hydrogen nucleus with spin (1/2) will have two orientations when a magnetic field B_o is applied. These spins will align with or against the direction of the magnetic field, and the energy states of the nucleus split.

In the lower energy state, α, a magnetic moment is parallel to the direction of the field. At equilibrium, the population of nuclei in this lower state is greater than that of the higher energy state, β. Nuclei in the lower state, α can be excited using electromagnetic radiation, which causes the nuclei to change their energy states. For the higher state, β the magnetic moment is antiparallel to the magnetic field [64, 65]. The energy state can be given by:

$$E = -m\gamma \hbar B_{\mathrm{o}} \tag{2.2}$$

where m=±1/2 a magnetic quantum number of nuclei. There is a difference in energy between the eigenstates ΔE due to the applied field. This difference in energy depends on the strength of the external magnetic field and is given by [64, 66]

$$\Delta E = \gamma \hbar B_{\mathrm{o}} \tag{2.3}$$

The angular processional frequency (ω) of a nucleus is termed the Larmor frequency and is given by 2.4. In case the external magnetic field is applied in the Z- direction, known as B_Z, [67, 68], given by equation (2.5)

$$\omega = \gamma \mathrm{B_o} \tag{2.4}$$

$$\omega_{eff} = \omega_0 + \gamma B_Z \tag{2.5}$$

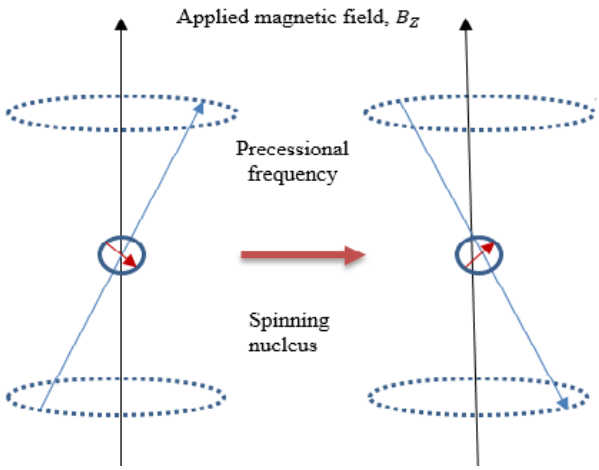

Figure 2.1: Precession of a nuclear in an external magnetic field. The small arrows indicate to when the magnetic moment with or against the applied magnetic field.

Atomic nuclei within a liquid move randomly within the applied external magnetic field through a process of diffusion (Brownian motion). If this applied field has a spatial dependence, a field gradient, then this causes processional frequencies to vary with time. It is this phenomenon that enables NMR to quantify the diffusion of the nuclei through the detection of the resultant time dependence of the processional frequencies [69].

2.2.1 Stokes−Einstein Theory

The diffusion coefficient,D_i known as the self-diffusion coefficient, can be defined by equation 2.6, where the position of the molecule or ion in the medium is indicated by the diffusion distance of particle, r_i, at long time *t:*

$$D = \lim_{t\to\infty} \frac{1}{6t} \langle | r_i(t) - r_i(0) |^2 \rangle \qquad (2.6)$$

The average displacement of ions or molecules in three directions is zero, but the mean square of the diffusion displacement of particle, i, can be determined by:

$$\langle r_i^{\,2} \rangle = 6Dt \tag{2.7}$$

The value of the diffusion coefficient depends on the shape of ions/molecules, their size, and the viscosity of the solution they are within[59, 68]. The relationship between translational diffusion of ions/molecules and the thermal energy in a viscous medium can be determined by the classical Stokes−Einstein equation.

$$D_i(T) = \frac{1}{\eta} \times \frac{k\,T}{4\,\pi f R_H} \tag{2.8}$$

where k is the Boltzmann constant, T is the temperature, η is the viscosity of the solution and R_H is the effective Stokes radius of the ion or molecule. f is a correction term and also known as micro-viscosity pre-factor, where f is equal to 1 when the diffusing ions sized are greater than the surrounding molecules [70]. It can also be f less than one if ion / molecule is smaller or similar to the size of particles in the viscous medium [59, 71]. According to McLaughlin, number 4 can be used instead of 6 in the Stokes-Einstein equation, when the size of ions is the same as that of the molecules of a solution [59, 72].

At room temperature, the values of diffusion coefficient are typically in the range between $10^{-9} m^2 s^{-1}$ and $10^{-12}\ m^2 s^{-1}$ for the small and large size of molecules in solution respectively [73, 74]. The Stokes effective radius, R_H, of ions can be determined by diffusion coefficient and the ratio of temperature to viscosity by using Stokes-Einstein equation. The effective hydrodynamic radius, $R_{H,i}$ can also be calculated through the volume or mass of one-mole component i, by the following equation[75]:

$$R_{H,i} \approx \frac{1}{2}\left(\frac{V_{m,i}}{N_A}\right)^{\frac{1}{3}} = \frac{1}{2}\left(\frac{M_i}{\rho N_A}\right)^{\frac{1}{3}} \tag{2.9}$$

where N_A is the Avogadro number, ρ is density, M_i is the molar mass, and $V_{m,i}$ is the molar volume. Equation 2.8 is used in many studies and has been shown to give reasonable approximate value for the effective radius of ions [59, 74-76].

2.2.2 Bloembergen−Purcell−Pound (BPP) Theory

The Bloembergen, Purcell and Pound (BPP) theory explain the influence of the thermal motion of ions upon spin–spin interactions [77]. In NMR system of nuclei spin, ½ (e.g. Hydrogen nuclei) the relaxation times T_1 and T_2 are related to a rotational correlation time,τ_{rot} at Larmor frequency, ω the relaxation times can be determined by:

$$\frac{1}{T_1} = 2A\left(\frac{\tau_{rot}}{1+\omega^2{\tau_{rot}}^2} + \frac{4\tau_{rot}}{1+4\omega^2{\tau_{rot}}^2}\right) \quad (2.10)$$

$$\frac{1}{T_2} = A\left(3\tau_{rot} + \frac{5\tau_{rot}}{1+\omega^2{\tau_{rot}}^2} + \frac{2\tau_{rot}}{1+4\omega^2{\tau_{rot}}^2}\right) \quad (2.11)$$

where the spin-lattice relaxation time is, T_1, also termed the longitudinal relaxation and T_2 is the spin-spin relaxation time, also known as the transverse relaxation time. A is a constant defined as follows:

$$\mathrm{A} = \frac{3}{20}\,\gamma^4\hbar^2\left(\frac{\mu_0}{4\pi}\right)^2 r_{H-H}^{-6} \quad (2.12)$$

where γ is the gyromagnetic ratio of protons, ħ is the reduced Planck constant, μ_0 is the permeability of free space, and r_{H-H} is the distance between two protons [77, 78].

The longitudinal relaxation depends on the mobility and proximity of nuclei to each other[64]. Transverse relaxation can be caused by interactions between nuclei that have identical precessional frequencies, but with different magnetic quantum numbers. In this case, spin can be mutually exchanged between energy states without a net change in the populations of the states. This results in a line broadening in the NMR spectrum and contributes to the transverse relaxation. Experimentally, the relaxation time is approximately exponential and is governed by Equation 2.18. In the transverse relaxation measurement, the magnetization is kept within the XY plane [79].

2.2.3 Stokes−Einstein−Debye Theory

The relaxation times and the correlation time depend on temperature, resultant that three types of systems > Liquid system at a high-temperature limit and when relaxation times T_1 and T_2 are equal, which both of relaxation times increase as temperature increased. The second is a solid system at low temperature and $T_1 \neq T_2$, this because T_1 rises, while T_2 reduces. A translational system is the point between solid and liquid systems and known as a T_1 minimum at $\omega\tau = 0.62$ [59, 77, 78]. It is possible to calculate the values of the effective hydrodynamic radii, R_H for ions or molecules, using relaxation times when $\omega\tau \ll 1$, T_1 and T_2 reduce to the same simple formula dependent on τ_{rot}. Debye and Einstein's equation relates that to viscosity, and putting it all together gives a final relationship between NMR relaxation times and viscosity. The rotational correlation time, τ_{rot}can be calculated for spherical molecules/ions. With nuclei spin, ½ is given by:

$$\tau_{rot} = {}^{4}/_{3}\,\pi {R_H}^3 \frac{\eta}{K_B T} \tag{2.13}$$

where η is shear rate viscosity. According to BPP theory, at the high-temperature limit, the relaxation time T_1 and T_2 can be determined following by:

$$\frac{1}{T_1} = \frac{1}{T_2} = 10A\tau_{rot} \tag{2.14}$$

with A constant, Equations 2.13 and 2.14 are combined to give the correlation between the relaxation times and viscosity by:

$$T_1 = T_2 = \frac{3k_B}{(40\pi A\, f\, {R_H}^3)}\, {T}/{\eta} \tag{2.15}$$

These equations will be applied to experimental data to determine the correction term, f and the hydrodynamic radii, $R_{H,i}$ of ions in viscous solutions, in next chapters.

2.3 Experimental Technique

This section will present the methods which were used to study carbohydrate 1-ethyl-3-methylimidazolium acetate [C2mim] [OAc] solutions.

2.3.1 NMR Methods

A Nuclear Magnetic Resonance Bruker Avance II (400MHz) spectrometer with diffusion probe (Diff 50) was used. The measurement of relaxation times T_1 and T_2 have been performed on a 20 MHz "low" field Maran Benchtop NMR spectrometer.

2.3.1.1 NMR Diffusion

Diffusion was measured using the method of NMR stimulated echo pulse sequence with bipolar gradients [80, 81], which is produced by a combination of magnetic field gradients and radiofrequency pulses (PFGSE) [82, 83]. Figure 2.2 displays the NMR stimulated echo pulse sequence with bipolar gradients. Bipolar gradients, g is used for dephasing and rephasing the magnetization positions during the time is Δ, and δ is the pulse duration of the joint pair of bipolar pulses sequences $\pi/2$ and π are indicated to 90° and 180°[83]. Experimentally, attenuation of the signal of the intensity of ions in PFGSE is provided by Equation 2.16 [84, 85].

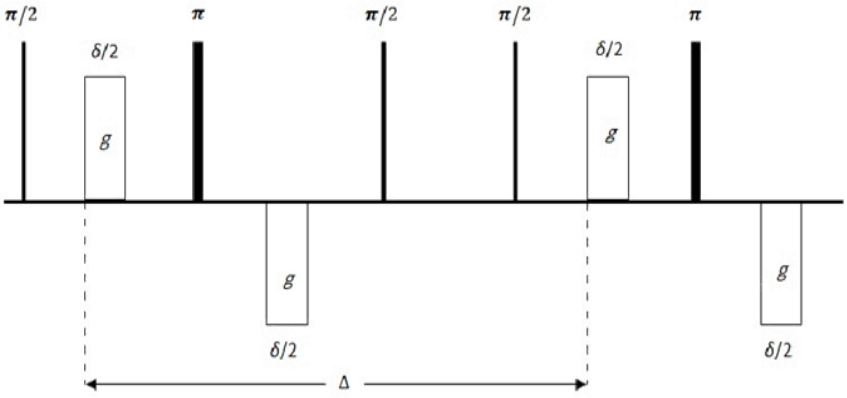

Figure 2.2: NMR stimulated echo sequence with bipolar gradients. It taken from ref [82].

$$ln(^{S_i}/_{S_{i0}}) = -D_i\gamma^2 g^2\delta^2(\Delta - {}^{\delta}/_{3} - {}^{\tau}/_{2}) \quad (2.16)$$

where D_i and S_i are a diffusion coefficient and the measured signal intensity of ions respectively. $S_{i,0}$ is an initial signal intensity, Δ the time between bipolar gradients, g the gradient strength, and τ is a period separating the starting of each pulse pair. The parameters were $\Delta = 60$ms and the duration of the gradient pulses, $\delta =$ 2-5ms, and g was incremented 20Tm^{-1} (gradient field strength was confirmed using water at 20 °C) [86] , and τ was kept constant at 2ms [59, 87, 88].

2.3.1.2 Spin Lattice Relaxation Time T_1

The inversion recovery method is given by the pulse sequence 180°x-τ-90°x and is utilised to measure the relaxation time T_1. Figure 2.3 displays the inversion recovery pulse sequence used to measure T_1. After the initial 180º pulse the net sample magnetisation M points along the negative Z-direction and then during τ M relax until it returns to the original and equilibrium position, pointing parallel to the positive Z-direction.

The magnetisation *M* rotates around the *X*- direction when, the 90º pulse is applied and then M, is transferred to the Y– direction [64, 79], where its size is then measured. This is repeated for various tau values and M_z as a function of τ is recorded. This function is then fitted to a single relaxation time expression given by:

$$M_Z = M_0\left(1 - 2exp^{-\tau/T1}\right) \tag{2.17}$$

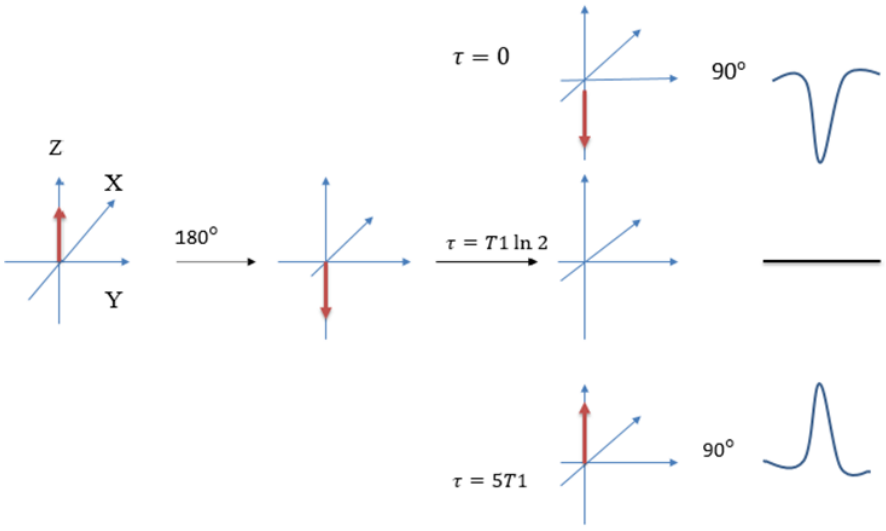

Figure 2.3: The inversion recovery pulse sequence to measure T_1.

2.3.1.3 Spin– Spin Relaxation Time T_2

The pulse sequences for measuring spin-spin relaxation time, T_2, was developed by Carr and Purcell in 1954 [69]. Experimentally, T_2 is measured by ‘‘90°x-τ/2-(180°x-τ/2-measure-τ/2)n’’, which is known as Carr Purcell Meiboom Gill (CPMG) sequence [69, 79]. Figure 2.4 shows the pulse sequence for the (T_2) measurement and its effect on

nuclear spins [89]. The value of magnetisation in the y-direction can be calculated by the equation:

$$M_y = M_0 \, exp^{-\tau/T2} \tag{2.18}$$

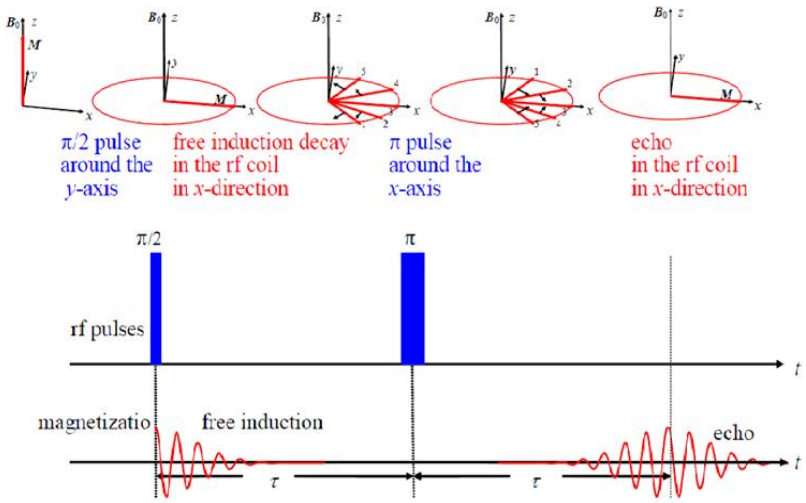

Figure 2.4: The measurement of the transverse relaxation time T_2 measurement. (taken from ref [90])

where M is magnetisation in the applied field B_0 after ‘‘90°’’ pulse sequence applied at the echo time, τ. After ‘‘90°’’ the magnetisations in XY plane and will gradually decay with decays at the rate of T_2*. This decay happened due to the inhomogeneous magnetic field, and spin-spin relaxation time. Therefore, the ‘‘180°’’ pulse sequence is employed to eliminate the inhomogeneous field [69, 71, 87, 90].

2.3.2 Rheology Method

A dynamic stress-controlled rheometer (Kinexus Ultra, from Malvern) using equipped with a cone-plate geometry (4°- 40 mm) and a temperature control system, using software called rSpace. A thin film of low-viscosity silicone oil was added around the edges of the plates to prevent moisture-contamination during the viscosity measurements. The Cross – Viscosity Equation has been used on a hypothetical basis that there is a change in the formation and structure of fluids at different shear rates [91]. The Cross – Viscosity equation was used to obtain the zero shear rate viscosity μ_0 of a solution.

$$\mu = \frac{\mu_0 + \mu_\infty . \alpha \gamma^n}{1 + \alpha \gamma^n} \tag{2.19}$$

where; γ is shear rate s^{-1}, μ_∞ is the viscosity at infinite shear rate, *n*, is the flow behaviour index (from 0 to 1), while α is the consistency index for shear-thinning fluids [91]. The intrinsic ability of a salute to raise the viscosity of a solvent at a given temperature is quantified by an intrinsic viscosity [η] [92]. There are several steps needed to determine an intrinsic viscosity. Starting with Relative viscosity, η_r can be calculated following by:

$$\eta_r = {}^{\eta}/_{\eta_0} \tag{2.20}$$

where η is the viscosity of polymer solution and η_0 is the viscosity of the solvent. The specific viscosity, η_{sp} of solutions were extracted from relative viscosity, which η_{sp} can obtain by

$$\eta_{sp} = \eta_r - 1 \tag{2.21}$$

The specific viscosity uses to measure intrinsic viscosity[η] by this equation.

$$[\eta] = \lim_{c \to 0} \eta_{sp} / c \tag{2.22}$$

where η is the viscosity of the solution, and η_0 is ionic liquid viscosity. From intrinsic viscosity, one can obtain information about the molar mass and solvent thermodynamic property.

Wolf approach was developed for carbohydrate in ionic liquids and used to determine the intrinsic viscosity [93, 94] and η can be calculated $[\eta]$ by

$$\ln \eta_r = \frac{c[\eta] + Bc^2[\eta][\eta]^{\cdot}}{1 + Bc[\eta]} \tag{2.23}$$

where B is a constant and c is a concentration of polymer in solution. The part $[Bc^2[\eta][\eta]^{\cdot}]$ of Equation 2.23 can be ignored because it is very small. Then by using the Huggins Equation to fit all the data in a single master curve.

$$\eta_{sp} = [\eta]c + k_H([\eta]c)^2 + A([\eta]c)^n \tag{2.24}$$

where A, n and $[\eta]$ were obtained from least squares analysis to a data point and k_H is the Huggins constant, which is typically in the range of 0.3 to 0.5 [92-95].

2.3.3 Carbohydrates Dissolved in Ionic Liquid [C2mim] [OAc] using NMR Spectroscopic

Nuclear Magnetic resonances (NMR) spectroscopy is used to investigate the interaction between the ions and carbohydrate molecules. The NMR chemical shift technique is employed to explore the new hydrogen bonds in these systems. The first carbohydrates were dissolved in IL [C2mim] [OAc] are cellulose and then glucose. Zhang et al., reported that the dissolution of cellulose can be determined by the interaction between cellulose molecules and ions of IL [C2mim] [OAc], which is hydrogen bonding interactions, these occur when the acetate anions [OAc] bonds to hydrogen atoms of the cellulose hydroxyl groups, and also by the imidazolium cations [C2mim] bonding with oxygen atoms of the OH groups of cellulose [6, 96]. Youngs et al., studied the interaction between anions acetate and hydroxyl groups in glucose solution by using pulse field gradient (PFG NMR). It found that the cations interact less with glucose in hydrogen bonding than that of the anion [97]. The interaction between ions of the ionic liquid and glucose molecules can be determined by measuring diffusion coefficients, activation energy and chemical

shift. It found that hydrogen bonds in glucose / IL [C2mim] [OAc] reduced the degree of ionic paring [98-100], where the anion prefers to associate with hydroxyl groups of glucose. The anions are found to diffuse slower, than unexpected, this might be due to anions diffusing as a member of ion aggregations [101, 102].

2.3.4 Material and Samples Preparation

The ionic liquid 1-ethyl-3-methylimidazolium acetate [C2mim] [OAc] solvent was purchased from Sigma-Aldrich (purity ≥ 97%, highest obtainable). This section will present the three types of carbohydrates – D-xylose, xylan and cellulose – which were dissolved in the ionic liquid [C2mim] [OAc]. D-xylose and cellulose powders were obtained from Sigma Aldrich with a purity of ≥ 99% for NMR and viscosity measurements. Xylan was extracted from pulping of primary birch wood in the form of a white powder, and it was obtained from the company Billerud Korsnas.

The carbohydrate composition of xylan is by dry weight fraction: xylose 88%, glucose 6%, galactose 4.4%, arabinose 1.4% and mannose 0.3%. There are other components in xylan, such as lignin and ash. D-xylose, xylan and cellulose powders were dried in vacuum at 50°C for 24h before use. D-xylose and xylan were individually dissolved in [C2mim OAc] solvent to prepare two sets of five samples with different weight fraction (weight fraction: 1%, 3%, 5%, 10% and 15%). Xylose samples have transparent colour, even if increase the weight fraction in solution, whereas the colour of xylan samples start with yellow to dark brown on adding a high concentration. Low concentrations of these carbohydrates took ~48h to dissolve in [C2mim] [OAc] while high concentrations (5%, 10% and 15%) approximately one week, these samples were prepared without heating. Carboyhdrate solutions were stirred under nitrogen gas in an MBraun Lab Master 130 Atmospheric chamber preserved at the level of a dew point between -70 ℃ and -40 ℃. The NMR tubes of samples were sealed to prevent contamination with water from the atmosphere within the chamber. NMR spectroscopy used to check whether there is water

in samples by examining the spectrum of IL[C2mim] [OAc] and looking for a resonance peak around 5 ppm, the water peak. The blends samples were prepared from two carbohydrates in 0.9 ml [C2mim] [OAc] and 0.1g of the total of carbohydrates with different concentrations. The carbohydrates consisted of xylan and cellulose, with xylan weight fraction ranging from 0-100%. These carbohydrate polysaccharides have different crystallinity percentage. For instance, the crystallinity of cellulose has the highest between 50% to 75% [19], while xylan has low crystallinity compared to cellulose, it could be due to xylan having a variety of structures [36]. The molar mass M_{GU} of ‘‘glucose unit’’ for cellulose and xylan are 162, and 131 g/mol, respectively.

Chapter 3

Investigation of the Influence of *D*-Xylose and Cellobiose on the Ionic Liquid 1-Ethyl-3-Methylimidazolium Acetate [C2mim] [OAc]

3.1 Introduction

The ionic liquid. 1-Ethyl-3-Methylimidazolium Acetate [C2mim] [OAc] is commonly used to dissolve different types of carbohydrate polysaccharide and monosaccharide, such as cellulose, glucose and xylose to investigate their influence on the diffusing particles in a viscous medium. This chapter will present the comparison between two carbohydrates monosaccharides (xylose and cellobiose) have when dissolving in 1-ethyl-3-methylimidazolium acetate [C2mim] [OAc]. There are two steps have been done, 1) Xylose in IL [C2mim] [OAc] solutions, to understand the dissolution of IL [C2mim] [OAc] using ^{1}H NMR spectroscopy, diffusion (9T / 400 MHz) , and low field NMR (0.5T / 20 MHz) relaxometry, across the temperatures range (20 °C to 70 °C). 2) The diffusion data of xylose will be compared to cellobiose data, which is taken from Ries et al. [41], to understand the influence of carbohydrate structure, in particular, the number of available OH groups, has on that the ions. The zero shear rate viscosity of xylose solution was measured. This viscosity data and diffusion, as well as relaxation time data, were employed to measure the correction term *f* and effective hydrodynamic radii, using both of Stokes-Einstein-Debye-relationships. The intrinsic viscosity of xylose and cellobiose

was calculated using the Wolf approach. It is also interesting to make a comparison between two carbohydrates polysaccharides, therefore; next chapter will show the dissolution of xylan in IL[C2mim] [OAc] and compared to cellulose data.

3.2 Experimental Methods

3.2.1 NMR Methods

NMR diffusion coefficient and low- field relaxation time T_1 and T_2 were measured using the techniques presented with details in Section 2.3.1. The diffusion coefficient of anions and cations for xylose and cellobiose solutions with different weight fractions were measured across temperatures ranging between 20 °C to 70 °C. The data of diffusion coefficients for xylose were compared to cellobiose data.

3.2.2 Viscosity Method

All rheological measurements were done for all xylose solutions using equipped with a cone-plate geometry (4°- 40 mm) and a temperature control system, using software called rSpace, as detailed in Section 2.3.2. Steady-state measurements were recorded for temperature between 20 °C to 60 °C inclusive in 10 °C steps. The viscosity-shear rates were from 0.01 to 200 s^{-1}. Before the experiment was run, a thin film of low-viscosity silicone oil was applied around the edges of the plate to prevent moisture contamination during the viscosity measurements. Each measurement for each concentration sample was repeated several times to get accurate data.

3.2.3 Materials and Sample Preparation

Xylose powder was dried under vacuum at 50°C for 24h before use. Xylose was dissolved in [C2mim] [OAc] solvent to prepare five samples with different concentrations (weight fraction: 1%, 3%, 5%, 10% and 15%). The resultant volume of each sample was ~ (1g). All xylose solutions were prepared in an MBraun Lab Master 130 Atmospheric chamber. Low concentrations of xylose took~ 24h to dissolve in [C2mim] [OAc] while high concentrations (5%, 10% and 15%) approximately 72h. All xylose solutions were placed in the NMR tubes with depths less than 1 cm to reduce convection currents on heating in the NMR machine. The NMR tubes of samples were sealed within the chamber to prevent contamination with water from the atmosphere By doing this, we followed the guidance set out by Annat et al [103].

3.3 Results and Discussion

3.3.1 NMR Diffusion

^{1}HNMR spectroscopy, diffusion, and low field relaxometry, across the temperatures range (20 °C to 60 °C), were used to examine the influence of xylose on the ions of the IL [C2mim] [OAc]. The ^{1}H NMR spectrum displays seven peaks, each peak corresponds to a chemically distinct proton within the ionic liquid molecule, recall Figure 1.1 [18]. During measurements of NMR diffusion, it was found that the diffusion coefficients of all cations resonances were equal. An Arrhenius type equation was used to model the temperature dependence of the self-diffusion coefficients of the ions $D_{cat/an}$ in 15% of cellobiose, CB, and all the xylose weight fractions %.

$$D_{(cat,an)} = D_0 \, exp^{\left(\frac{-E_{A,D}}{RT}\right)} \tag{3.1}$$

where E_A is the translational activation energy for the ions, R is the universal gas constant, T is temperature, and D_0 is the zero activation energy limiting value (sometimes known as the high temperature limiting value) of the diffusion coefficients for the ions [41]. In Figure 3.1(a, b) the solid lines are the Arrhenius fits. The mobility of anions and cations decrease with an increase in xylose weight fraction. The values of diffusion coefficients are increased with increase in temperature, as expected. These values indicate the diffusivities of anions and cations are similar. At low temperature, the values of diffusion decrease gradually with the addition of xylose. From Figure 3.1 both ions diffuse in 15% of cellobiose slightly slower than 15% of xylose. For instance D_{cat} are $8.2*10^{-12}$m^{2}s^{-1}and $1.02*10^{-11}$m^{2}s^{-1} D_{an} are $5.8*10^{-12}$m^{2}s^{-1} and $7.7*10^{-12}$m^{2}s^{-1} for 15% of cellobiose and xylose respectively, at temperature 50 ℃.

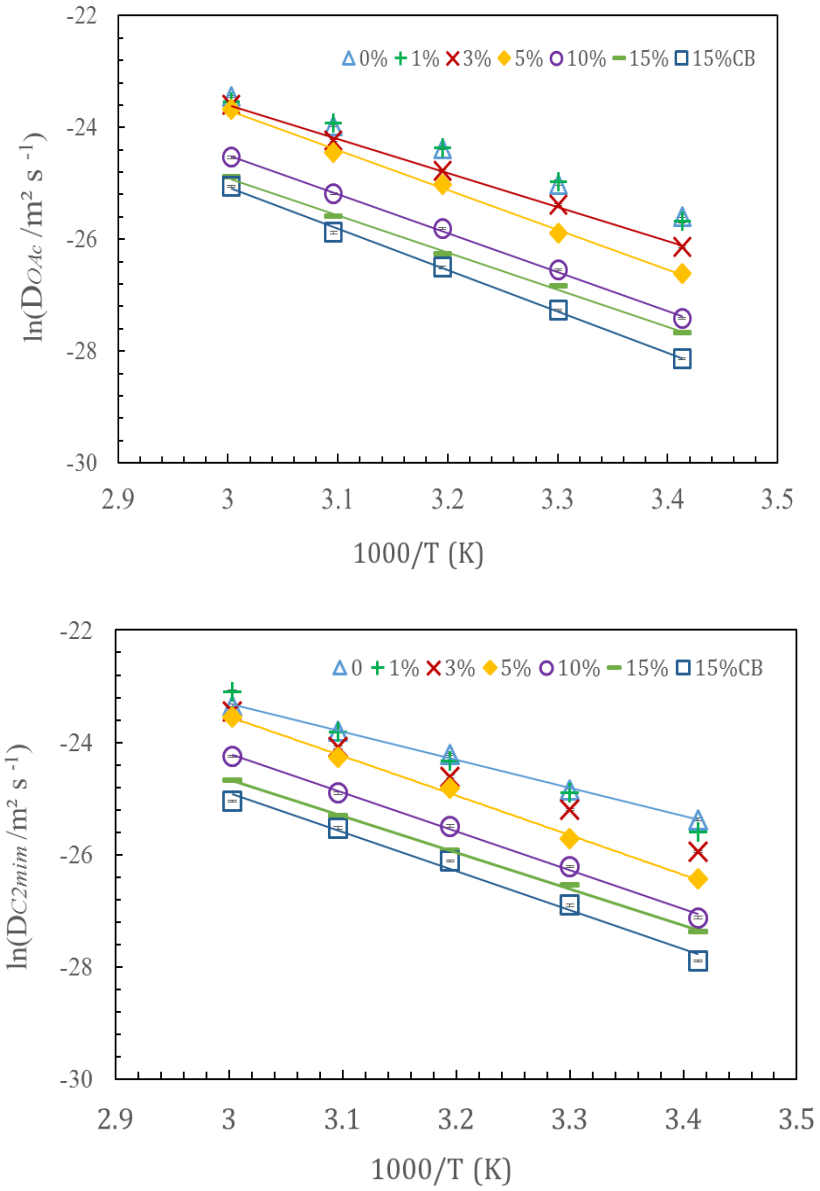

Figure 3.1: Arrhenius plots for the diffusion coefficients of (a) anions [OAC] and (b) cations [C2mim], for 15% cellobiose and all xylose weight fraction. Solid lines represented fits based on equation (3.1)and error bars are within the symbols used. [CB] means cellobiose.

The values of activation energies of diffusion coefficients of cations and anions for xylose and cellobiose solutions were calculated using Equation 3.1. Table 3.1 displays the values of activation energies of both ions increased with concentration at low concentrations, but for high concentrations of 10% and 15% of xylose solutions, it decreased slightly. The activation energies of ions gradually increased with an increase in cellobiose concentrations in solution. The values of activation energies of both ions indicated an insignificant difference between xylose and cellobiose systems for diffusion measurements.

Wt (%)	$E_{A,D}$ Xylose/kJ mol^{-1}		$E_{A,D}$ Cellobiose/kJ mol^{-1}	
	E[C2mim]+	E $[OAc]^-$	E[C2mim]+	E $[OAc]^-$
0	41.5 ± 1	43 ± 1	42 ± 1	43 ± 1
1	49.5 ± 2	50 ± 2	41 ± 1	43 ± 1
3	50 ± 1	51 ± 1	43 ± 2	45 ± 2
5	59 ± 2	59 ± 2	43 ± 1	44 ± 1
10	57 ± 2	58 ± 1	49 ± 2	50 ± 2
15	54 ± 1	55 ± 2	58 ± 4	61 ± 2

Table 3.1: The activation energies values of cations and anions for all xylose and cellobiose solutions.

Figure 3.2 presents the ratio of diffusion coefficients of anions to cations as a function of temperature for xylose and cellobiose. The ratio of diffusion coefficients of the anion to the cations for all xylose and 1% and 15% cellobiose concentrations were calculated from the data which is presented in Figure 3.1. As the temperature increased the ratio of anion [OAc] to cation [C2mim] diffusivities remained constant, with only a slight dependence on the xylose weight fraction. The 1% and 15% cellobiose solution are also shown as a comparison with this data displaying a similar temperature dependence. The ratio of anion [OAc] diffusion coefficients to that of cation [C2mim] is less than 1. This is known as ‘anomalous’ diffusion since the anion is geometrically smaller than the cation and therefore is expected to diffuse instead faster (i.e. the geometrically larger cation diffuses relatively faster than expected). The ratio of diffusion coefficients of the anions to the

cations is barely affected by the addition of xylose. Here it can be inferred that both carbohydrates have a similar dissolving mechanism. Figure 3.2 shows the data point of 15% of cellobiose jumped up at 60℃; this may be caused due to the current convection.

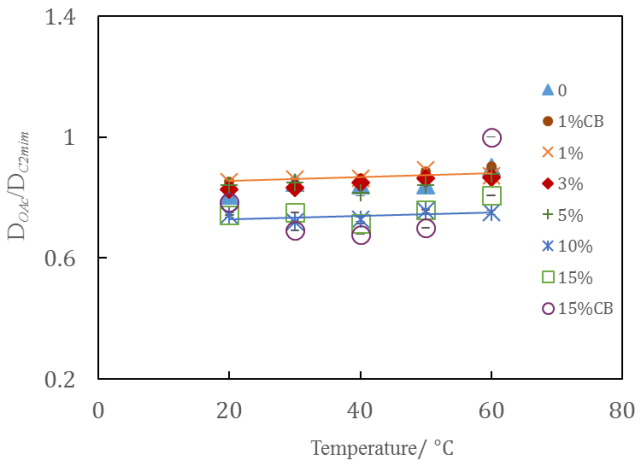

Figure 3.2: The ratio of diffusion coefficients of anions to cations as a function of temperature for xylose and cellobiose. Solid lines correspond to linear fits and error bars within the symbols sizes.

3.3.1.1 The Chemical Shift of Protons Resonances

The chemical shift of protons was determined during NMR diffusion measurements. The resonance frequency, δ, for a proton in parts per million (ppm), and Δδ is the change of these frequencies from the pure IL [C2mim] [OAc] positions caused by the addition of xylose. Figure 1.1 shows the labelling of proton resonances in the structure of IL [C2mim] [OAc]. The chemical shift $\Delta\delta$ of protons resonances was calculated using δ resonance peak 5 as the reference position. Protons of imidazolium ring [C2mim] have negative values of Δδ and relatively large movement peak 2, which is the most acidic proton. Peak 6 belongs to the anion [OAc] and peak 7 to a cation methyl group, and these both display positive values of Δδ. Figure 3.3 shows at 40℃, the movement of peak positions, this indicates that the addition of xylose and cellobiose disrupts the associated ions in the IL [C2mim] [OAc] and also given is the spectrum of 10% xylose/IL[C2mim] [OAc] solutions at 40℃. The reason for this is presumably the formation of H-bonding between

the IL and the OH groups in carbohydrates respectively. The anion [OAc] prefers to form H-bonds with the hydroxyl groups of carbohydrates, which moves them downfield, rather than remain associated with the protons in the imidazolium ring [C2mim]. It is interesting to note that the Δδ on the addition of xylose is almost identical to the chemical shift movements on the addition of cellobiose, suggesting that the dissolution process in both instances is similar.

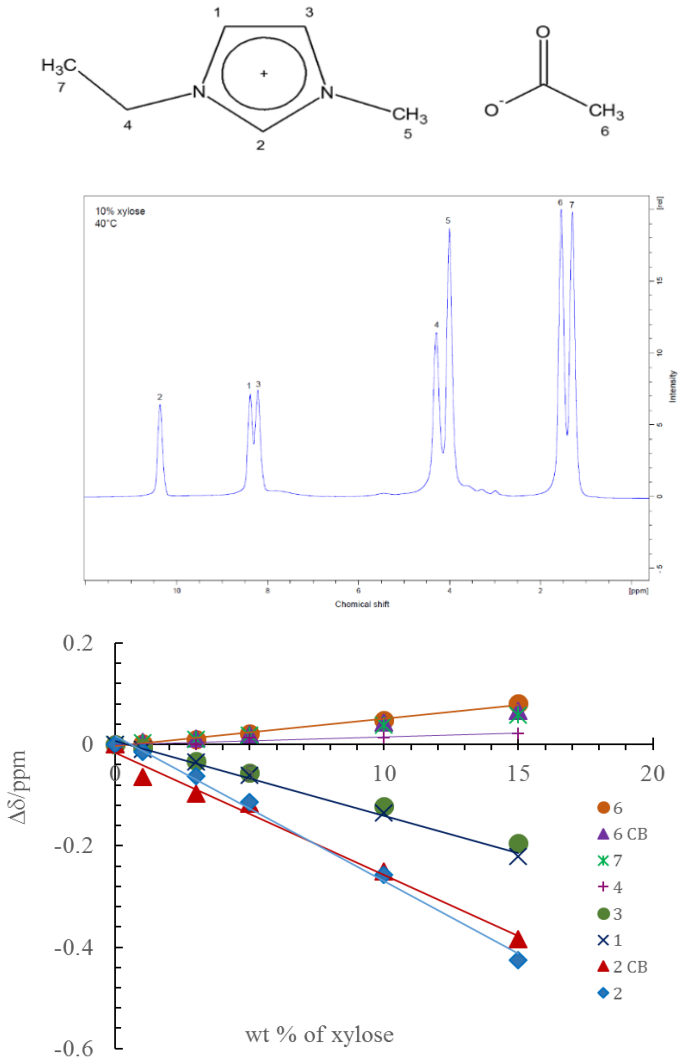

Figure 3.3: The chemical shift of protons resonances Δδ (ppm) versus weight fraction of xylose and cellobiose, CB, and spectrum of 10%/ IL[C2mim] [OAc] solutions at 40 °C. Error bars are within the symbols sizes.

3.3.2 Stokes−Einstein Analysis

Stokes-Einstein theory was employed to obtain an insight into the correlation between microscopic (diffusion) and macroscopic (viscosity) properties of ions and molecules. Stokes-Einstein Equation 2.8 is applied to experimental data to determine the correction term f, also known as the micro-viscosity pre-factor, it works as a key to determining the diffusion of ions in xylose and cellobiose systems, as discussed in section 2.2.1. The hydrodynamic radius, $R_{H,i}$ of ions was calculated by Hall et all using Equation 2.9. The values of the effective hydrodynamic radius are for the anion 2.2 Å and the cation 2.8 Å [59]. These values of $R_{H,i}$ are used in Equation 2.8.

Figure 3.4 (a, b) shows the correlation between translational diffusion of cations and anions and the ratio of temperature (K) to the viscosity ($Pa\ s$) to the viscosity of pure IL [C2mim] [OAc] and 15% cellobiose and all xylose concentrations. The cellobiose and xylose solutions follow the Stokes-Einstein Equation. It is possible to note that these carbohydrates have similar behaviour in IL [C2mim] [OAc]. All data of pure ionic liquid, 15% of cellobiose and all xylose solutions are combined from different temperatures into a single master plot. From Figure 3.4 the gradients are used to determine the correction term, f, as shown in Figure 3.5.

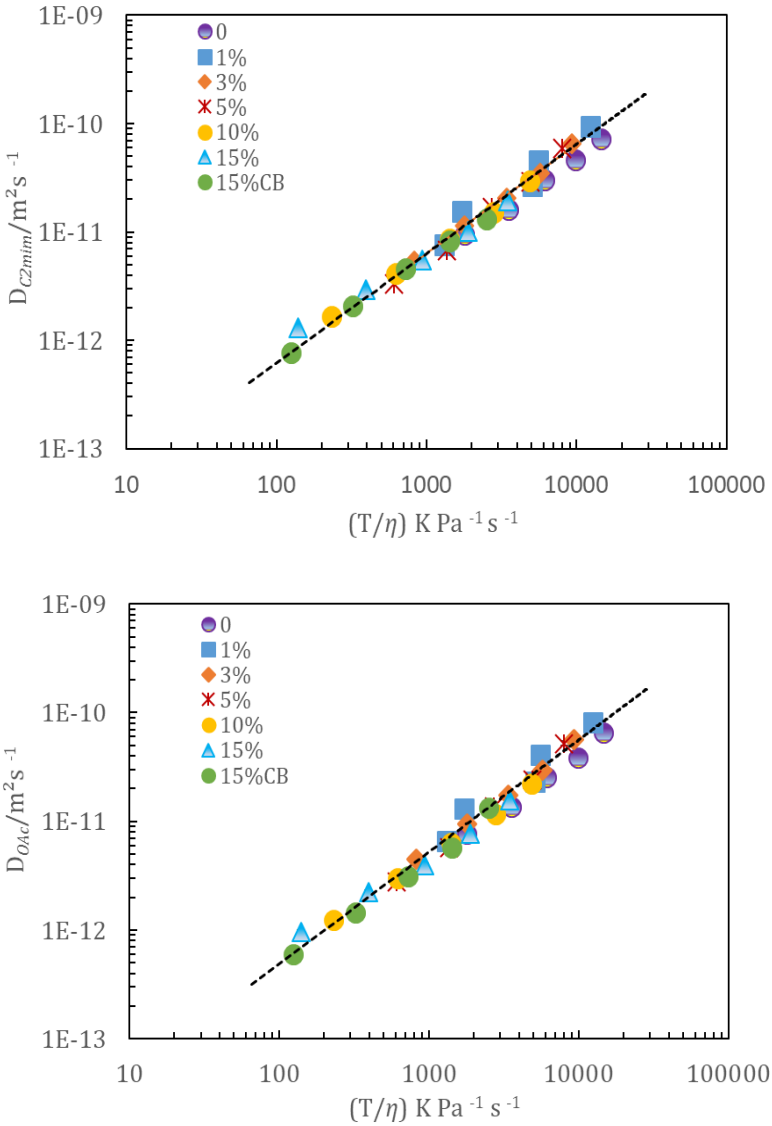

Figure 3.4: NMR diffusion coefficients of cations(a) and anions (b) against the ratio of temperature to the viscosity of pure IL [C2mim] [OAc] and 15% cellobiose and all xylose concentrations. Dashed lines are provided as visual guide and Error bars are within the symbols sizes.

McLaughlin reported that when the sizes of ions are the same as that of the molecules of the solution, then $f < 1$, but f is equal to 1 when the diffusing particle is large compared to the molecules of the viscous medium [75]. Figure 3.5 presents the correction term, f, of cations and anions as a function of weight fraction of xylose. The result shows the correction term of the diffuses anion faster than cation.

The f for anions ≥ 1 at high concentrations, this indicates that the anions diffuse close to as expected. The cation f is less than one, which means the cations are diffusing faster than expected.

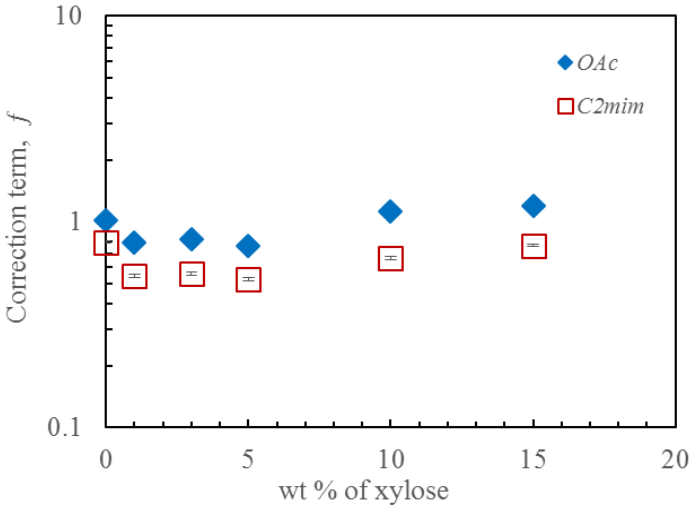

Figure 3.5: The correction term, f, of cations and anions as a function of weight fraction of xylose. The error bars are in the same size of symbols used

3.3.3 NMR Low−Field Relaxometry

Experimentally, low-Field Relaxation (0.5 T and 20MHz) T_1 and T_2 of different xylose concentrations (1%, 3%, 5%, 10%, and 10% of cellobiose) were measured across the range of temperatures 30 °C to 70 °C. The values of T_1 and T_2 relaxation times increase with an increase in temperature, but these values decrease with xylose concentration increases in solution.

Figure 3.6 (a, b) shows T_1 is very close to T_2 for all xylose, and there is the insignificant difference between 10% of cellobiose and xylose. At low field relaxation, xylose is found to be in the liquid regime across all selected temperatures. We will discuss this data in more details later.

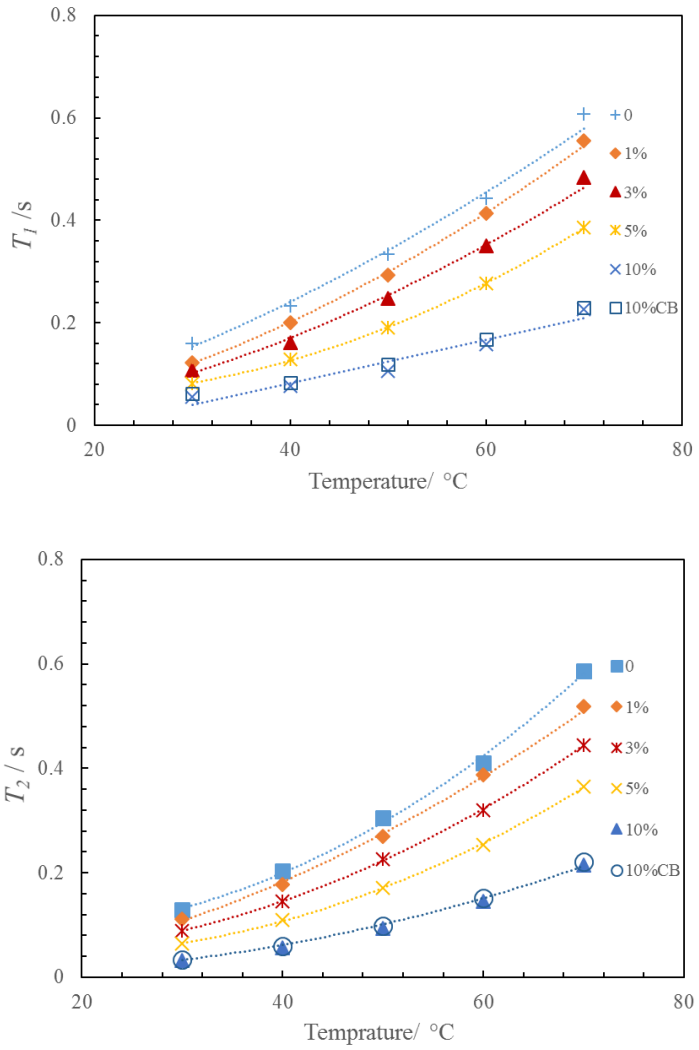

Figure 3.6: NMR relaxation times T_1 and T_2 as a function of temperature at 20 MHz, for all xylose concentrations with 10% cellobiose. Error bars are within data size and the dashed lines to guide the eye.

Low field relaxation times T_1 and T_2 have an inadequate chemical resolution to distinguish between ions; therefore, the calculated values of the activation energy, $E_{T1,T2}$ is an average value of both ions. The activation energy gives essential insight into transport characteristics. An Arrhenius equation is modelled to calculate the activation energy of relaxations times, $E_{T1,T2}$, which gives the following:

$$ln\, T_{1,2} = ln\, T_0 + \frac{E_{T1,T2}}{RT} \tag{3.2}$$

Where T_0 is relaxation time at infinite temperature, R is the universal gas constant and T is temperature. Table 3.2 displays the values of activation energies of T_1 and T_2 relaxations for xylose and cellobiose concentrations (1%, 3%, 5% and 10%). There are the insignificant difference between the values of activation energies of relaxation time T_2 for xylose and cellobiose. E_{T2} of 15% of cellobiose was slightly higher than 15% of xylose.

Wt%	$E_{T1,T2}$ Xylose/kJmol^{-1}		$E_{T1,T2}$ Cellobiose/kJmol^{-1}	
0	31 ± 1	33 ± 1	31 ± 1	33 ± 1
1	32 ± 1	34 ± 1	30 ± 1	34 ± 1
3	33 ± 1	35 ± 1	31 ± 1	35 ± 2
5	33 ± 1	37 ± 2	27 ± 1	38 ± 2
10	30 ± 1	41 ± 2	30 ± 1	44 ± 2

Table 3.2: Activation energies of T_1 and T_2 relaxations for xylose and cellobiose/IL [C2mim OAc].

3.3.4 Viscosity–Temperature Analysis

The viscosity measurements of different xylose concentrations (1%, 3%, 5%, 10% and 15%) were measured across the range of temperatures 20 °C to 60 °C inclusive. The Cross-Viscosity Equation 2.19, was used, to determine the zero-viscosity η_0 of xylose solution at selected temperatures.

Figure 3.7a shows the steady state flow curves of xylose / [C2mim] [OAc] solutions for various concentrations at 40 °C. The data from 0 to 10 s^{-1} had a low signal to noise ratio and thus was ignored for 1%, 5%, 10% and 15% of xylose solution, but the low signal started from 0 to 1 s^{-1} for 3% xylose. Figure 3.7b shows the viscosity decreased as temperature increased, as expected. The influence of xylose concentration on solution viscosity is more significant at low temperatures; than high temperatures. Figure 3.7c shows the experimental data for each concentration is plotted as ($\ln \eta_0$) against inverse temperature. Viscosity values increase with xylose weight fractions and decrease with temperature. Xylose solutions behave in a remarkably similar way to cellobiose. The diffusivity of ions in a viscous medium can be determined through their activation energy, using an Arrhenius−type equation as:

$$ln(\eta) = \ln(\eta_0) + {E_{A,\eta}}/{RT} \tag{3.3}$$

Where; η_∞ is the value of limiting viscosity, E_A is activation energy, T is temperature and R the molar gas constant [104].

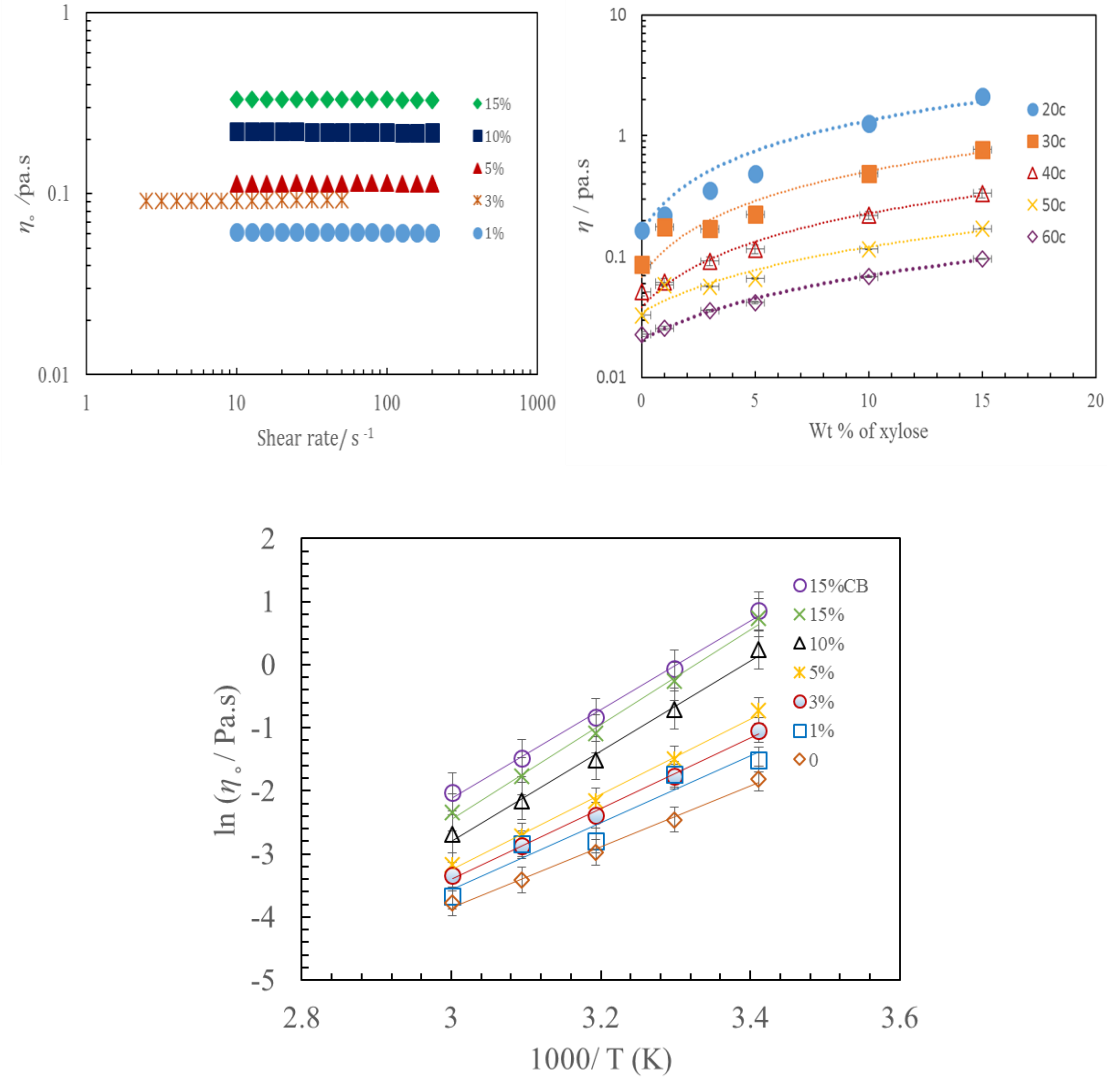

Figure 3.7:a) The zero viscosity of xylose / [C2mim] [OAc] solutions at different weight fractions as a function of shear rate/s. b) Viscosity as function of weight fraction of xylose across arrange of temperatures. Dashed line to guide the eye. c) The logarithmic plots of the viscosity of pure [C2mim] [OAc] and 15% cellobiose and xylose in IL [C2mim] [OAc] solutions versus inverse temperature. Lines are linear approximations. Error bars are within the size of the symbols used.

The activation energy of viscosity is related to the energy required for molecules to move past each other, allowing flow [59]. An Arrhenius Equation 3.3 was applied to the experimental data to calculate the activation energy of viscosity for carbohydrates solutions. Table 3.3 presents the values of viscosity activation energies of xylose compared to cellobiose at similar temperatures. The activation energy of viscosity increased with the addition of carbohydrate weight fractions. The $E_{A,\eta}$ of xylose is slightly higher than $E_{A,\eta}$ of cellobiose. From Table 3.3, it was found that the values of activation energies of ions indicated an insignificant difference between xylose and cellobiose systems for viscosity measurements.

Wt%	$E_{A,\eta}$ Xylose/kJmol^{-1}	$E_{A.\eta}$ Cellobiose/kJmol^{-1}
0	40 ± 2	40 ± 2
1	44 ± 6	39 ± 2
3	46 ± 2	41 ± 2
5	50 ± 3	44 ± 2
10	50 ± 3	50 ± 2
15	63 ± 3	58 ± 2

Table 3.3: The activation energies of viscosity for xylose and cellobiose solutions with uncertainties values.

3.3.5 Stokes−Debye−Einstein Analysis

Low field relaxation times (20 MHz) were measured across temperatures (70 °C - 30 °C). Relaxation times T_1 and T_2 have the inadequate chemical resolution to distinguish between ions; therefore, the values of the hydrodynamic radii size, $R_{H,i}$ were calculated as averaged value over both ions. Stokes- Einstein-Debye Equation was used to consider the rotational correlation time of diffusing ions and to calculate the values for the radius of ions in a viscous medium, $R_{H,i}$, as discussed in Section 2.2.3.

Figure 3.8 (a, b) displays the correlation between the relaxation time and the ratio of temperature to the viscosity for carbohydrates concentrations. Figure 3.8a shows the dependence of relaxation times T_1 on the ratio of temperature to viscosity for 10% cellobiose and D-xylose concentrations. All data collapsed together to form one master line, which may be due to them having the same number of OH groups. The gradient for each concentration is approximately equal to 1. This helped compare relaxation times T_1 and T_2 and viscosity systems at selected temperatures. Figure 3.8b shows that same relationship holds almost as well for relaxation time T_2. The slope was used to calculate the value of the effective hydrodynamic radii for T_1 and T_2 using Equation 2.15. Figure 3.9 will display the hydrodynamic radii, $R_{H,i}$ values of relaxation time T_1.

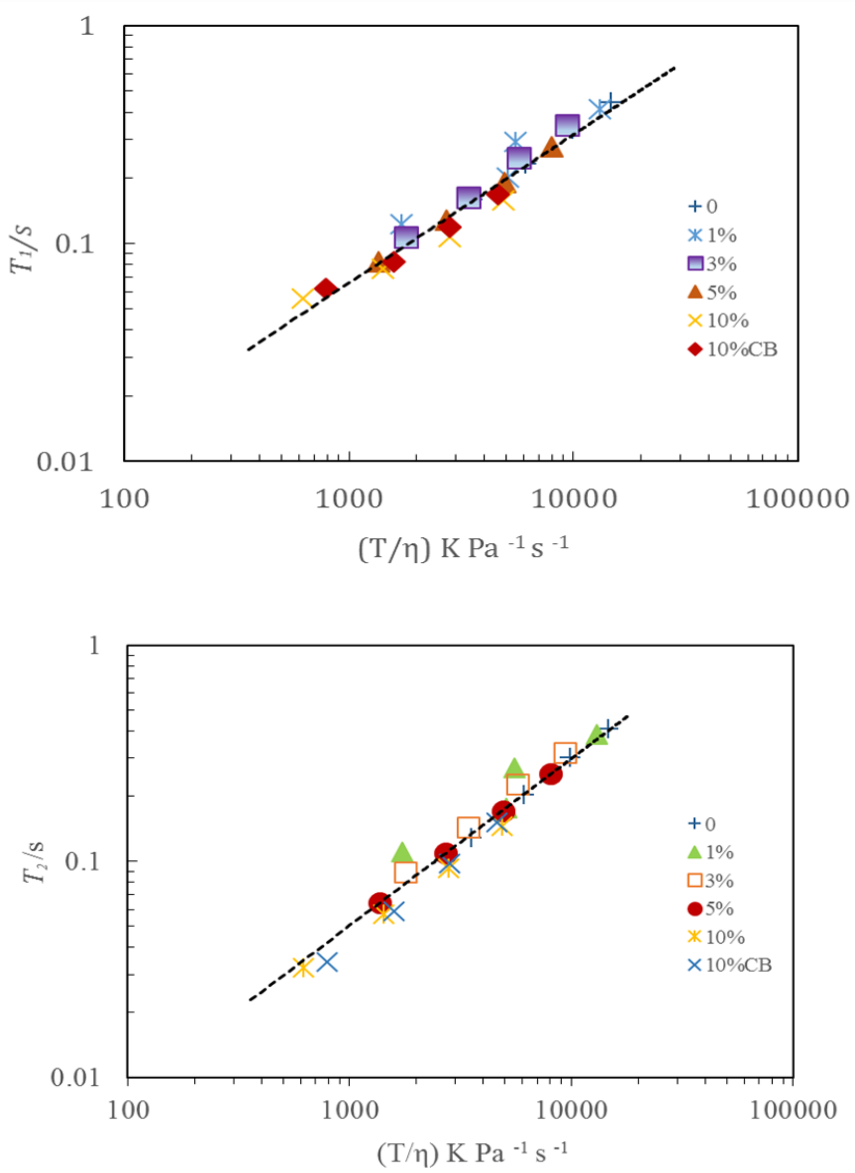

Figure 3.8: The relaxation times T_1 and T_2 dependence on the ratio of temperature to viscosity for 10% cellobiose [CB] and D- xylose concentrations. Error bars are within data points. Dashed lines are provided as a visual guide.

Figure 3.9 shows the hydrodynamic radius in D-xylose solutions and the hydrodynamic radius of the averaged ions (2.5 Å) of pure IL [C2mim] [OAc]. It is visible from that the value of the hydrodynamic radius of averaged ions increases for (1%, 3%, 5% and 10%) xylose concentrations and are between 3.5 Å to around 4 Å. The size of ions does not change, but how they move can be influenced by the interactions with D-xylose. The values of hydrodynamic radii for all the xylose concentrations and all the temperatures, for T_1, is almost equal to or slightly greater than T_2 experimentally.

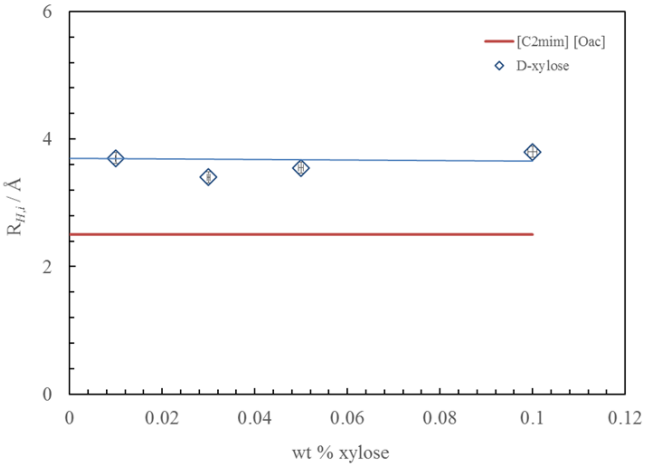

Figure 3.9: The values of effective hydrodynamic of radii against the xylose weight fractions and the hydrodynamic radius of the averaged ions of pure IL [C2mim] [OAc] and errors are within the size of data points.

3.3.6 Intrinsic–Viscosity Analysis

In this work, the intrinsic viscosity is determined by using the viscosity-shear rate data. The intrinsic viscosity, $[\eta]$ was obtained by processing the data of viscosity at selected temperatures through the following steps. First of all, we used the zero viscosity of xylose solutions mean Newtonian viscosity values presented in Figure 3.7a. The Second step, the calculations were done employing relative viscosity, where η_{rel} of xylose solution calculated by applying Equation 2.20, where is the viscosity of each xylose concentration

divided by the viscosity η_0 of pure IL[C2mim] [OAc]. Figure 3.10a shows concentration-dependence of the relative viscosity of xylose solutions. The relative viscosity increases with increase in xylose into a solution. The highest values of η_{rel} were at 20 ℃, alongside gradual decreases with increase in temperature. The values of relative viscosity increase with an increase in xylose, For instance, η_{rel} for 1% and 15% of xylose are 1.4Pa. s and around 13 Pa. s. At high temperatures, such as 60 ℃ , η_{rel} the values for 1, 3, 5, 10 and 15% of xylose are 1, 1.6, 2, 3 and 4.2 Pa. s, respectively. After that, the specific viscosity was determined by applying Equation 2.21.

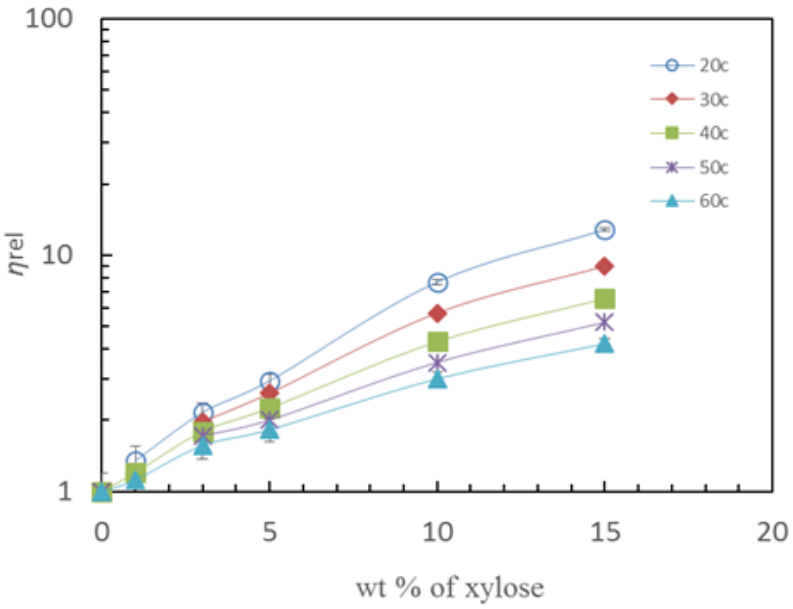

Figure 3.10: Relative viscosity as a function of xylose weight fraction between 20°C to 60 °C. Error bars within the symbols sizes and dashed lines are to guide the eye.

Figure 3.11a shows the specific viscosity, η_{sp} as a function of xylose solution across arrange of temperature. The η_{sp} spreads out with the increase in temperature, the highest values of specific viscosity for 10% and 15% of xylose at 20 ℃. Finally, the intrinsic viscosity is calculated by using Equation 2.23 (the squared part with constant *B* was ignored in the equation because it is relatively very small) in the Wolf approach, and then Equation 2,24 was used to fit the data into a master curve.

The Wolf approach involves plotting the natural logarithm of relative viscosity, η_{rel} versus the weight fraction of xylose. The weight fraction of xylose multiplied to the density of the IL [C2mim] [OAc] is 1.1 g/cm^3. This means the numerical values of concentrations have used to calculate the intrinsic viscosity are between 0.0121 g/cm3 and 0.182 g/cm3, which from low to high concentration. Figure 3.11b shows the intrinsic viscosity plotted as a function of temperature, alongside data for cellobiose as a comparison. The values of xylose intrinsic viscosity [η] are greater than the corresponding cellobiose values at the lower temperature. The intrinsic viscosity of cellobiose was influenced slightly by temperature, as shown in Figure 3.11b. The intrinsic viscosity [η] values significantly reduce with increasing temperature for xylose solutions showing that the quality of the solvent reduces with increase in temperature. The intrinsic viscosity of cellobiose slightly decreased compared to xylose.

The values of intrinsic viscosity [η] of xylose were around 22 ml/g at 20 °C and slightly decreased with increasing temperature to reach 10 ml/g at 60 °C. The values of intrinsic viscosity [η] of cellobiose were around 13 ml/g at 20 °C and slightly decreased with increasing temperature to reach 9.97 ml/g at 60 °C.

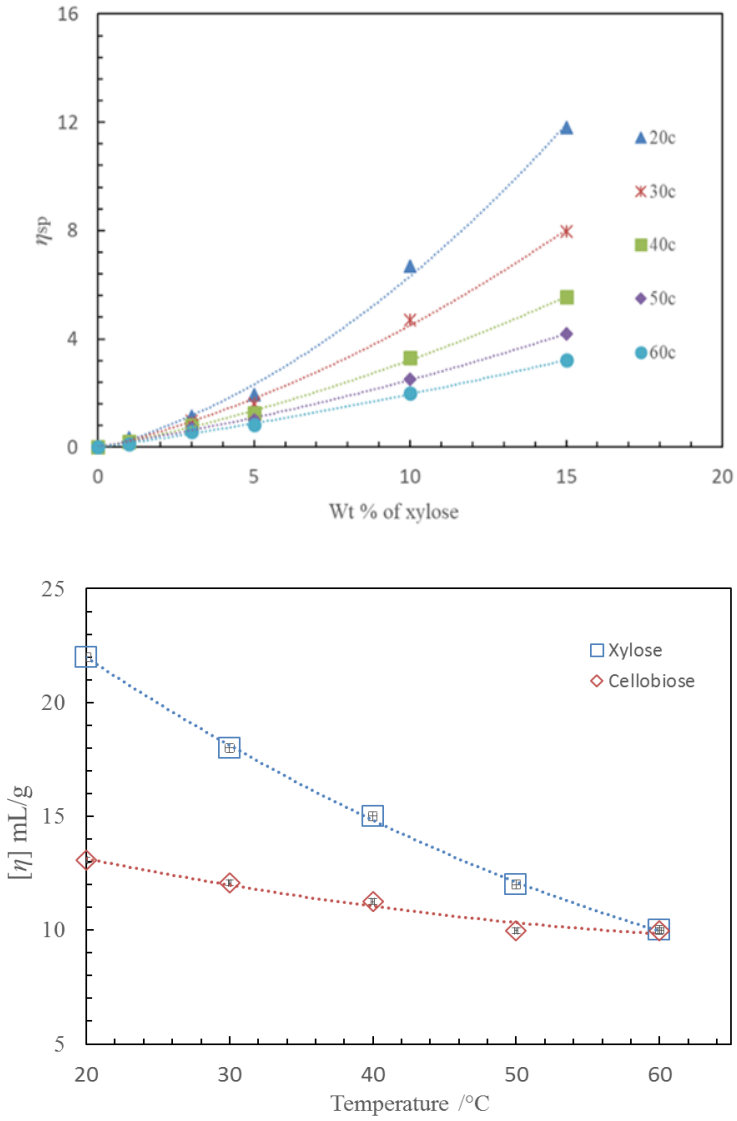

Figure 3.11: a) Specific viscosity as a function of xylose weight fraction between 20°C to 60 °C. b) Intrinsic viscosity [η] of cellobiose and xylose solutions as a function of temperature / °C. Error bars are within the symbol size. Solid and dashed lines are to guide the eye.

Figure 3.12 presents the correlation between the relative viscosity and concentration-intrinsic viscosity, c[η] across temperature 20℃ to 60℃. In Figure 3.12, all the intrinsic viscosity data of xylose solutions are combined for different temperatures into a single master curve, at selected temperatures.

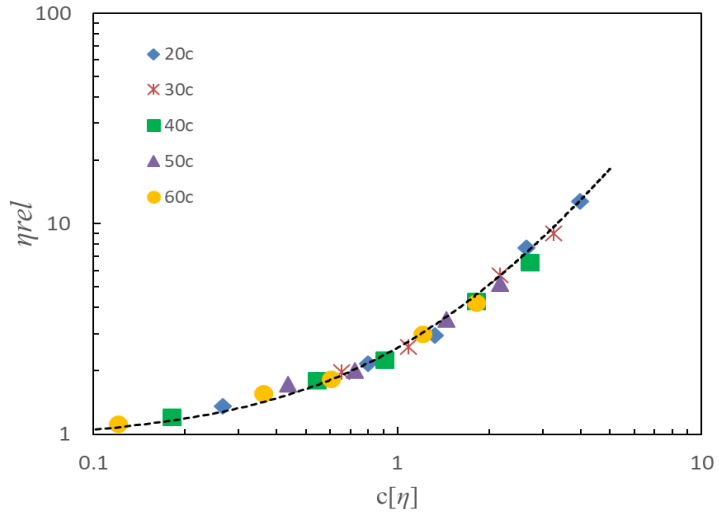

Figure 3.12:Master plot of relative viscosity against $c[\eta]$ for xylose / [C2mim] [OAc] solutionsfor temperature from 20 °C - 60 °C and xylose concentrations (1%, 3%, 5%, 10% and 15%). Error bars within the symbols sizes and dashed line are to guide the eye.

3.4 Conclusion

NMR technique is employed for chemical characterisation and was used to measure diffusion properties as well as molecular relaxation dynamics at various temperatures. The values of diffusion coefficients of ions reduced with increases in xylose weight fractions and decreases in temperature. The ratio of the diffusion coefficient of anions to cations was less than 1. This is known as ‘‘anomalous’’ diffusion because the anion is geometrically smaller than the cation and so would be expected to diffuse faster not slower than the cation. This indicates anions are not diffusing slowly, but it is possible these anions diffuse as part of an aggregation of ions.

The changes in ^{1}H chemical resonance frequencies $\Delta\delta$ for proton by adding xylose is almost identical to the chemical shift movements of cellobiose, suggesting that the dissolution method in both instances is similar.

The Arrhenius equation was used in both microscopic and macroscopic systems to determine the activation energy for ions. Stokes-Einstein equation was used to determine the correction term, f and it decreased with increasing xylose concentration by weight. Stoke-Debye-Einstein Equation was applied to experimental data.

Relaxation times (20 MHz) T_1 and T_2 were measured across a temperature range (70 °C-30 °C). This work found that for all the xylose concentrations and all the temperatures T_1 is approximately equal to or slightly greater than T_2 experimentally. The values of activation energy for both relaxation times are similar. The values of hydrodynamic radii were determined by using the correlation between the relaxation times T_1 and T_2 and the ratio of temperature to viscosity for all xylose concentrations. The zero shear viscosities were obtained for all xylose concentrations. The intrinsic viscosity of homogeneous solutions for xylose in the solvent [C2mim] [OAc] was calculated. In overall, it can be noted that from diffusion and viscosity measurements and chemical shift technique, xylose and cellobiose have a similar dissolving mechanism in IL [C2mim] [OAC].

Chapter 4

Investigation of the Influence of Xylan and Cellulose on the Ionic Liquid 1-Ethyl-3-Methylimidazolium Acetate [C2mim] [OAc]

4.1 Introductions

The dissolving of xylan in 1-ethyl-3-methylimidazolium acetate [C2mim] [OAc] solutions, were examined at temperatures (20 °C – 70 °C) using rheology, nuclear magnetic resonance (NMR) spectroscopy, diffusion, high (9.5T / 400 MHz) and low field (0.5T / 20 MHz) relaxometry. The influence of xylan on the ions of IL [C2mim] [OAc] is compared a previous study on cellulose / IL [C2mim] [OAc], this cellulose data taken from ref [41]. The zero shear rate viscosity of xylan solutions were measured. The activation energy of diffusion, relaxation time and viscosity were calculated. The intrinsic viscosity of xylan was calculated using Wolf approach. The overlap concentration was determined for xylan solutions and compared to cellulose. The main aim of this chapter is to understand the interaction of ions in xylan and compared to cellulose solutions.

4.2 Experimental Method

4.2.1 NMR Method

NMR diffusion coefficient and high and low field relaxation time T_1 and T_2 were measured using the techniques was presented with details in Section 2.3.1. The diffusion coefficient of anions and cations for xylan solutions with different weight fractions % were measured across temperatures range of 20 °C to 70 °C. All xylan solutions were placed in the NMR tubes with depths less than 1 cm to reduce convection currents on heating in the NMR machine. By doing this, we followed the guidance set out by Annat et al [103].

4.2.2 Rheology Method

All xylan viscosity measurements were measured using equipped with a cone-plate geometry (4°- 40 mm) and a temperature control system, using software called rSpace, as detailed in Section 2.3.2. Steady-state measurements were recorded from 20 °C to 60 °C inclusive in 10 °C steps. The viscosity-shear rates were from 0.1 to 100 s-1. Before the experiment was run, a thin film of low-viscosity silicone oil was added around the edges of the plate to prevent moisture contamination during the viscosity measurements. The cross-viscosity equation 2.20 used to get the accurate zero-shear-rate viscosity of xylan solution. The Wolf approach used to determine the intrinsic viscosity of these solutions and using the Huggins Equation 2.24 to fit all the data into a master curve.

4.2.3 Material and Sample Preparations

Xylan powder was dried under vacuum at 50°C for 24h before use. Xylan was dissolved in [C2mim] [OAc] solvent to prepare five samples with different concentrations (weight fraction: 1%, 3%, 5%, 10% and 15%). The resultant volume of each sample was ~ (1g). All Xylan solutions were prepared in an MBraun Lab Master 130 Atmospheric chamber. For more details is in Section 2.3.3. Low concentrations of xylan took~48h to dissolve in [C2mim] [OAc] while high concentrations (5%, 10% and 15%) approximately 1 week, without heat. All samples tubes were sealed within the chamber to prevent contamination with water from the atmosphere.

4.3 Results and Discussion

4.3.1 NMR Diffusion

The influence of xylan on the diffusion properties of the ions of the IL [C2mim] [OAc] was examined using ^{1}HNMR spectroscopy, diffusion, and low field relaxometry, across the temperatures range (20 °C to 70 °C). The ^{1}H NMR spectrum displays seven peaks, each peak corresponds to a chemically distinct proton within the ionic liquid molecule, recall Figure 1.1. Temperature increases both the diffusivity of cations [C2mim] and anions [OAc], but an increase in concentrations of xylan decreases them. The reason for this is that the viscosity is increased by the presence of xylan and decreased by increasing temperature and there is an inverse relationship between diffusion and viscosity, through the Stokes-Einstein relationship. Figure 4.1 (a, b) shows the diffusion coefficients of cations and anions as a function of the inverse of temperature for all xylan solutions. The values of diffusion coefficients of cations appear to be similar to that of the anions. The values of diffusion coefficients of the imidazolium cations [C2mim] to those of the acetate anions [OAc] are near to 1.

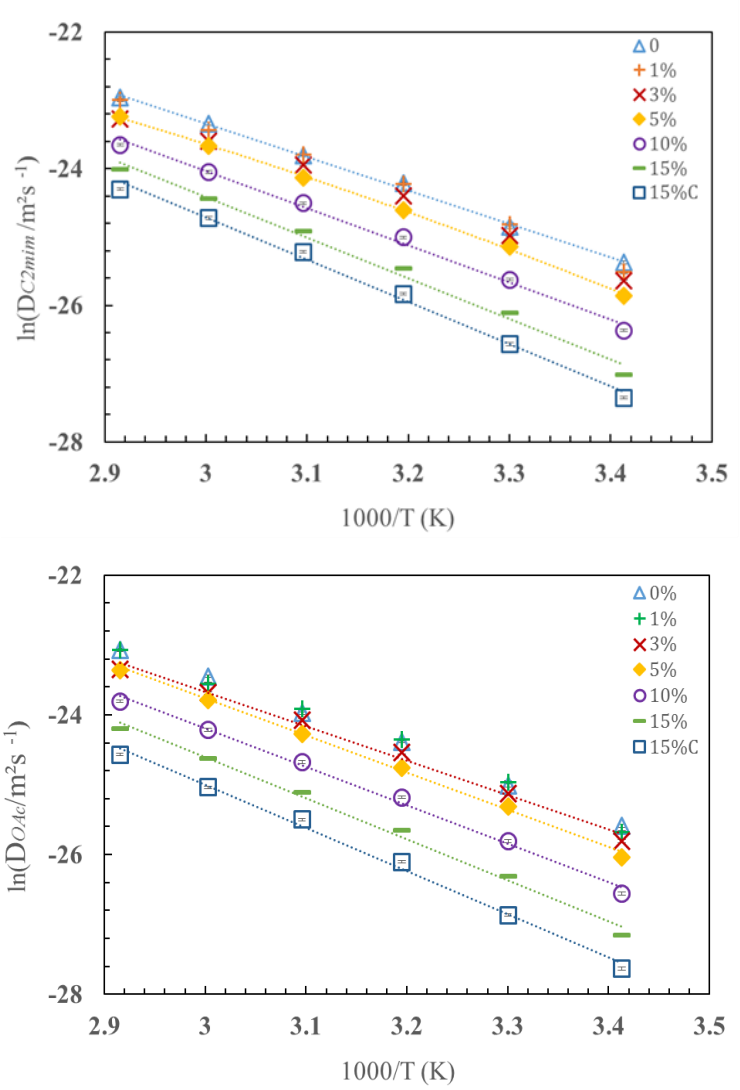

Figure 4.1: The diffusion coefficients of cations [C2mim] (a) and anion [OAc] (b) as a function of the inverse of temperature for 15% cellulose, [C] and xylan concentrations. Dashed lines represent fits based on equation 3.1, uncertainties are shown.

The activation energies of the diffusivity of ions are related to the energy required for molecules to move past each other, enabling flow [59]. The experimental data for each concentration plotted as ($\ln D_{OAc,C2mim}$) against inverse temperature, was taken from Figure 4.1. The activation energies were extracted from the slope of the linear fits to this data using Equation 3.1. Table 4.1 presents the values of activation energies of self-diffusion of cations and anions for all samples of xylan and cellulose.

Wt%	$E_{A,D}$ Xylan / kJmol^{-1}		$E_{A,D}$ Cellulose / kJmol^{-1}	
	$[C2mim]^+$	$[OAc]^-$	$[C2mim]^+$	$[OAc]^-$
0	41 ± 1	42 ± 1	41 ± 1	42 ± 1
1	41 ± 2	43 ± 2	40 ± 1	41 ± 1
3	39 ± 2	41 ± 2	40 ± 1	41 ± 1
5	43 ± 1	44 ± 1	40 ± 1	40 ± 1
10	45 ± 2	46 ± 2	45 ± 4	45 ± 4
15	49 ± 2	49 ± 2	51 ± 2	51 ± 2

Table 4.1: The values of the activation energies of self-diffusion of cations and anions for all xylan and cellulose weight fractions solutions.

Figure 4.2 shows that as the temperature is increased the ratio of anion [OAc] to cation [C2mim] diffusivities remains constant, with only a slight dependence on the xylan concentration. The 1% and 15% cellulose solutions are also shown as a comparison with this data displaying a slightly stronger concentration dependence and a similar weak temperature dependence. The ratio of anion [OAc] diffusion coefficients to that of cation [C2mim] is less than 1. This is known as 'anomalous' diffusion since the anion is smaller geometrically than the cation and therefore is expected to diffuse instead faster, but is found experimentally to diffuse slower. Consequently, the addition of xylan hardly affects this ratio. This similar weak concentration dependence suggests a similar dissolving mechanism for both carbohydrates, indicating that the reduction in mobility of both ions has the same source, presumably a change in the local effective micro-viscosity.

If the anion experienced more and/or stronger interactions with the carbohydrate in hydrogen - bonding then this would preferentially reduce the diffusivity of the anion.

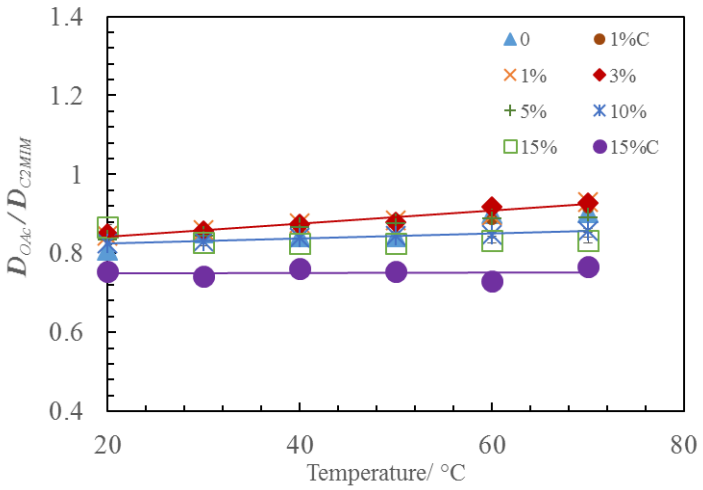

Figure 4.2: Ratio of the diffusion coefficient of the anion to the cation as a function of temperature. Solid lines correspond to linear fits. Error bars are within the symbols sizes and [C] indicates cellulose.

4.3.1.1 The Chemical Shift of Proton Resonances

The numbers shown in the structure of the IL [C2mim] [OAc] in Figure 1.1 are used to indicate the labelling of proton resonances. The chemical shift $\Delta\delta$ of protons resonances was calculated using δ resonance peak 5 as a reference position. In Figure 4.3 the results are displayed, for 40 ℃, where δ is the resonance frequency for a proton in parts per million (ppm), and $\Delta\delta$ indicates the change of this frequency from the pure IL [C2mim] [OAc] positions caused by the addition of xylan. Protons of imidazolium ring [C2mim] have negative values of $\Delta\delta$ and relatively large movements; particular peak 2, which is the most acidic proton. Peak 6 belongs to the anion [OAc] and peak 7 to a cation methyl group and these both display positive values of The chemical shift $\Delta\delta$ of protons resonances. The movement of peak positions indicates that the addition of carbohydrate polymers disrupts the associated ions in the pure IL [C2mim] [OAc]. The reason for this

is presumably the formation of H-bonding between the IL and the OH groups of xylan and cellulose respectively.

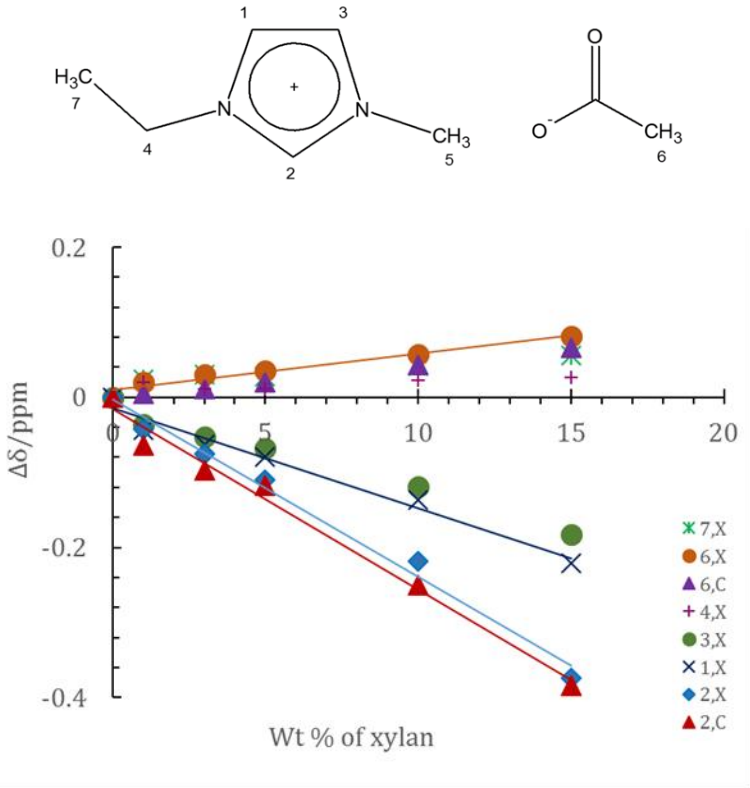

Figure 4.3: The chemical shift of protons resonances Δδ (ppm) versus weight fraction of xylan, X and cellulose, C at 40 °C Error bars are within the symbols sizes. The lines are guides to eye.

The anion [OAc] prefers to form H-bonds with the carbohydrates, which moves them downfield, rather than remain associated with the protons in the imidazolium ring [C2mim]. It is interesting to note that the Δδ on the addition of xylan is identical to the chemical shift movements on the addition of cellulose, implying that the dissolution process in both instances is similar.

4.3.2 Stokes−Einstein Analysis

Stokes-Einstein theory was used to investigating the interaction between ions of the IL [C2mim] [OAc] and the carbohydrate molecules. By using the correction term f, also known as the micro-viscosity pre-factor as a key to determining the diffusion of ions in xylan and cellulose systems, as discussed in section 2.2.1. The experimental data of the correlation between diffusion coefficients of ions and the ratio of the temperature to the viscosity is employed to calculate the correction term, f, using Stokes-Einstein Equation 2.8. The hydrodynamic radius, $R_{H,i}$ of ions was calculated by Hall et all using Equation 2.9. The values of the effective radius are for the anion 2.2 Å and the cation 2.8 Å [59]. These values of $R_{H,i}$ are used in Equation 2.8. Figure 4.4 (a, b) shows the correlation between the diffusion coefficients of anions and cations and the ratio of temperature to viscosity values. The diffusion coefficients of cations and anion of IL [C2mim] [OAc] are slowly decreased with an increase in carbohydrate polymers concentrations. However, this gradual reduction of diffusion coefficients came with a strong increase in viscosity and therefore a decoupling of the local micro and larger scale macroscopic viscosities.

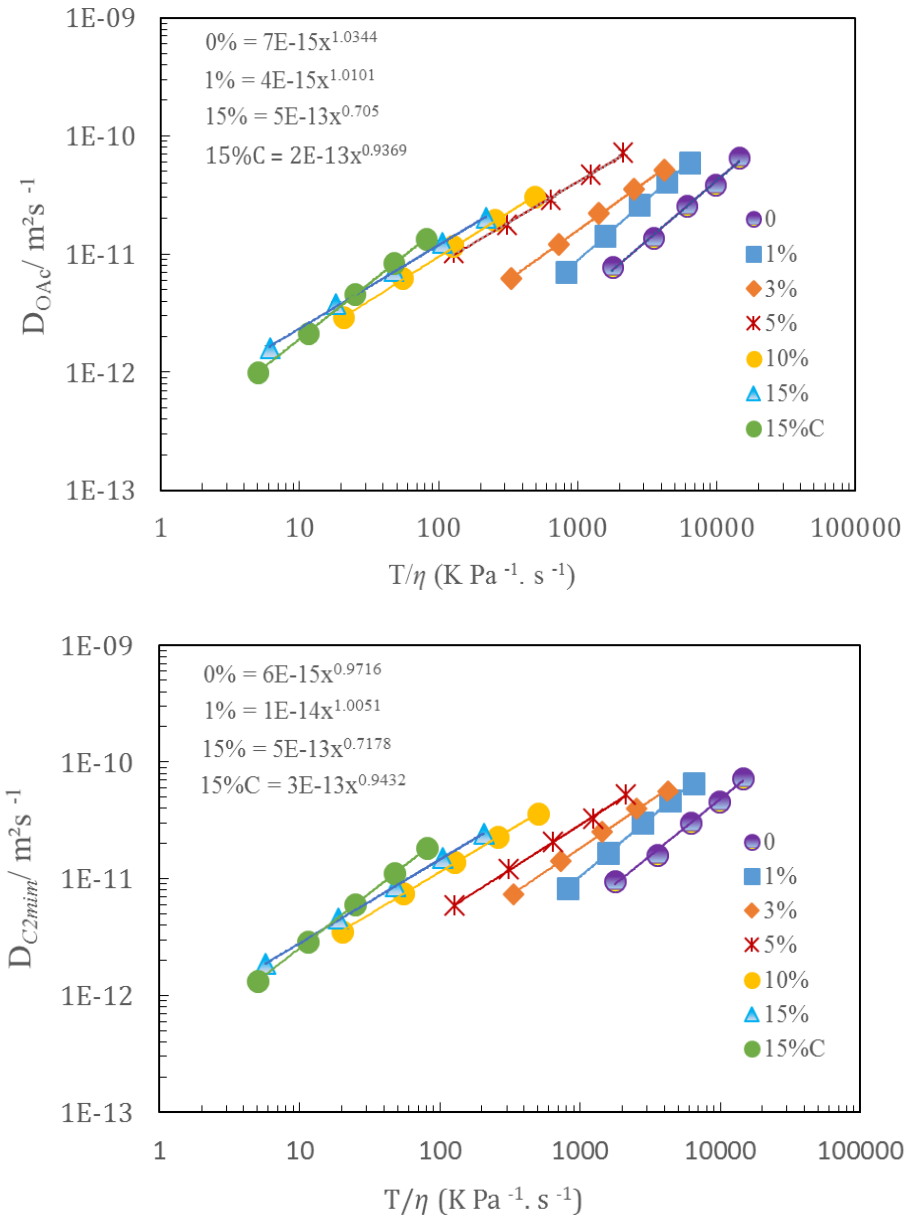

Figure 4.4: NMR diffusion coefficient of anions (a) and cations (b) against the ratio of temperature to the viscosity of pure IL [C2mim] [OAc] and 15% cellulose and all xylan concentrations.Solid lines are provided as a visual guide and Error bars are within the symbols sizes.

Figure 4.5 shows the correction term *f* for cation [C2mim] and anion [OAc] as a function of weight fraction of xylan. According to McLaughlin, when the sizes of ions are the same as that of the molecules of the solution, then $f \approx 1$, but f is equal to 1.5 when the diffusing particle is large compared to the molecules of the viscous medium [75]. The correction term decreased with increased xylan concentration. It is interesting to note that the anions have $f \sim 1$ so diffuse as expected, but the cations are less than one, this indicates the cations diffuse faster than expected. In Figure 4.5 the f drops off with the increase in xylan concentration, this due to the decoupling between the macroscopic and microscopic viscosities. Macroscopic entanglements are formed at concentrations above the overlap concentration and these dramatically increase the sample viscosities, but these large structures do not significantly alter the mobility of the ions, being quantified via the diffusion coefficients. This difference between what is happening microscopically and macroscopically is driving the decrease in *f* with increase in concentration.

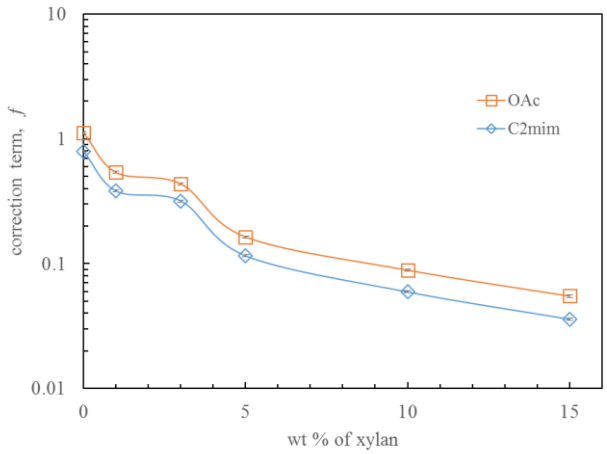

Figure 4.5: The correction term f as a function of weight fraction of xylan. The solid lines are provided as a visual guide. Error bars are within the symbols sizes.

4.3.3 NMR Relaxometer

4.3.3.1 High-Field Relaxation Time T_1 and T_2

High field (9.5T / 400 MHz) proton spin-lattice relaxation T_1 is measured for 1% and 10 % of xylan in IL [C2mim] [OAc], across temperatures (20 °C to 70 °C). At temperatures less than 40 °C at 400 MHz the system is in the solid regime, above this temperature, it is in the liquid regime. This is indicated by the observed minimum in T_1, which is classically taken as the divide between liquid and a solid regime in NMR measurements.

Figure 4.6 (a, b) shows the high field relaxation time T_1 for 1% and 10% of xylan. All the proton resonances of 1% xylan solution shown in Figure 4.6a, apart from peak 7, have a clear minimum. This minimum indicates a transition from solid to liquid-like behaviour. Resonance at peak 7 shows liquid behaviour, in that it monotonically increases with increasing temperature. This reveals that the end of the tail attached to the cation in the system. The mobility of protons corresponding to peaks 2 and 5 is less than the other protons, as their minima occur at the highest temperature, so they are in the solid regime right up to the highest temperatures measured in this study. In the temperature range 20 ℃ to 70 ℃, the proton resonances for peak 1, 3 and 6 show a minimum around 40 ℃.

Figure 4.6b shows the temperature dependence of the high field T_1 data for 10 % xylan. All the T_1 values have been decreased by the addition of xylan, showing that mobility of all the protons has been reduced. Notably, peak 2, the most acidic proton has had the greatest reduction in its T_1 values with the added increase in xylan.

This is surprising in that it is normally argued that the anion interacts with the polysaccharide most strongly and it should, therefore, be this peak that is affected the most. Peak 7 displays the proton resonances having the highest mobility which gives the highest T_1 as compared with the other protons. This means peak 7 goes from a liquid to solid response.

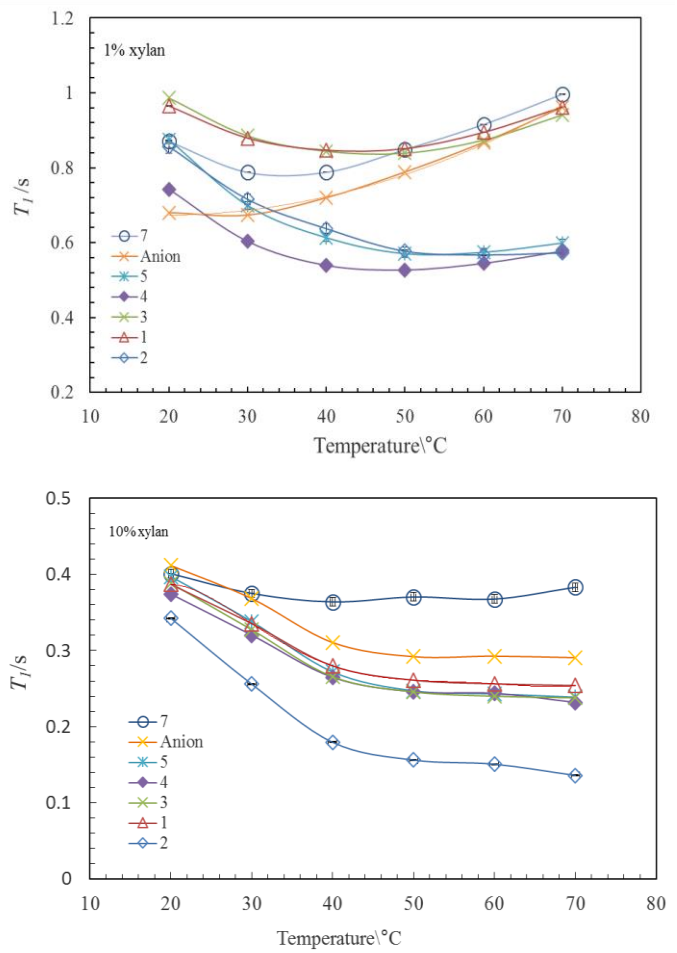

Figure 4.6: High field relaxation time T_1 for (a) 1% and (b) 10% of xylan at various temperatures.The solid lines to guide the eyes and error bars are within the data points.

The high field relaxation time T_2 for all xylan solutions were measured. This work presents 1% and 10% as an example. The values of relaxation time T_2 rise with temperature increase. Figure 4.7a shows the 1% xylan solution, the Peak 7 is the most significant increase as temperature increases. Anion (peak 6) and cation (Peak 7) behaviours considerably close. Peak 2 the most acidic proton has the lowest value. The values of imidazolium cation ring (Peaks 1 and 3) are the same with an increase in temperature.

Figure 4.7b shows the diffusing of ions for 10% of xylan in relaxation system. Peak 2 diffusing slower than other cations ring and anion behaved similarly to rest of cations (Peaks 4, 5 and 7).

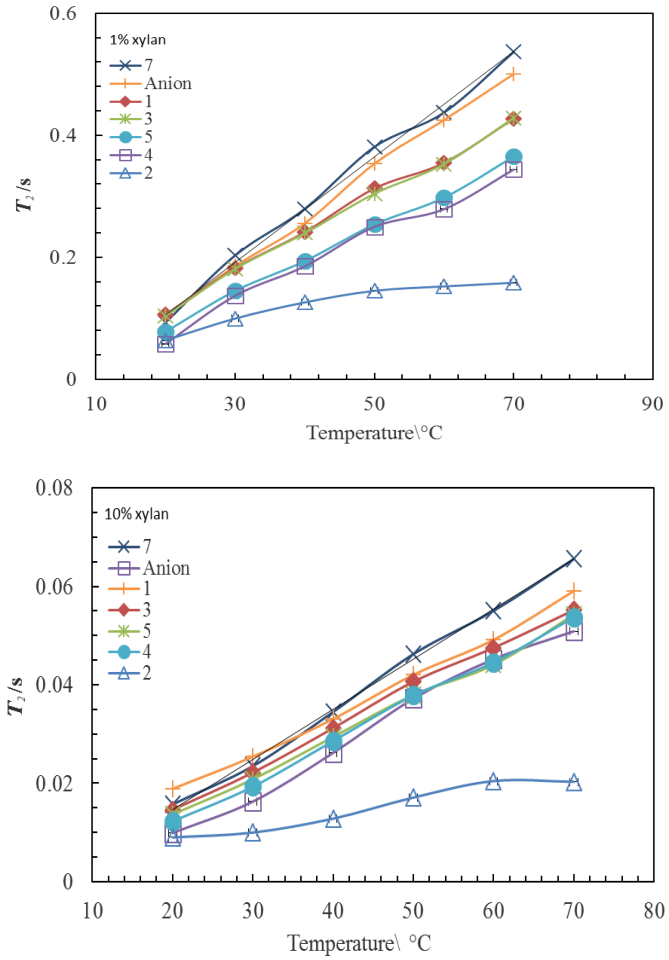

Figure 4.7: High field relaxation time T_2 (a) for 1% and (b) for 10% of xylan at various temperatures. The solid lines to guide the eyes. Error bars are within the symbols sizes.

4.3.3.2 Low-Field Relaxation Times T_1 and T_2

Figure 4.8(a, b) show the low-field relaxation time T_1 and T_2 plotted as a function of temperature for 15% of cellulose and xylan concentrations. Here the relaxation T_1 and T_2 times are in the liquid regime, as at 20 MHz the system is like a liquid, but at 400 MHz it's solid. They all increase in value with an increase in temperature. At low fields (20MHz) it is not possible to chemically distinguish between the cation and anion; instead, an average over all the protons is recorded.

Figure 4.8 (a, b) displays the relaxation time measurements reveal that T_2 is slightly less than or approximately equal to T_1 at 20 MHz. This suggests that rotational motion is the dominant mechanism for NMR relaxation [79]. It can see in Figure 4.8a that an increase in temperature causes an increase in T_1 and conversely an increase in xylan decreases T_1. The relaxation time T_1 is related to the mobility of the protons, with an increase here indicating an increase in mobility or, in other words, a decrease in the local micro-viscosity. The values of T_1 for 15% of the cellulose are positioned between the 5% and 10% of xylan. Therefore, the mobility of the protons at 15% of the cellulose is higher compared to 15% of xylan.

Figure 4.8b shows T_2 decreases with increasing xylan concentration in the inverses of the temperature range (K^{-1}). The T_1 at 0% xylan which is 100% Pure IL [C2mim] [OAc] linearly increases with increasing temperature. In contrast, adding the xylan to the solutions decreases the mobility of the protons and hence decreases T_2. The reason is that the viscosity has increased and this has the effect on the T_2 through the subsequent rotational mobility of the protons. Relaxation time T_2 of 15% of the cellulose is between the values of 5% and 10% of xylan solutions, as with T_1.

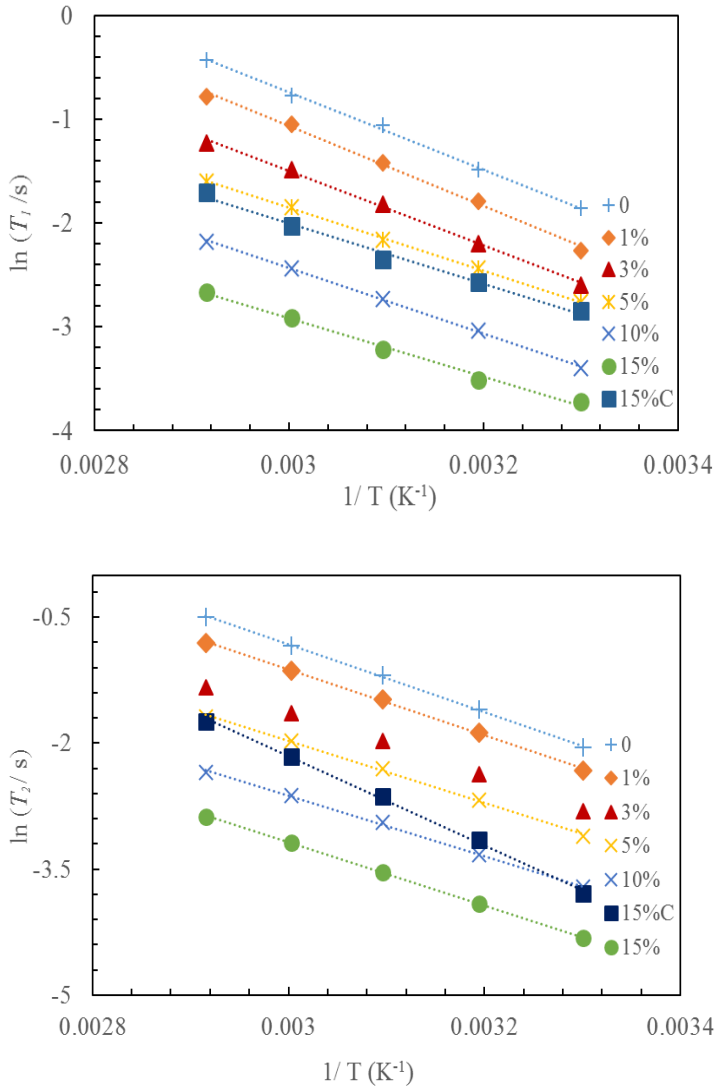

Figure 4.8: Arrhenius plots for relaxation times T_1 (a) and T_2 (b) against the inverse of temperature, for 15% cellulose and all xylan weight fractions. Solid lines represented fits based on Equation (3.2), and error bars within the symbols sizes.

The data of T_1 and T_2 relaxations for xylan and cellulose concentrations (1%, 3%, 5% 10% and 15%) from Figure 4.8 (a, b), were used to determine activation energy, employing Equation 3.2. Table 4.2 displays the values of activation energies of T_1 and T_2 relaxations for xylan and cellulose concentrations. It can be concluded that the values of activation energies of T_1 for xylan and cellulose are quite similar. In contrast, there are

significant differences between the values of activation energies of relaxation time T_2 for both carbohydrates. This could be indicative of chemical exchange in NMR relaxation systems. This result compared to the activation energy of relaxation time for carbohydrate monosaccharides in the previous chapter, it found that there is the slight difference between the values of activation energies of relaxation time T_2 for xylose and cellobiose.

Wt%	$E_{T1,T2}$ Xylan/kJmol^{-1}		$E_{T1,T2}$ Cellulose/ kJmol^{-1}	
	T_1	T_2	T_1	T_2
0	31 ± 1	33 ± 1	31 ± 1	33 ± 1
1	32 ± 1	33 ± 1	30 ± 1	34 ± 1
3	30 ± 1	32 ± 1	31 ± 1	35 ± 1
5	32 ± 1	31 ± 1	27 ± 1	35 ± 1
10	26 ± 1	30 ± 1	30 ± 1	38 ± 1
15	23 ± 1	31 ± 1	24 ± 1	44 ± 1

Table 4.2: Activation energies of T_1 and T_2 relaxations for xylan and cellulose/IL [C2mim] [OAc].

4.3.4 Viscosity−Temperature Analysis

The measurements of viscosity of different xylan concentrations (1%, 3%, 5%, 10% and 15%) were measured across the range of temperatures 20 °C to 60 °C inclusive. The Cross–Viscosity Equation 2.19, has been used on a hypothetical basis that there is a change in the formation and structure of fluids at different shear rates [91]. Figure 4.9a shows a steady state flow curves of xylan / [C2mim] [OAc] solutions for various concentrations at 40 °C. The data from 0.1 to 100 s had low signal to noise ratio and thus were ignored. Equation 2.19 was used to model the data in to determine the values of zero-shear–rate viscosity of xylan solution. Figure 4.9b shows the viscosity values as a function of xylan concentration (the logarithm scale used to make the figure clearer).

The viscosity dependence increases with adding this polymer through an increase in temperature, however, the largest values of xylan viscosity at 20℃. Figure 4.9c presents the experimental data for each concentration is plotted as ($\ln \eta_0$) against inverse temperature (K). The activation energies were extracted from the slope of the linear fits to this data using Equation 3.3.

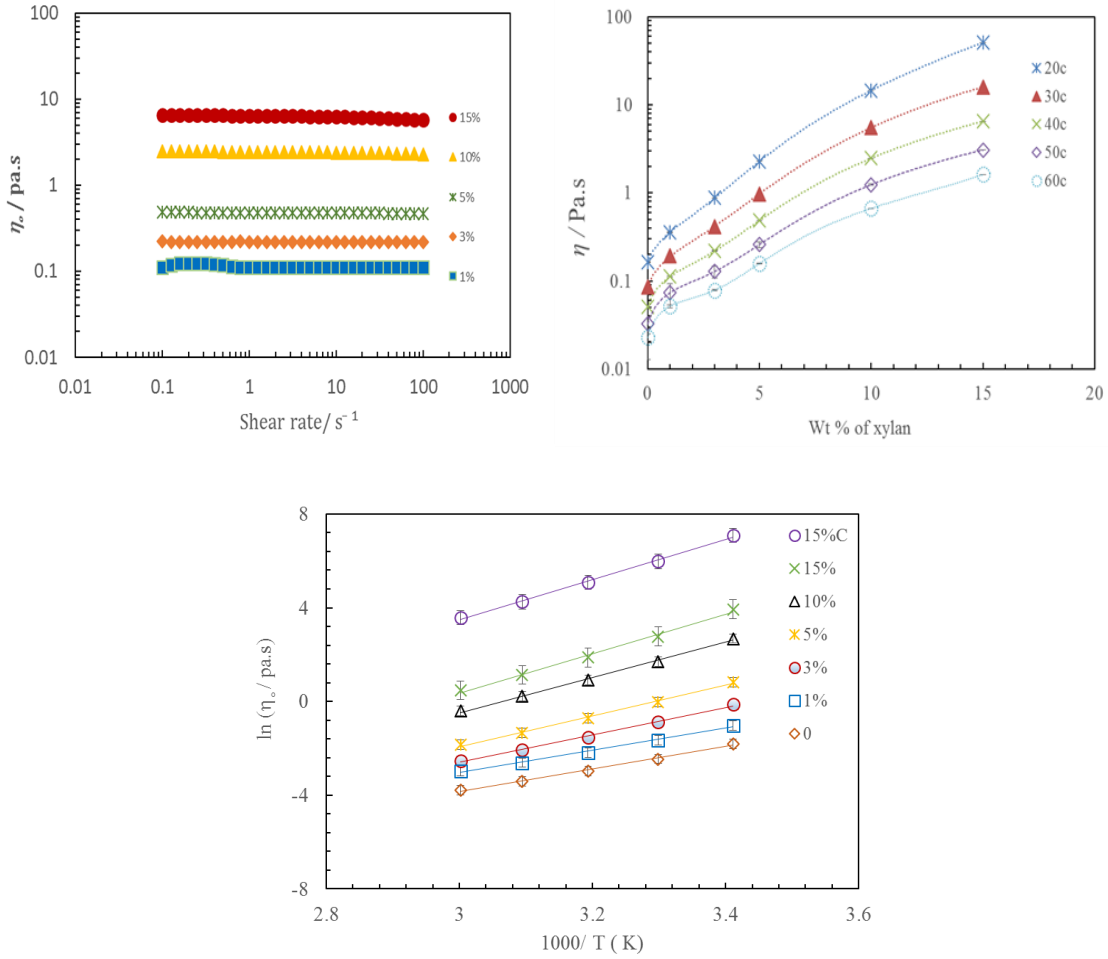

Figure 4.9:a) Viscosity-shear rate dependences of all xylan/[C2mim] [OAc] solutions recorded at 40 °C. The size of error bars is approximately within the data points. b) The natural logarithm of viscosity values as a function of xylan concentration. c) Logarithmic plots of the viscosity of pure [C2mim] [OAc] and 15% cellulose and xylan in IL [C2mim] [OAc] solutions versus inverse temperature. Lines are linear approximations. Error bars are within the symbol sizes.

The activation energy, $E_{A,\eta}$ of viscosity is related to the energy required for molecules to move past each other, enabling flow [105]. The activation energies of viscosity increase with increasing carbohydrates. Table 4.3 presents there is an insignificant difference between the activation energies values of viscosity for xylan and cellulose solutions. The values of activation energies of viscosity, $E_{A,\eta}$ increased slightly sharper then that observed for diffusion. The values of activation energies in viscosity system significantly increased from 50 kJ/mol to 71 kJ/mol for concentrations 3% to 15%, as compared to diffusion system from 40 kJ/mol to 51 kJ/mol in cellulose and xylan solutions from Table 4.1. It can be concluded that the values of activation energies of ions indicated an insignificant difference between xylan and cellulose systems, even with increase weight fractions, for diffusion, relaxation times and viscosity measurements.

Wt (%)	$E_{A,\eta}$ xylan /kJ mol^{-1}	$E_{A,\eta}$ cellulose /kJ mol^{-1}
0	40 ± 2	40 ± 2
3	39 ± 2	44 ± 2
3	49 ± 1	50 ± 2
5	54 ± 2	53 ± 2
10	62 ± 2	63 ± 2
15	70 ± 3	71 ± 2

Table 4.3: The comparison of the activation energy of viscosity of cellulose and xylan weight fractions into solutions.

4.3.5 Stokes−Debye−Einstein Analysis

Experimentally, relaxation times were measured across the temperature (70 °C - 30 °C). Low field (20 MHz) relaxation times T_1 and T_2 have an insufficient chemical resolution to distinguish between ions; therefore, the values of the hydrodynamic radii, $R_{H,i}$ calculated is an averaged value over both ions. Stokes- Einstein-Debye Equation was applied to consider the rotational correlation time of diffusing ions and from that calculate the values for the radius $R_{H,i}$ of ions in the viscous medium. Figure 4.10 (a, b), presents that the relationships between relaxation times and the ratio of temperature to viscosity (T/η).

Figure 4.10a presents relaxation time T_1 between 0.01 to 1s for all xylan weight fraction combined from different temperatures into a single master plot, while 15% of the cellulose is not connected with them. This is because cellulose is the most effective at increasing the viscosity, due to its higher molecular weight as compared with the xylan. Figure 4.10b shows that same relationship holds approximately as well for relaxation time T_2. The slope is used to calculate the value of the effective hydrodynamic radii for T_1 and T_2 using Equation 2.15. The values of hydrodynamic radii for all the xylan concentrations and all the temperatures T_1 is roughly equal to or slightly higher than T_2 experimentally.

The Stokes-Debye-Einstein equations worked remarkably well. It is only on the addition of a polymer (xylan/cellulose) above the critical overlap concentration that they begin to fail. The result will display the hydrodynamic radii, $R_{H,i}$ values of relaxation time T_1 against xylan weight fractions in Figure 4.11.

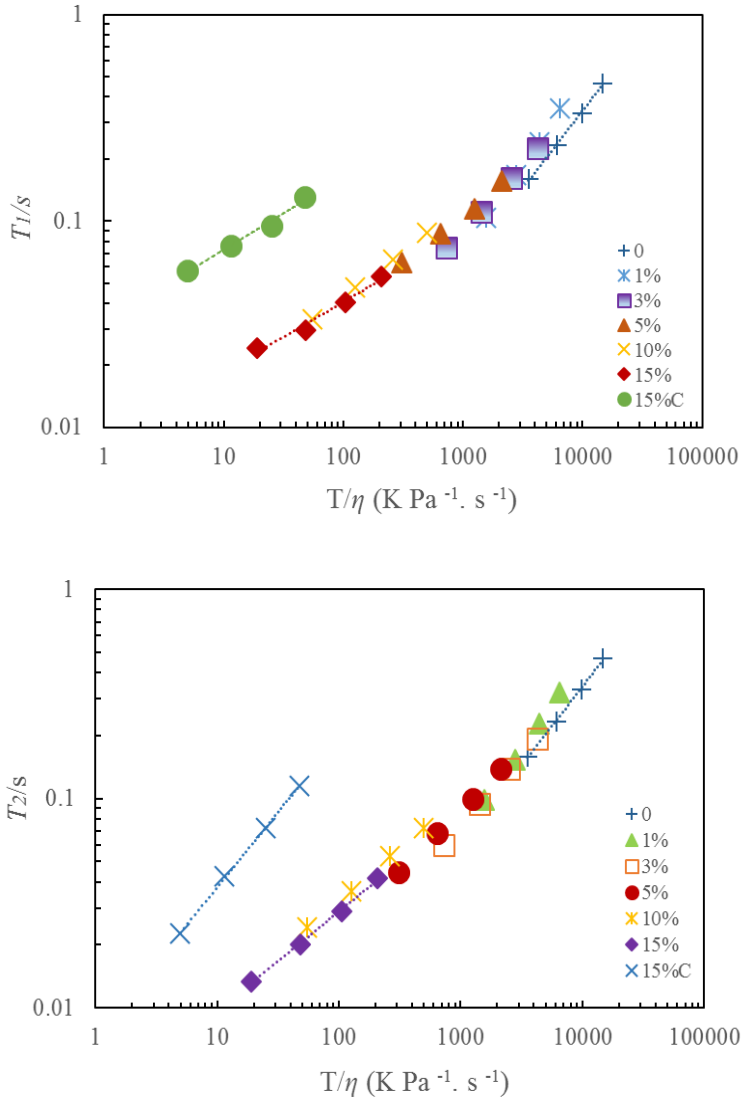

Figure 4.10: (a) The relaxation time T_1dependence on the ratio of temperature to viscosity for each xylan, (b) for T_2. The error bars are within symbols sizes. The dotted lines are provided as visual guide. [C] means cellulose data.

Figure 4.11 shows the hydrodynamic radius of the averaged ions of pure IL [C2mim] [OAc] 2.5 Å and the hydrodynamic radii, $R_{H,i}$ values of relaxation time T_1 against xylan weight fractions (1%, 3% and 5%) is around 3Å, the values of hydrodynamic radii of ions in high concentrations 10% and 15% around 2Å. The values of $R_{H,i}$ decreased with increasing of xylan concentrations, this due to the entanglement in solution [106]. The polymers (xylan/cellulose) structures do not significantly affect the mobility of the ions, which is here measured via the NMR diffusion and relaxation times, but due to entanglements that form they can support stress that dramatically increases the zero shear rate viscosity.

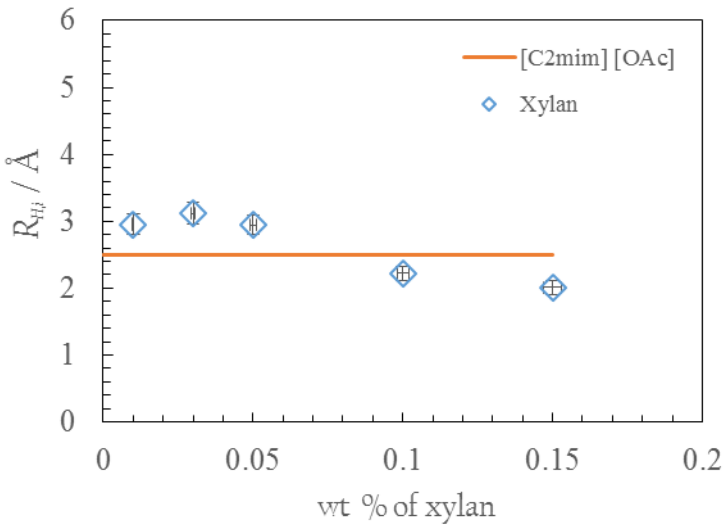

Figure 4.11: The values of effective hydrodynamic radii size against the xylan weight fractions and the hydrodynamic radius of the averaged ions of pure IL [C2mim] [OAc]. The error bars are within symbols sizes

4.3.6 Intrinsic–Viscosity Analysis

The intrinsic viscosity was obtained through several steps. Firstly, we used the zero viscosity of xylan solutions from the Newtonian viscosity values presented in Figure 4.9a. Secondly, the relative viscosity, η_{rel} of xylan calculated using Equation 2. 20, where the viscosity of each xylan concentration divided by the viscosity of pure IL [C2mim] [OAc] at the corresponding temperature. Figure 4.12a then the shows concentration dependence

of the relative viscosity for the xylan solutions. The relative viscosity increases with increase in xylan. The highest values of η_{rel} were at 20 ℃, while this gradually decreases with increase in temperature. After that, the specific viscosity determined by applying Equation 2.21 to the relative viscosity data. Finally, the intrinsic viscosity is calculated by using Equation 2.23 (the squared part with constant *B* was ignored in the equation because it is relatively small), and then Equation 2.24 was used to create a master curve. The Wolf approach involves plotting the natural logarithm of relative viscosity, η_{rel} versus the weight fraction of xylan. The weight fraction of xylan multiplied by the density of the IL [C2mim] [OAc] equal to 1.1 g/cm^3. This means the numerical values of concentrations have used to calculate the intrinsic viscosity are between 0.0121 g/cm3 and 0.182 g/cm3, which from low to high concentration. Figure 4.12b shows the intrinsic viscosity plotted as a function of temperature, alongside data for cellulose as a comparison. The values of cellulose intrinsic viscosity [η] are greater than the corresponding xylan values.

The intrinsic viscosity [η] values reduce with increasing temperature for both carbohydrates showing that the quality of the solvent reduces with an increase in temperature. The cellulose data was taken from ref [41]. The values of intrinsic viscosity [η] of xylan solutions are low compared to cellulose, approximately 1/3 the size.

The values of intrinsic viscosity [η] of xylan were around 38 ml/g at 20 °C and slightly decreases with increasing temperature to reach 23 ml/g at 60 °C. It is possible to suggest that the main reason for this is that the size of xylan molecules are smaller than those of the molecules of cellulose.

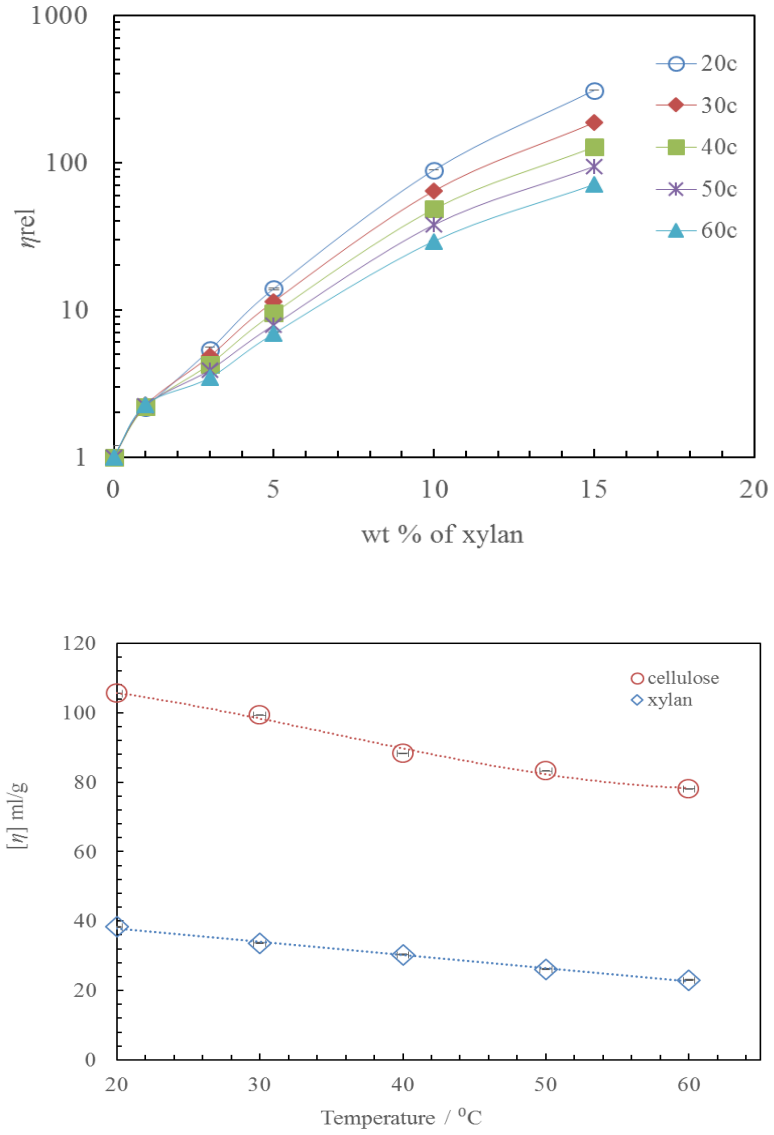

Figure 4.12: a) Relative viscosity as a function of xylan weight fraction between 20°C to 60 °C. b) Intrinsic viscosity [η] as a function of temperature / °C for cellulose and xylan solutions(cellulose data are taken from ref [105]). Error bars within the symbols sizes and the dotted lines are to guide the eye.

Figure 4.13 shows the relative viscosity plotted as a function of xylan concentrations −intrinsic viscosity c[η] for temperature from 20 °C − 60 °C. All data on xylan solutions are combined from different temperatures into a single master curve. The values of intrinsic viscosity can be used to determine the overlap concentration of the polymer.

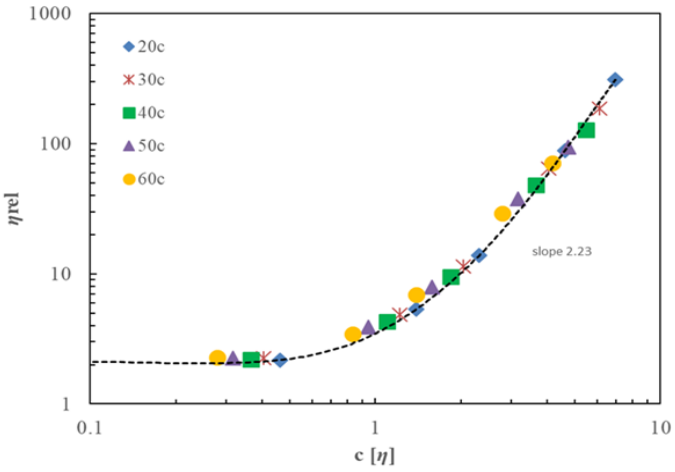

Figure 4.13: Master plot of relative viscosity against c[η] for xylan/ [C2mim OAc] solutions for temperature from 20 °C−60 °C and xylan concentrations (1%, 3%, 5%, 10% and 15%. Error bars are within the symbols sizes and dotted lines are to guide the eye.

The overlap concentration c^* is the crossover point between dilute and semi-dilute systems. The c^* is independent of the concentration of polymer [104] and it can be determined by:

$$C^* = 1/[\eta] \tag{4.1}$$

where [η] is the intrinsic viscosity of a viscous medium [104, 106, 107]. The overlap concentration of xylan system calculated and compared to cellulose is shown in Table 4.4. The resultant is $c^*_{20} = 0.03$ and $c^*_{60} = 0.04$ of xylan weight fraction, whereas for cellulose is $c^* = 0.01$ at low and high temperatures. The intrinsic viscosity decreases and the overlap concentration increase with an increase in temperature. The overlap concentration of xylan is higher than cellulose.

This is expected due to the molecular weight differences between the two carbohydrate polymers.

T / ℃	Overlap concentration c^*	
	Cellulose	Xylan
20	0.01 ± 0.001	0.03 ± 0.002
30	0.01 ± 0.001	0.03 ± 0.002
40	0.01 ± 0.001	0.03 ± 0.002
50	0.01 ± 0.001	0.04 ±0. 002
60	0.01± 0.001	0.04 ± 0.002

Table 4.4: The overlap concentration of xylan and cellulose systems at selected temperatures.

4.4 Conclusion

NMR spectroscopy is employed for chemical characterisation and was used to measure diffusion properties as well as molecular relaxation dynamics at various temperature. The values of diffusion coefficients of ions reduced with increasing in xylan weight fractions and increasing in temperature. The ratio of the diffusion coefficient of anions to cations is less than 1. This is known as ‘‘anomalous’’ diffusion because the anion is geometrically smaller than the cation and so would be expected to diffuse faster not slower than the cation.

The changes in ^{1}H chemical resonance frequencies $\Delta\delta$ for the proton in adding of xylan is almost identical to the chemical shift movements of cellulose, suggesting that the dissolution method in both instances is similar. High field relaxation time T_1 and T_2 were measured for 1% and 10 % of xylan in IL [C2mim OAc], across temperatures (20 °C to 70 °C). The T_1 at temperatures less than 40 °C at 400 MHz the system is in the solid regime, above this temperature, it is in the liquid regime. The values of relaxation time T_2 rise with temperature increases. Relaxation times (20 MHz) relaxation T_1 and T_2 were measured across the temperature (70 °C-30 °C).

This work found that for all xylan concentrations and all the temperatures T_1 is approximately equal to or slightly greater than T_2 experimentally. Stokes-Einstein equation used to determine the correction term, f and it decreased with increasing xylan concentration by weights. Stoke- Debye-Einstein Equation was applied on the experimental data, to determine the values of effective hydrodynamic of radii for the all xylan concentrations. The values of $R_{H,i}$ decreased with increasing of xylan weight fraction.

The Cross- viscosity equation was used to obtain the zero shear viscosity. The Arrhenius equation was used in both microscopic and macroscopic systems to determine the activation energy for ions. The intrinsic viscosity of homogeneous solutions for xylan and cellulose in the solvent [C2mim] [OAc] were calculated. The micro-viscosity of cellulose is higher than xylan; this indicated to the size of molecules of cellulose. The overlap concentration determined by using Equation 4.1, was applied to both of carbohydrates using their intrinsic viscosity values. The overlap concentration of xylan is higher than cellulose where c^* found of xylan is approximately between 3% and 4%, while for cellulose is 1%, across arrange of temperatures (20 ℃ to 60℃). This is expected due to the molecular weight differences between the two polymers.

Chapter 5

Hydroxyl Group of Five Carbohydrates (Glucose, Cellobiose, Xylose, Cellulose and Xylan)

5.1 Introduction

This chapter presents the influence of carbohydrate weight fractions of glucose, cellobiose, xylose, cellulose and xylan on the properties of ions of [C2mim] [OAc] from 20 ℃ to 60 ℃. The data of glucose, cellobiose and cellulose solutions were taken from ref [41]. The data of xylan and xylose were measured and compared to this previous data. BPP theory was applied on the relaxation time T_1 to calculate the correlation time τ, it was discussed in section 2.2.2. Stokes–Debye − Einstein Equation 2.13 was used to determine the correction terms, f also known as the micro-viscosity pre-factor of anions and cations in carbohydrates solutions. The reduction in diffusivity of ions was determined by the associated fraction α of ‘‘glucose unit’’ per molecule of IL [C2mim OAc], where (‘‘glucose unit’’ involves $D-$ glucose, $D-$ glucopyranose, $D-$anhydroglucopyranose, $\beta-D-$xylose) [41]. The activation energy of diffusion coefficients and relaxation time T_1 was calculated and plotted against the associated fraction α of ‘‘glucose unit’’ per molecule of IL [C2mim] [OAc].

5.2 Analysis and Discussion

5.2.1 NMR Diffusion

The diffusion coefficients of anion [OAc] and cation [C2mim] as a function of carbohydrates concentrations, which are glucose, cellobiose, xylose, cellulose and xylan at 40 ℃, is shown in Figure 5.1. The values of diffusion coefficients of anions decrease with the increase of carbohydrate concentration in solutions. The most significant decrease was with the addition of glucose, and xylan was the least effective. It can be observed that the rate of reduction in diffusion coefficients of ions is influenced by carbohydrates differently. Xylan and cellulose have 2 and 3 OH groups per ring, respectively, these polymers are less effective on the diffusivity of ions, except when the cellulose is at a high concentration if compared to other carbohydrates. These carbohydrates such as cellobiose and xylose have each one of them 4 of OH group per ring work similarly together. Glucose with five OH group per ring has the most significant effect on the diffusion coefficients of the ions of IL [C2mim] [OAc].

In Figure 5.1 (a, b), the diffusion coefficients of cations appear similar to that of the anions for these carbohydrates. The data shows there is an insignificant difference between the diffusion coefficients of anion to cations. The results are found similar for all measured temperatures.

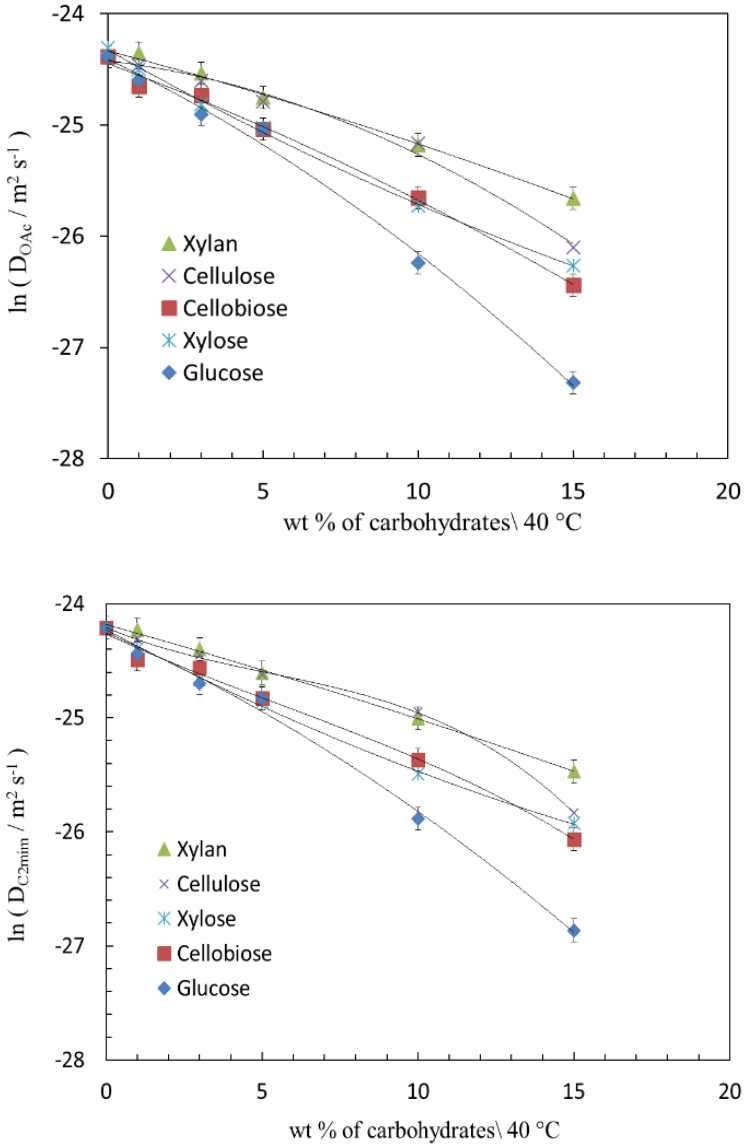

Figure 5.1: The diffusion coefficients of (a) anion [OAc] and (b) cation [C2mim] as a function of carbohydrates weight fractions, which are glucose, cellobiose, xylose, cellulose and xylan at 40 ℃. Solid lines are provided as a visual guide and error bars are shown.

5.2.2 The Investigation of the Influence of Hydroxyl Group of Carbohydrates on the Diffusivity of Ions of the Ionic Liquid 1-Ethyl-3-Methylimidazolium Acetate [C2mim] [OAc]

It is possible to determine the decrease in diffusion coefficients of ions compared to their original states in an ionic liquid by the number of Hydroxyl group, OH, per mass of carbohydrate. The number of the hydroxyl group can be determined from the carboxylate structure, where glucose ($C_6H_{12}O_6$) is classified as simplest carbohydrates, consisting of five OH groups. Cellobiose ($C_{12}H_{22}O_{11}$) is classified as a disaccharide and consists of two $D-$glucopyranose units connected by a β (1→4) bond, and each $D-$glucopyranose has four OH groups. Cellulose ($C_6H_{10}O_5$) is polymer and consists of $D-$anhydroglucopyranose units correlated with β (1→4) glyosidic bond, where each $D-$anhydroglucopyranose unit has three OH groups [32, 41]. $D-$Xylose ($C_5H_{10}O_5$) is a monosaccharide with four OH groups. As for xylan ($C_6H_8O_4$) , it is a polysaccharide consisting of $\beta-D-$xylose units correlated with β (1→4) glyosidic bond and possesses two OH groups per ring [24, 43]. This will discuss it in the next section.

Studies have shown that it is possible to understand the interaction between ions of ionic liquid and carbohydrate molecules based on the associated fraction α of ‘‘glucose unit’ OH groups per molecule of IL [C2mim] [OAc]within the solution. Remsing et al. studied glucose and cellobiose dissolved in 1-butyl-3-methylimidazolium chloride [BMIM] [Cl] individually, using NMR measurements. It was found that there was a 1:1 ratio of chloride anions to the OH groups for glucose and cellobiose [108]. Ries et al. investigated the influence of hydroxyl group of carbohydrates, which are glucose, cellobiose and cellulose on the diffusing of cations and anions of [C2mim] [OAc] [41].

The associated fraction α of ‘‘glucose unit’’ per molecule of IL [C2mim] [OAc], where this ‘‘glucose unit’’(involves *D*-glucose, *D*-glucopyranose, *D*-anhydroglucopyranose, $\beta-D-$xylose) was used instead of weight fraction carbohydrates. In this work, the effect of OH group of xylose and xylan on the ions of [C2mim] [OAc] were examined and compared to previous data of glucose, cellobiose and cellulose solutions taken from ref [41] at 20 ℃ to 60 ℃.

An associated fraction, α can be calculated following by:

$$\alpha = N \times \frac{M_{IL}}{M_{GU}} \times \frac{\phi}{100 - \phi} \quad (5.1)$$

where N is the number of hydroxyl group per ring, M_{IL} and M_{GU} are the molar mass of IL [C2mim OAc] and carbohydrates ‘‘glucose units’’. ϕ is weight fraction of carbohydrates [41, 108].

Figure 5.2 (a, b) shows the natural logarithm of diffusion coefficients of cations (a) and anions (b) as a function of the associated fraction of ‘‘glucose units’’ per molecule of IL [C2mim] [OAc] at 40 ℃. The molar ratio α of cations and anions was determined using Equation 5.1. The M_{GU} of ‘‘glucose unit’’ are 180, 171, 162, 150 and 131 g/mol for glucose, cellobiose, cellulose, xylose and xylan, respectively. The N of OH groups for the same order of carbohydrates are 5, 4, 4, 3, and 2. The M_{IL} of pure IL [C2mim] [OAc] is 170 g/mol and ϕ is the carbohydrates weight fraction. Therefore; N of cellulose used as a fixed value of 3, to get the linear fit, the best overlap is calculated by a subsequent least–squares fit [41].

The aim of the linear fit is to measure the reducing in the diffusivity of ions with the increase in the number of OH groups to molecules of IL [C2mim] [OAc]. The results show the numerical values of the mobility of cation (D_{C2mim}) and anion (D_{OAc}) in carbohydrate systems are similar, with an uncertainty on all those values ± 0.2 m^2 s^{-1}. In these semi-log plots, each of the diffusion coefficients of cations and anions for all carbohydrates collapsed into a single master curve. Both of cellobiose and xylose are having an N of 4 OH groups per ring, where there be four anions around each molecule of them, and there was the same number of cations. It can be noted that there is a similar influence for each OH group of carbohydrates in decreasing the diffusion properties of ions. In Figure 5.2 (a, b) the slopes of the linear fit are -3.3 ± 0.2 and -2.7 ± 0.2 for anions and cations, respectively, with their uncertainties.

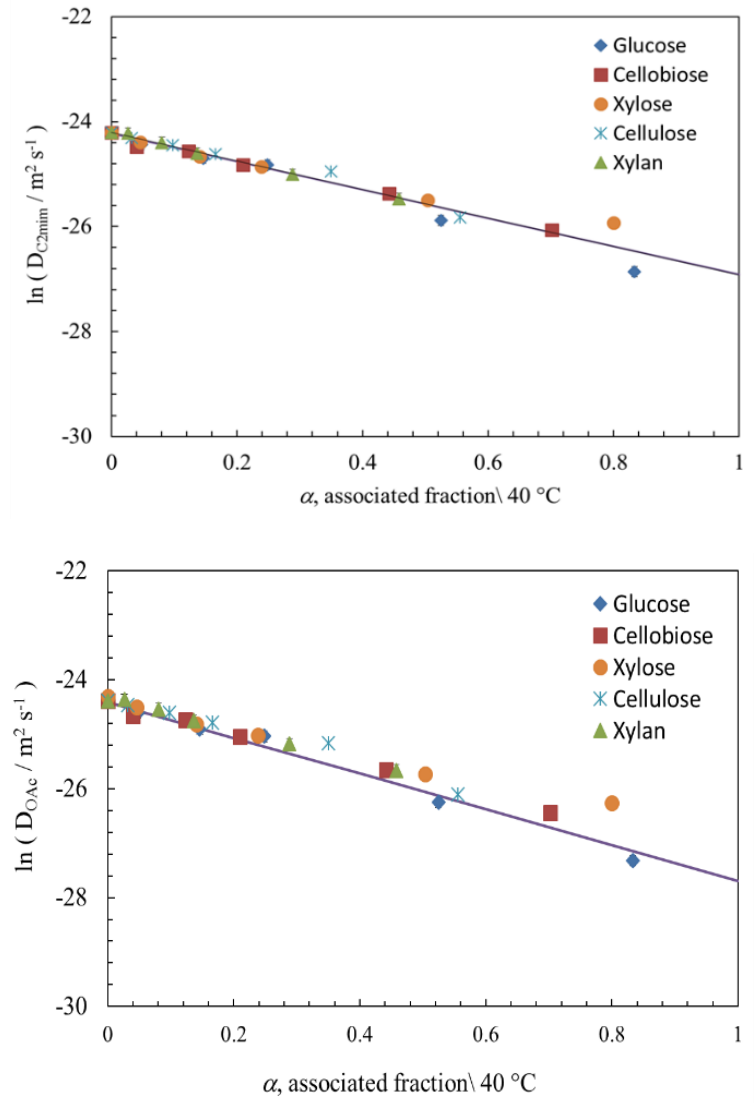

Figure 5.2: a) Diffusion coefficients of the cations $D_{(C2mim)}$ and b) anions $D_{(OAc)}$ at 40 ℃, as a function of α associated fraction, having an N are 5,4,4,3,2 for glucose, cellobiose, xylose, cellulose and xylan, respectively. Solid lines indicate to the linear fit to the data. Error bars are within the symbols sizes.

The interaction between the ions with molecules surrounded by a viscous medium can be understood by determining the activation energy of diffusional dynamics. An Arrhenius Equation 3.1 was used on experimental data of carbohydrate systems, where D_0 describes a basic property of each ion itself, and it is treated the same for all carbohydrates solutions as a global fitting parameter. The values of D_0 for cation is $1.4 * 10^{-3} \pm 0.2$ m^2 s^{-1} and for anion is $1.6 * 10^{-3} \pm 0.2$ m^2 s^{-1} [41]. The results in Figure 5.3 (a, b) shows the activation

energy of cations [C2mim] and anion [OAc] against the same associated fraction α used for glucose, cellobiose, xylose, cellulose and xylan with ratio of OH group 5:4:4:3:2 per molecule of IL [C2mim] [OAc]. In Figure 5.3 all the data collapsed into a single master plot where the activation energy of cations diffusion is very similar to anion diffusion with uncertainties given. The slopes of activation energies for cations and anion diffusions are 46.2±0.2 kJ/mol and 46.8±0.2 kJ/mol, respectively.

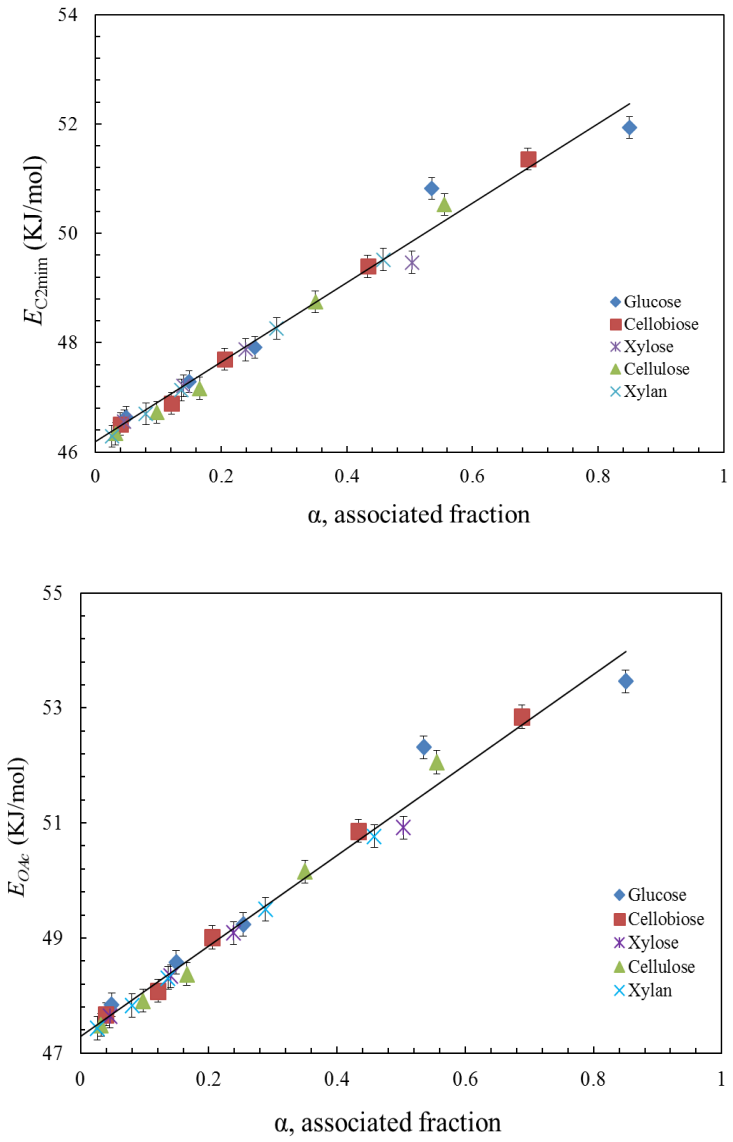

Figure 5.3: The activation energy of diffusion coefficients of cations [C2mim] (a) and anions [OAc] as a function of the associated fractions α for glucose, cellobiose, xylose, cellulose and xylan with ratio of OH group 5:4:4:3:2 per molecule of IL [C2mim] [OAc]. The solid lines indicated to a linear fit to the data. The error bars are shown.

5.2.2.1 The Chemical Shift of Proton Resonances

The changes of protons resonances positions $\Delta\delta$ in parts per million (ppm) are determined by using the δ resonance of each in pure IL [C2mim] [OAc] as a reference point. Figure 5.4 shows ^{1}H chemical shift of ions of peaks 2 and 6 for all carbohydrate solutions plotted as a function of α, associated fraction at 40 ℃. These carbohydrate solutions are for glucose, G, cellobiose, CB, xylose, X, cellulose, C and xylan, XY. Peak 2 is the most acidic proton from imidazolium ring cations. Peak 6 is an anion [OAc] and displays a positive value of Δδ. The imidazolium cations' positions indicate that the addition of these carbohydrates with their the ratio of OH group to the molecule of IL[C2mim] [OAc] 5:4:4:3:2, disrupt the associated ions in the pure IL [C2mim] [OAc]. The anions in all carbohydrate solutions followed the same trend with the increase in α associated fraction. All data of carbohydrate solutions fall onto a single master plot. The other resonances are not shown in order to enhance clarity in Figure 5.4.

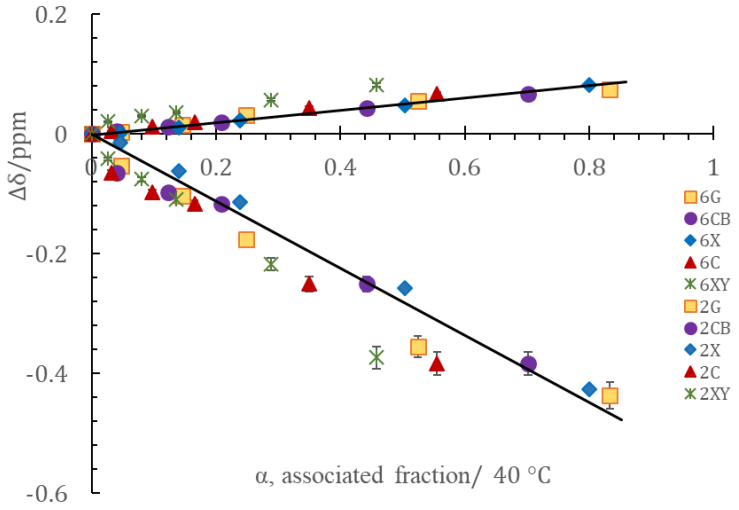

Figure 5.4: The chemical shift of protons resonances Δδ (ppm) for glucose, G cellobiose, CB, xylose, X, cellulose, C and xylan, XY versus α associated fraction at 40 °C. Error bars are shown and the lines guide the eyes

5.2.3 NMR Low−Field Relaxation Time T_1

The experimental data of Low field (20 MHz) relaxation times T_1 plotted against the associated fractions α of hydroxyl groups of carbohydrate systems. The associated fractions α was calculated using Equation 5.1 as discussed in section 5.2.2. Here, the associated fraction α of ‘‘glucose unit’ ’per molecule of IL [C2mim OAc] was used as a key to determine the influence of carbohydrates on averaged ions in the relaxation system.

Figure 5.5a shows the natural logarithm of relaxation time plotted as a function of carbohydrate weight fraction at 40 ℃. The values of relaxation time T_1 decrease with the increase in carbohydrates’ weight fractions as expected. Although there is an overall reduction in relaxation time, this proportion is not determined by the number of OH groups, unlike the diffusion. It was observed that xylan and cellulose have numbers of OH groups per ring, which are 2 and 3, respectively; however, xylan has the most significant effect on the relaxation time, while the lowest is cellulose. Carbohydrates such as cellobiose and xylose with 4 OH group per ring, work well. Glucose, although it has the largest number of OH group, has less effect on the value of relaxation time T_1 than xylan in [C2mim OAc].

Figure 5.5b presents the relaxation time T_1 against the α associated fraction of hydroxyl groups of carbohydrates, having an N as 5,4,4,3,2 of glucose, cellobiose, xylose, cellulose and xylan, respectively. In Figure 5.5b the data of carbohydrates, in the order of glucose, cellobiose, xylose, cellulose and xylan with the ratio of N 5:4:4:3:2, were lying on the linear fit, except the xylan data which worked separately. We speculate that it might be caused by the chemical exchange of ions in xylan solution.

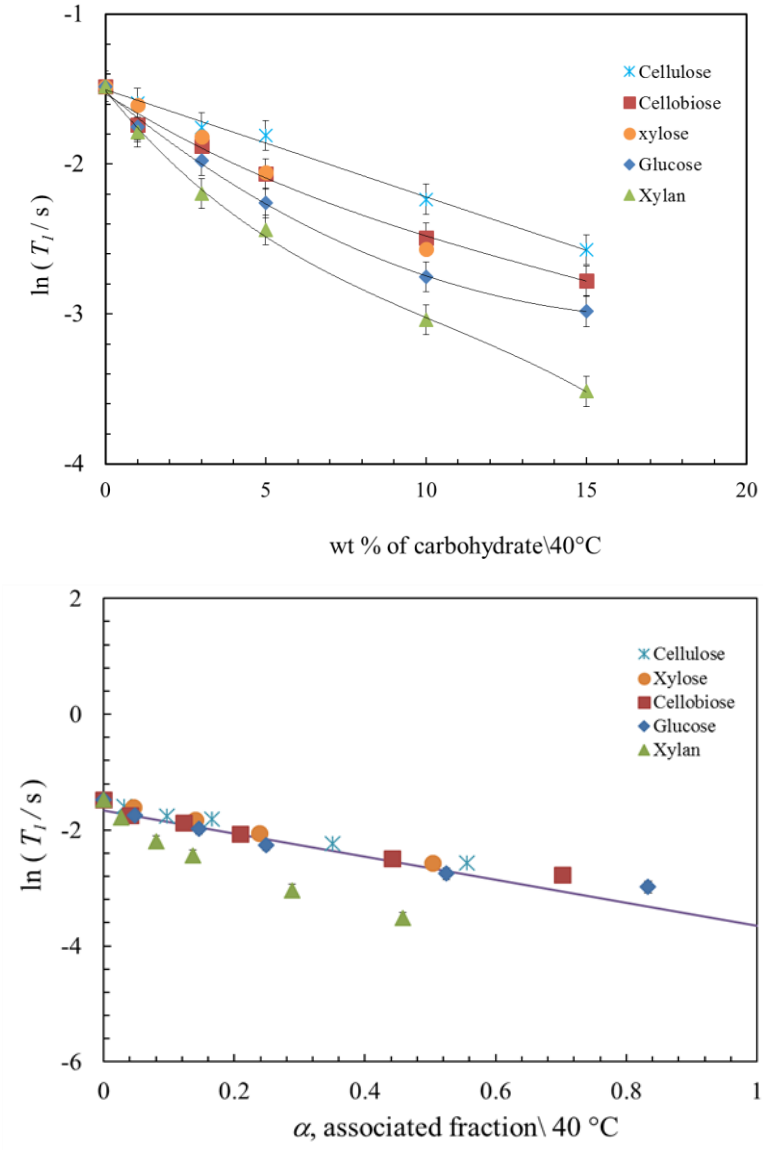

Figure 5.5: At 40 ℃, a) The natural logarithm Relaxation time T_1 as a function of all carbohydrate concentrations. b) The natural logarithm of relaxation time against the α associated fraction of hydroxyl groups of carbohydrates, having an N to be 5:4:4:3:2 of glucose, cellobiose, xylose, cellulose and xylan, respectively. The solid lines indicated to the linear fit and error bars are within the symbols sizes.

5.2.4 Stokes−Einstein Analysis

The influence of carbohydrates on the diffusivity of ions can be determined by the associated fraction, α of ‘‘glucose unit’ ’per molecule of IL [C2mim OAc] and also by the correction term f, as it discussed in section 2.2.1. Therefore; Stokes-Einstein Equation 2.8 was applied on experimental data. Figure 5.6 and Figure 5.7 show the correlation between diffusion coefficient of anions and cations against the ratio of temperature to viscosity for 3% and 10% of each glucose, cellobiose, xylose, cellulose and xylan. We used semi-log for clarity in these Figures. The diffusivity of anions increased with an increase in the ratio of temperature to viscosity, as expected. The most effective at increasing viscosity is cellulose and then xylan, while glucose, cellobiose and xylose have relatively low viscosities. In Figure 5.6a the diffusion coefficients of anions for 3% of each glucose, cellobiose and xylose are collapsed together into a master curve, while the values of diffusion coefficients of anions xylan and cellulose behave independently. In Figure 5.6b there is almost the same correlation contains for the cations.

It is interesting to note how ions behave at high concentrations of various carbohydrate systems. Figure 5.7 (a, b) shows the correlation between the diffusion coefficient of anions and cations to the ratio of temperature to the viscosity at 10% for cellobiose and xylose, which still fall into a master curve. The diffusivity of anions for cellulose and xylan increase with the increase in the ratio of temperature to viscosity. There is an insignificant difference between the values of diffusion coefficients of anion and cations at each weight fraction of carbohydrates.

The numerical values of diffusion coefficients were affected by the number of OH groups of each carbohydrate, but they do not influence the viscosity measurements. For example, glucose and cellobiose systems have a similar viscosity, but the difference in diffusion coefficient is due to their OH groups.

The hydrodynamic radius $R_{H,i}$ of ions was calculated by Hall et all using Equation 2.9. The values of the effective radius are for the anion 2.2 Å and the cation 2.8 Å [59]. These values of $R_{H,i}$ are used in Equation 2.8. The gradients from the relationship between the diffusion coefficient and the ratio of temperature to the viscosity, are obtained from all concentrations of carbohydrates solutions, as it will show the results late on.

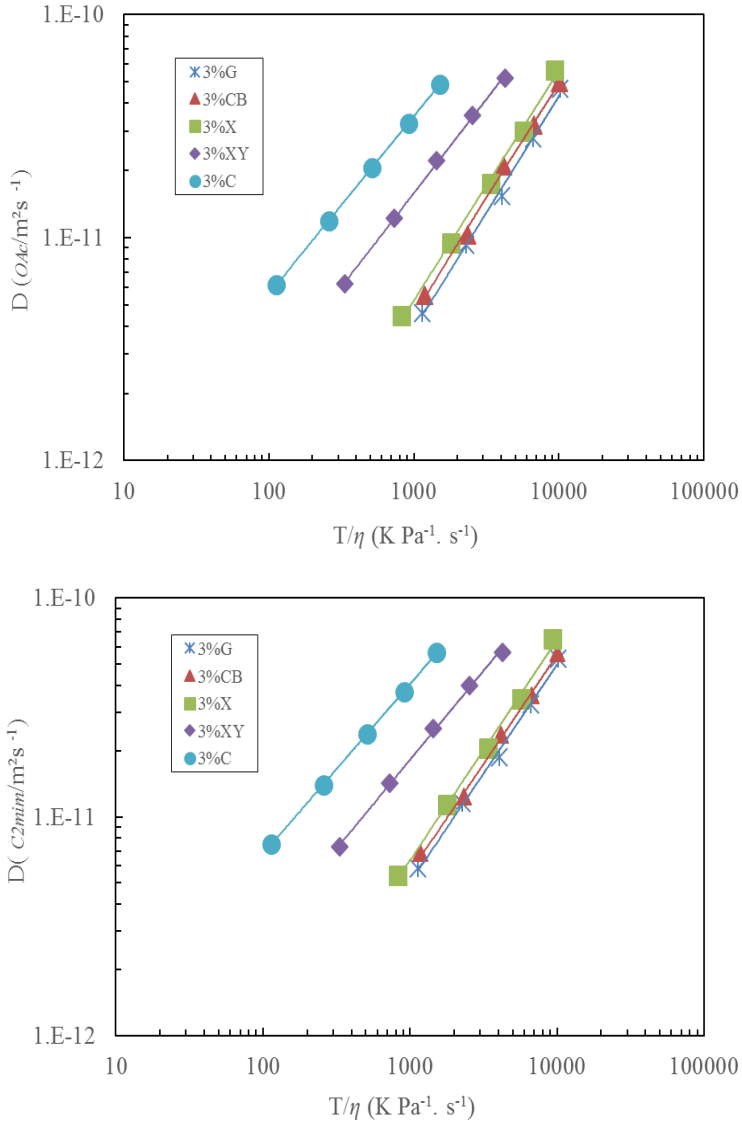

Figure 5.6: NMR diffusion coefficient of cations (a) and anions (b) against the ratio of temperature to the viscosity 3% of glucose, G cellobiose, CB, xylose, X, cellulose, C and xylan, XY. Solid lines are provided as a visual guide and error bars are within the symbols sizes.

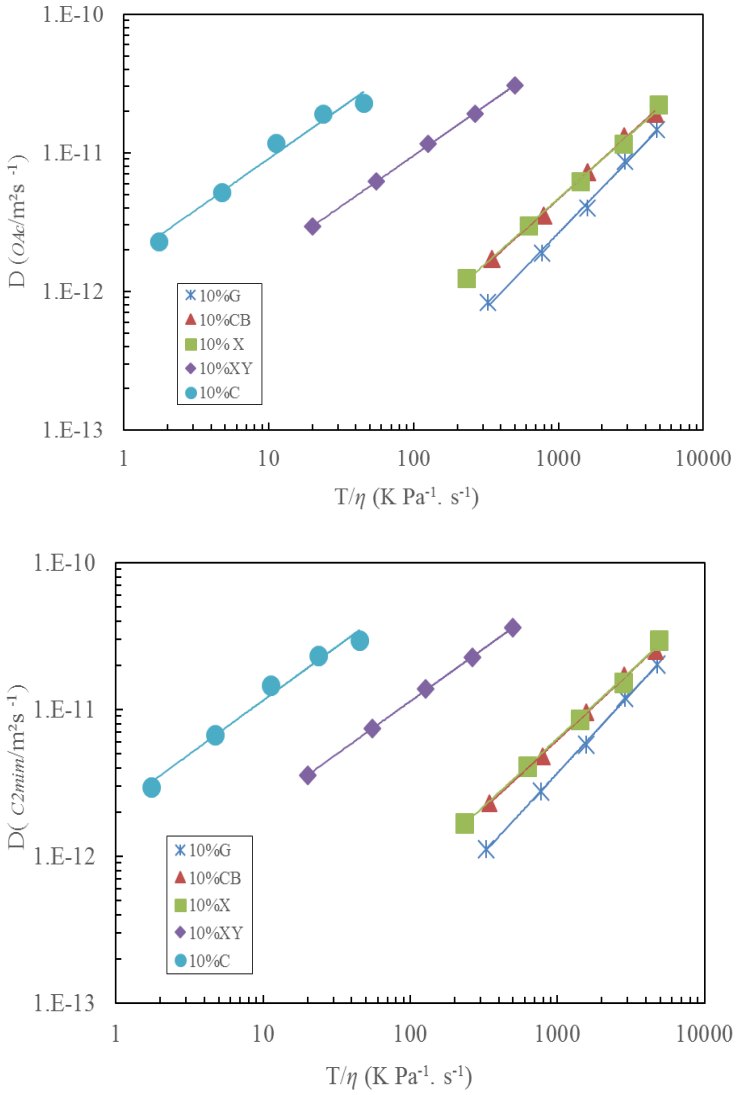

Figure 5.7: NMR diffusion coefficient of cations (a) and anions (b) against the ratio of temperature to the viscosity of 10 % of glucose, G cellobiose, CB, xylose, X, cellulose, C and xylan, XY. Solid lines are provided as a visual guide and error bars are within the symbols sizes.

The gradients from Figure 5.6 and Figure 5.7 shown as the example of the data used to calculate the correction terms f, of different carbohydrates. Figure 5.8 (a, b) shows the correction term f of cations and anions as a function of weight fractions of glucose, cellobiose, xylose, cellulose and xylan.

It is interesting to note that in glucose, cellobiose and xylose solutions, their anions have $f \approx 1$ so they diffuse as expected, but the cations are less than one, this is the known anomalous behavior- the cations diffuse faster than expected. In Figure 5.8 there is a large drop in f of anion and cation in cellulose and then xylan solutions. This due to the decoupling between the macroscopic and microscopic viscosities and cellulose has the larger molecular weight and so the larger deviations.

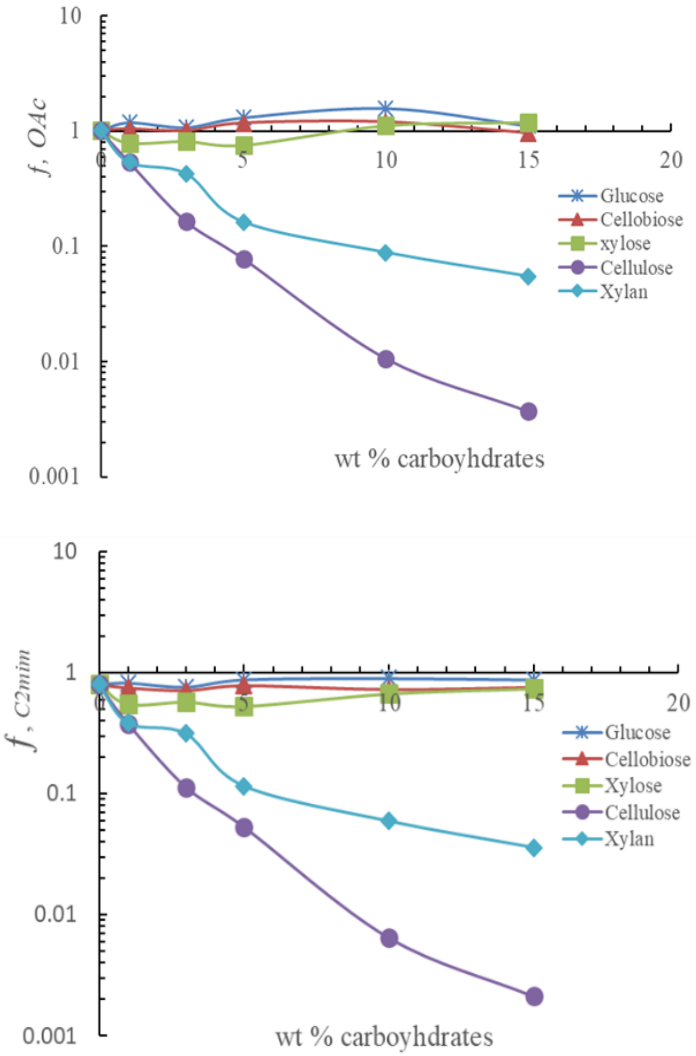

Figure 5.8: The correction term f of cations (a) and anions (b) as a function of weight fractions of glucose, cellobiose, xylose, cellulose and xylan. Solid lines are provided as visual guide. Error bars are within the symbols sizes.

5.2.5 Stokes−Debye−Einstein Analysis

It is possible to relate two parameters of microscopic NMR relaxation time (20 MHz) and macroscopic viscosity by using Stokes −Debye− Einstein Equation 2.15, as discussed in section 2.2.3. The technique of relaxation times T_1 and T_2 has an insufficient chemical resolution to differentiate between ions; therefore, the values of the hydrodynamic radii, $R_{H,i}$ calculated is the averaged value over both ions. Equation 2.15 was applied to experimental data of the relaxation time T_1 for carbohydrate systems in the following order: glucose, cellobiose, xylose, cellulose and xylan with concentrations (1%, 3%, 5%, 10% and 15%) across the temperature (70 °C - 30 °C) to determine the hydrodynamic radii.

Figure 5.9 (a, b) shows the rotational correlation time T_1 and the ratio of the temperature to the viscosity (T/η) for 3% and 10% of glucose, cellobiose, xylose, cellulose and xylan. We used logarithm scales for clarity. Figure 5.9a presents the relaxation time T_1 between 0.01 to 1s for glucose, cellobiose, xylose and xylan which increased with the increase in the ratio of (T/η). These carbohydrates were combined into a single master plot. The cellulose is most effective with the increase in viscosity. Figure 5.9b shows the same relationship holds for 10% of carbohydrate systems. It is interesting to note that 10% of the cellulose is most effective with the increase in viscosity. The relaxation time T_1 for 10% of glucose, cellobiose and xylose behave similarly with an increase in the viscosity. Similar results are found for all concentrations measured.

The gradients from the correlation between relaxation time T_1 and ratio of (T/η) are used to calculate the values of hydrodynamic radii, $R_{H,i}$ for all carbohydrate systems by employing Equation 2.15. The results of all carbohydrate systems can be seen in Figure 5.10.

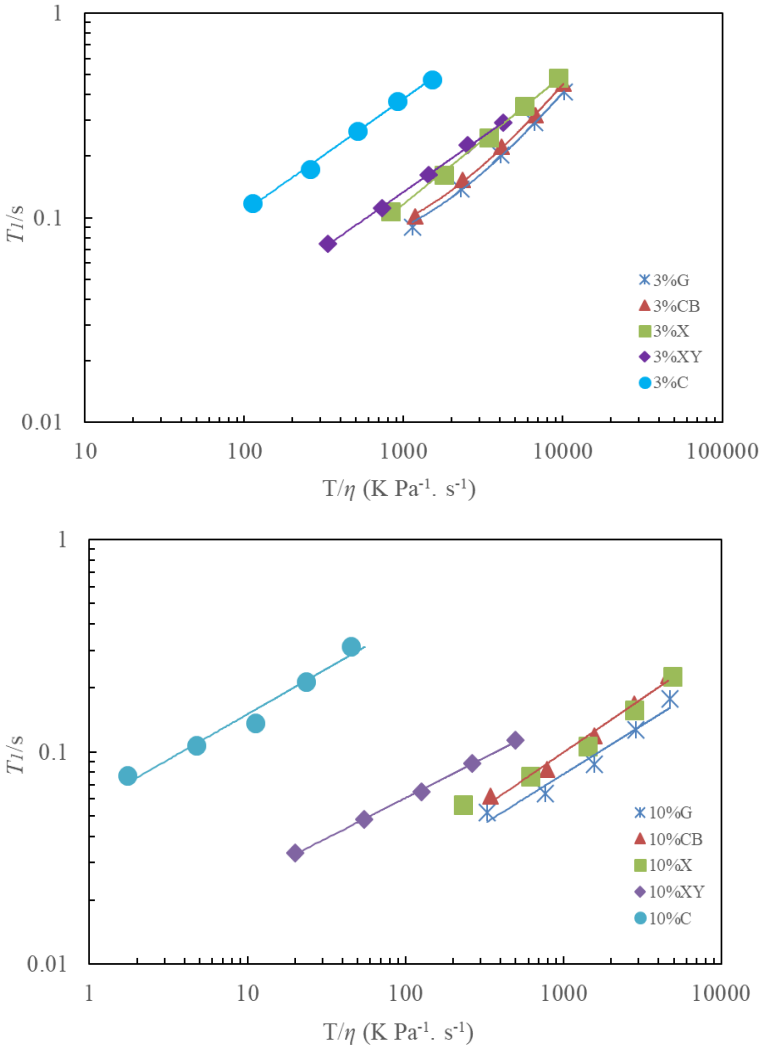

Figure 5.9: Relaxation time T_1 versus the ratio of the temperature to the viscosity of carbohydrate systems for 3% (a) and 10% (b) of glucose, G cellobiose, CB, xylose, X, cellulose, C and xylan, XY. The solid lines to guide eyes and the error bars within the symbols sizes.

Figure 5.10 displays the values of hydrodynamic radii, $R_{H,i}$ against all carbohydrate weight fraction at selected temperatures. The sizes of the ions are not in reality changing. Carbohydrates influence the values of $R_{H,i}$, this results in a reduction of the diffusion of ions [106]. The size of the effective radius has the most considerable reduction in xylan solutions. The comparison between carbohydrates of glucose, cellobiose xylose and cellulose, shows values of $R_{H,i}$ remained the same with an increase in the concentration of carbohydrates. However, the values of $R_{H,i}$, gradually decreased at high concentrations of these carbohydrates, except glucose. This is possible due to the decoupling between macroscopic and microscopic viscosity once entanglements have started to form.

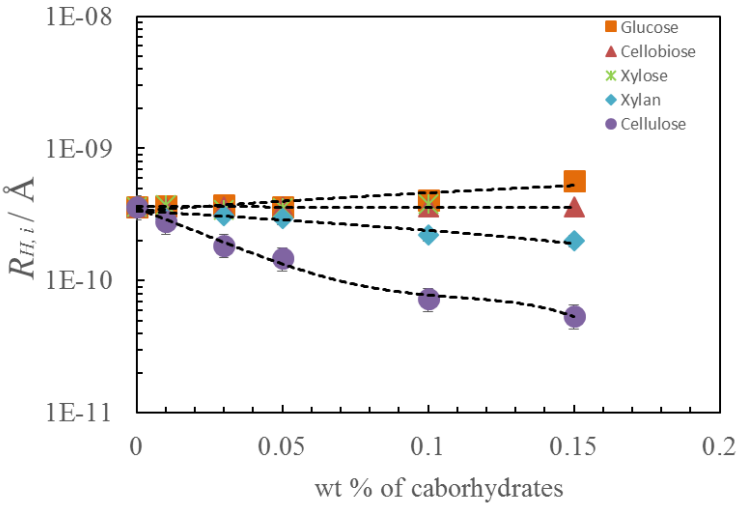

Figure 5.10: The values of effective hydrodynamic of radii versus carbohydrate weight fractions. The dashed points are used to guide the eyes, and errors are within the symbols sizes.

The basic of BPP theory as was discussed in Section 2.2.2, was applied to the experimental data of relaxation time T_1 to calculate the correlation time, τ using Equation 2.10, at 20 MHz. After that, the value of correlation time, τ was used to determine the activation energy for all carbohydrates systems. Arrhenius Equation is modelled to calculate the activation energy of correlation time, $E_{a,\tau}$, as follows:

$$ln\,\tau = ln\,\tau_0 + \frac{E_{a,\tau}}{RT} \tag{5.2}$$

where τ_0 is the correlation time at infinite temperature, and it is global value $3.23*10^{-15}$s and R is the universal gas constant, and T is temperature. Figure 5.11 shows the activation energies of correlation times plotted as a function of associated fraction α. The values of activation energies increased with an increase in the associated fraction α of ‘‘glucose unit’’ per molecule of IL [C2mim OAc], with uncertainties on all these values $\pm$ 0.1. The data of these carbohydrates fell on the straight line, except data of xylan/IL [C2mim] [OAc]; this system works differently when the associated fraction increases.

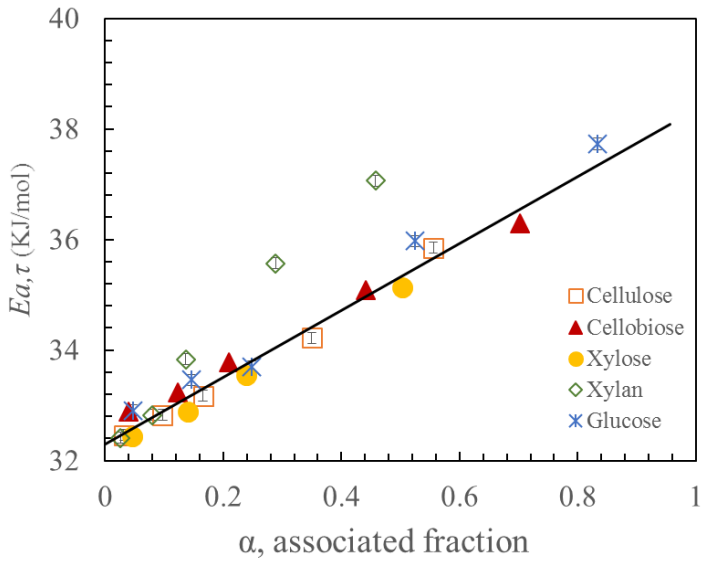

Figure 5.11: The activation energy of correlation time τ as a function of associated fraction α as defined by Equation 5.1. The solid line indicated to a linear fit to the data. The Error bars within the symbols sizes.

5.2.6 Intrinsic−Viscosity Analysis

This section presents the intrinsic viscosities of glucose and cellobiose. The intrinsic viscosity of cellulose was published, and for more information see ref [105]. The zero shear rate of viscosities of glucose and cellobiose in IL[C2mim] [OAc] employed to determine the intrinsic viscosities, using Equations 2.23 and 2.24 to fit the data. Figure 5.12a presents the specific viscosity as a function of glucose weight fractions across temperatures 20 ℃ to 60 ℃. The specific viscosity was determined from the relative viscosity using Equation 2.21. The specific viscosity of glucose / IL [C2mim] [OAc] increased as temperature decreased, as expected. Figure 5.12b shows the relative viscosity as a function of glucose concentrations – intrinsic viscosity multiplied by the concentration c[η]. All data of glucose solutions are combined from different temperatures into a single master curve.

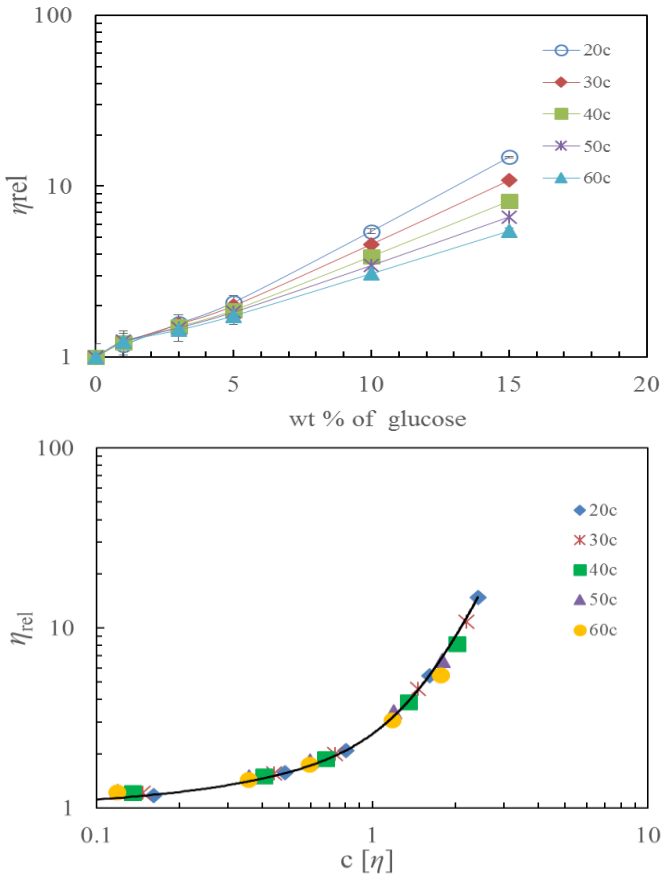

Figure 5.12 : a) The relative viscosity as a function of glucose weight fraction between 20°C to 60 °C. b) Intrinsic viscosity [η] as a function of temperature / °C for glucose. The error bars within the symbols sizes.

Figure 5. 13a shows the specific viscosity plotted against the weight fraction of cellobiose at selected temperatures. The specific viscosity reduced with the increase in temperature and addition of cellobiose in solution. Figure 5. 13b presents the relative viscosity as a function of xylan concentrations – intrinsic viscosity c[η]. Cellobiose data are also combined from different temperatures into a single master curve. The relative and intrinsic viscosities of glucose and cellobiose are much similar, as demonstrated in Figure 5.12 and Figure 5. 13.

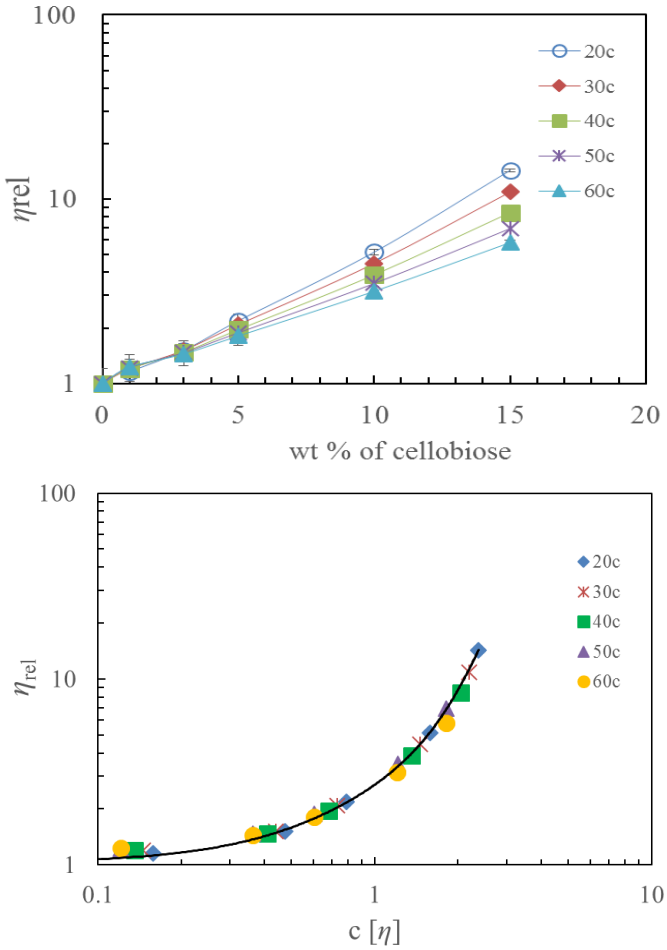

Figure 5. 13: a) The relative viscosity as a function of cellobiose weight fraction between 20°C to 60 °C. b) Intrinsic viscosity [η] as a function of temperature / °C for cellobiose. The error bars within the symbols size.

In Figure 5.14 displays the effect of temperature on five carbohydrate solutions, reducing the intrinsic viscosities. This is indicative of the quality of IL[C2mim] [OAc] decreased [105]. The cellulose solution obtained the large values of intrinsic viscosity, however, it decreased with temperature increases. After xylan, glucose, xylose and cellobiose have similar intrinsic viscosity values.

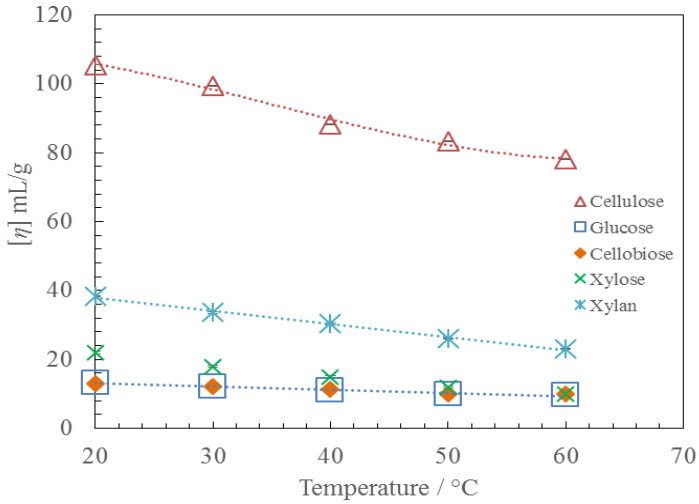

Figure 5.14: Intrinsic viscosity [η] as a function of temperature / °C for xylan and xylose solutions with glucose, cellobiose and cellulose, cellulose data taken from ref [105]. Error bars within the symbols sizes and dotted lines are to guide the eye.

5.3 Conclusion

The influence of carbohydrates on the diffusion coefficients of ions was determined by using the associated fraction, as shown in Figure 5.1. The associated fraction is calculated using Equation 5.1 for glucose, cellobiose, xylose, cellulose and xylan, respectively.

The diffusion coefficient of cations and anions was plotted as a function of the associated fraction of OH groups for all carbohydrate systems. All data of carbohydrate systems were lying on the straight line. The number of OH group of cellulose used as a fixed value to calculate the linear fit. The values of diffusion coefficients were affected by the ratio of OH group 5:4:4:3:2 per a molecule of IL[C2mim] [OAc].

The activation energy of cations and anions determined these carbohydrates, using the fixed values of D_0 for cation is $1.4 * 10^{-3} \pm 0.2$ m^2 s^{-1} and for anion is $1.6 * 10^{-3} \pm 0.2$ m^2 s^{-1} [41] in Arrhenius Equation.

The chemical shift of peaks imidazolium cation and anion for all carbohydrates solution was plotted as a function of the associated fraction. It shows that the anions are collapsed into a single line, while cations are disturbed by adding polymer. The correction term was determined using Stokes−Einstein Equation. It found that in glucose, cellobiose and xylose, the anions diffuse in a very similar way to cations. The correction term dropped off at high concentrations for xylan and cellulose. Stokes – Debye – Einstein Equation was also applied to the correlation between the relaxation time and the ratio of temperature to the viscosity. This was to determine the size of hydrodynamic radii of ions. Xylan obtained the lowest values of the effective radius.

The associated fraction of OH group was employed as a function of relaxation time T_1. It can be noted that xylan works individually with increase in the associated fraction. The BPP Equations was applied on the experimental NMR data using 20MHz, to measure the correlation time. Furthermore, Arrhenius Equation was modelled to calculate the activation energy. The intrinsic viscosity of glucose and cellobiose were determined using Wolf approach and Huggins Equation employed to fit all the data in a single master curve.

It found that the intrinsic viscosities of glucose and cellobiose have the smallest and similar values. The cellulose solution obtained the significant values of intrinsic viscosity; however, it decreased with temperature increases. After that xylan, and the intrinsic viscosity value of xylose is close glucose and cellobiose values.

Chapter 6

Investigation of the Effect of Xylan and Cellulose Blends on Diffusivity of the Ions of 1-Ethyl-3-Methylimidazolium Acetate [C2mim] [OAc]

6.1 Introduction

The purpose of this chapter is to investigate the interactions between xylan and cellulose mixtures in IL [C2mim] [OAc], as well as the mobility of ions in the carbohydrate solution with the use of primarily NMR diffusion, relaxation times (0.5 T/ 20MHz) and rheology methods, across a range of temperature, 20 ℃ to 60 ℃. The diffusion coefficient of anions and cations for the mixture of xylan and cellulose solutions with different weight fractions % were measured. The zero shear viscosity was determined using Cross – Viscosity equation 2.19. The viscosity data is plotted versus the composition of carbohydrates and inverse of temperature. An Arrhenius equation is modelled to calculate the activation energy of the diffusivity of ions in the viscous medium. The ideal mixing law is applied to diffusion and viscosity data.

6.2 Experimental methods

6.2.1 NMR methods

NMR diffusion coefficient and low- field relaxation time T_1 and T_2 were measured across temperatures range of 20 °C to 70 °C, using the techniques presented with details in Section 2.3.1. All mixture carbohydrates solutions were placed in the NMR tube with depths less than 1 cm to reduce convection currents on heating in the NMR machine. By doing this, we followed the guidance set out by Annat et al [103].

6.2.2 Viscosity method

All viscosity measurements of the mixtures carbohydrates solutions were measured using equipped with a cone-plate geometry (4°- 40 mm) and a temperature control system, using software called rSpace, as detailed again in Section 2.3.2. Steady-state measurements were recorded from 20 °C to 60 °C with a 10 °C step. The shear rates were from 0.1 to 100 s^{-1}. Before the experiment was run, a thin film of low-viscosity silicone oil was added around the edges of the plate to prevent moisture contamination during the viscosity measurements. A nuclear magnetic resonance (NMR) Bruker Avance II (400 MHz) spectrometer with pulsed field gradient ^1H NMR technique was used. A Benchtop NMR (20 MHz) was used to study low-field relaxation times T_1 and T_2 of carbohydrates solutions.

6.2.3 Materials and Sample Preparation

Xylan and cellulose powders were dried in vacuum at 50°C for 24h before use. NMR diffusion and viscosity measurements on 13 mixtures of the samples that were prepared from these carbohydrate polymers with 0.9 ml of IL [C2mim OAc] and 0.1g of the total of carbohydrate.

Table 6.1 shows the carbohydrate concentrations added to the solution, with xylan weight fraction ranging from 0-100%. The 0% corresponds to 100% of cellulose weight fraction. The 100% cellulose sample and 100% xylan were separately prepared. The polymers were mixed in to the IL [C2mim] [OAc] at the same time. Each sample took between 72 h to one week and was prepared without heating. Xylan concentrations were responsible for changing the colour of the samples (from transparent 0% to dark brown for 100% xylan).

The blends samples were stirred under nitrogen gas in an MBraun Lab Master 130 Atmospheric chamber preserved at the level of a dew point between -70 ℃ and -40 ℃. The NMR tubes of samples were sealed to prevent contamination with water from the atmosphere within the chamber. Five samples were prepared for each concentration of composition xylan and cellulose, and the measurements have repeated several times to obtain accurate data by reducing the percentage of error.

CONC %	0	5	10	20	30	40	50	60	70	80	90	95	100
Xylan	0	0.005	0.01	0.02	0.03	0.04	0.05	0.06	0.07	0.08	0.09	0.095	0.1
Cellulose	0.1	0.095	0.09	0.08	0.07	0.06	0.05	0.04	0.03	0.02	0.01	0.005	0

Table 6.1: The carbohydrate concentrations added to the solution, with xylan weight fraction ranging from 0-100%.

6.3 Results and discussion

6.3.1 NMR Diffusion

NMR Diffusion measurements are used to determine the mobility of ions in each mixture and from this investigate the interactions between xylan and cellulose in solution. The diffusion coefficients of all cation resonances were equal. The Arrhenius equation was applied to NMR diffusion data. Figure 6.1a the natural logarithms of the diffusion coefficients of anions for nine composition concentrations are plotted versus the inverse temperature. The anion diffusion increase with the increase in temperature. The data of $\ln D_{C2mim}$ and $\ln D_{OAc}$ have a slight concave dependence in the Arrhenius plot. Figure 6.1b shows the same relationship holds almost for cation diffusion.

From Figure 6.1 (a, b) the diffusion values of the cations and anions for the composition solutions are approximately the same, with uncertainties on all these diffusion values of ± 0.2 m^2 s^{-1}. The values of diffusion coefficients for 30% and 50% have lower values during temperatures increase. It can note that the concentrations of mixture polymers solutions are not in regular order in Figure 6.1 (a, b), as might be expected. Figure 6.2 (a, b) displays the diffusion of ions are behaving differently at the concentrations of blends polymers.

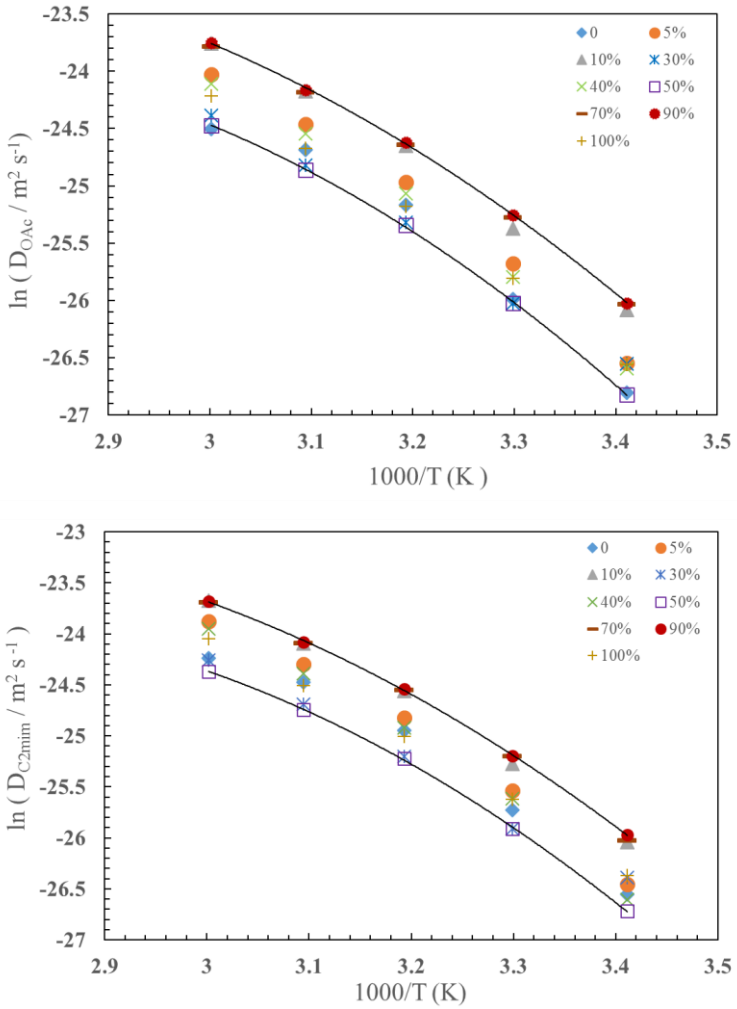

Figure 6.1: Natural logarithm of the diffusion coefficients for the anions (a) and cations (b) for the weight percentage of the xylan-cellulose mixture in [C2mim OAc]. The solid lines provided as a visual guide. Error bars are within the data points.

Figure 6.2 (a, b) shows the diffusion coefficients of anions as a function of the composition of polymers solutions at 40 ℃. It is found that the diffusion values of the anions compared to cation diffusion are approximately the same. These values fluctuated with an increase in xylan from 10 to 100 mg/l and decreased cellulose concentrations, that is kept fixed at 10% in total of concentration into solution. These fluctuations indicate to there is an interaction between the ions and the molecules of two compounds in solution, as it seems in peaks at particular concentrations.

The diffusion coefficients of anions and cations of the blends samples have unexpected behaviours, and this may indicate there are interactions due to the specific cellulose-cellulose, cellulose-xylan and xylan-xylan arrangements taking place particular stoichiometric ratios. The diffusion coefficients of ions were higher in the 10%, 70% and 90% xylan concentrations, whereas they were lower in the 0%, 30% and 50% concentrations, as shown in Figure 6.2 (a, b). In the xylan-cellulose mixture, interactions at 20% and 80% or 80% and 20% of weight fraction respectively, appeared lower for diffusion coefficients of both ions, which means that ions may have interacted with a higher number of OH groups in these mixtures. The same results are obtained for all temperatures measured. The diffusion measurements were repeated several times before starting the analysis of the data. So far, we do not have any idea why these peaks happened at these ratios, therefore; further analysis is required, it would be useful to use a computer simulation to give some insight on these interactions and possible polymer-polymer arrangements. The ideal mixing law was then applied to the diffusion data of complex solvent and polymer combination [41, 109]. The result will be discussed in detail later.

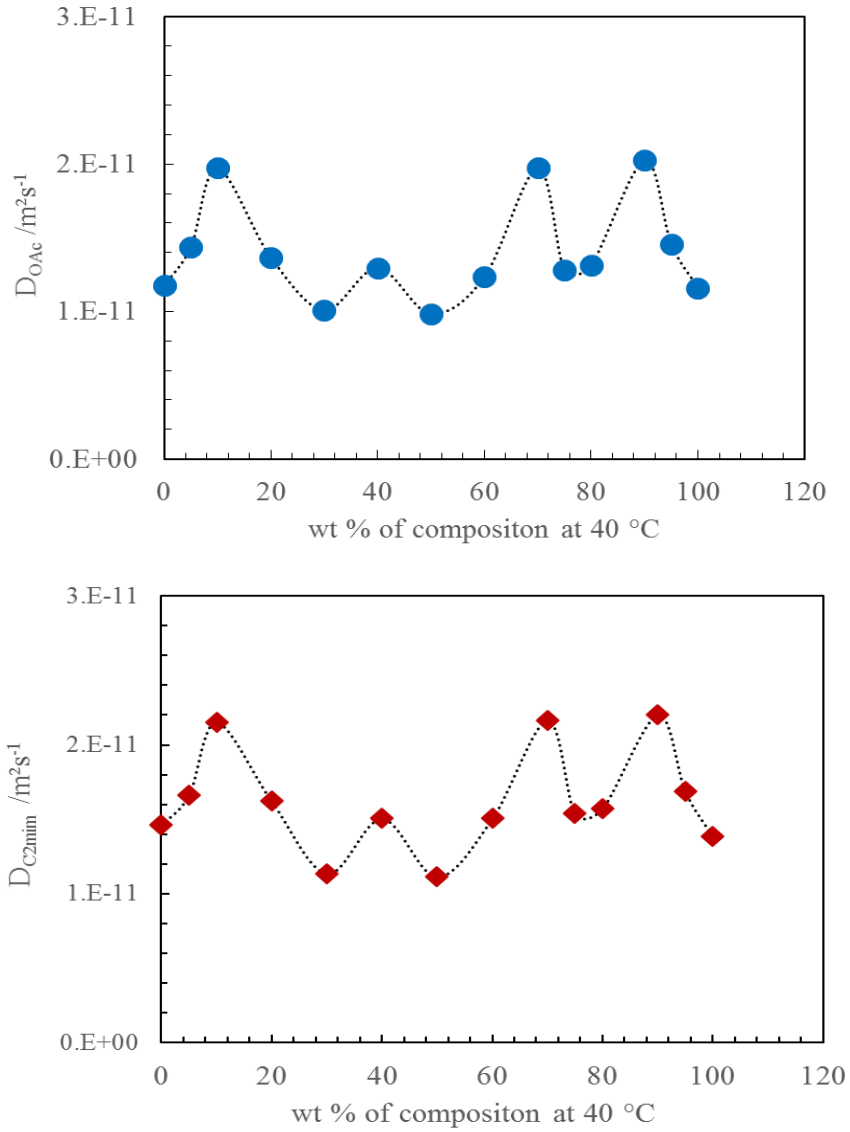

Figure 6.2: Diffusion coefficients for the anions (a) and cations (b) for the weight percentage of the xylan-cellulose mixture in [C2mim OAc] at 40 ℃. Dashed lines are provided as a visual guide. Error bars are within the data points.

The ratio of the anion to that the cation fluctuates between 0.8 and less than 1 with an increase in the composition of polymers in solution. Figure 6.3 presents the ratio of the anion diffusion coefficients to those of the cations as a function of composition (xylan and cellulose) concentrations and is less than 1 (D_{OAc}/D_{C2mim}< 1). This diffusion is called 'anomalous' diffusion since the anion is smaller geometrically than the cation and so is expected to diffuse instead faster.

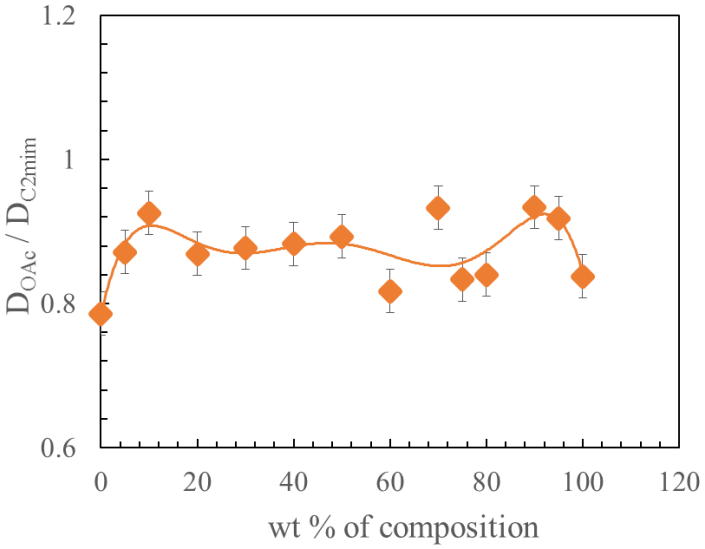

Figure 6.3: Ratio of the diffusion coefficients of the anions to the cations as a function of varying the concentrations of composition (xylan-cellulose). Error bars are displayed with symbols. The solid lines to guide the eyes.

6.3.1.1 ^{1}H Chemical Shift of Proton Resonances

The composition altered the positions of IL [C2mim OAc] proton resonances 1-7, as shown in Figure 1.1. Figure 6.4 displays the chemical shift, $\Delta\delta$ (ppm) versus weight fractions of composition (xylan-cellulose) at 30 °C. The chemical shift $\Delta\delta$ of protons resonances was calculated using δ resonance peak 5 as a reference position. The protons in the cation ring have negative values of $\Delta\delta$ with four peaks, while anion also has peak with positive values at 30ºC. The largest movement is in peak 2, which is the most acidic proton of the imidazolium ring. The chemical shift of both ions shown there 4 peaks,

which coincides with the peaks in the diffusion of cations and anions. This is independent evidence of interactions between cellulose and xylan, complementing the diffusion data. The chemical shift of proton peaks in composition solutions changed compared to the chemical shift of each polymer in IL [C2mim OAc] individually.

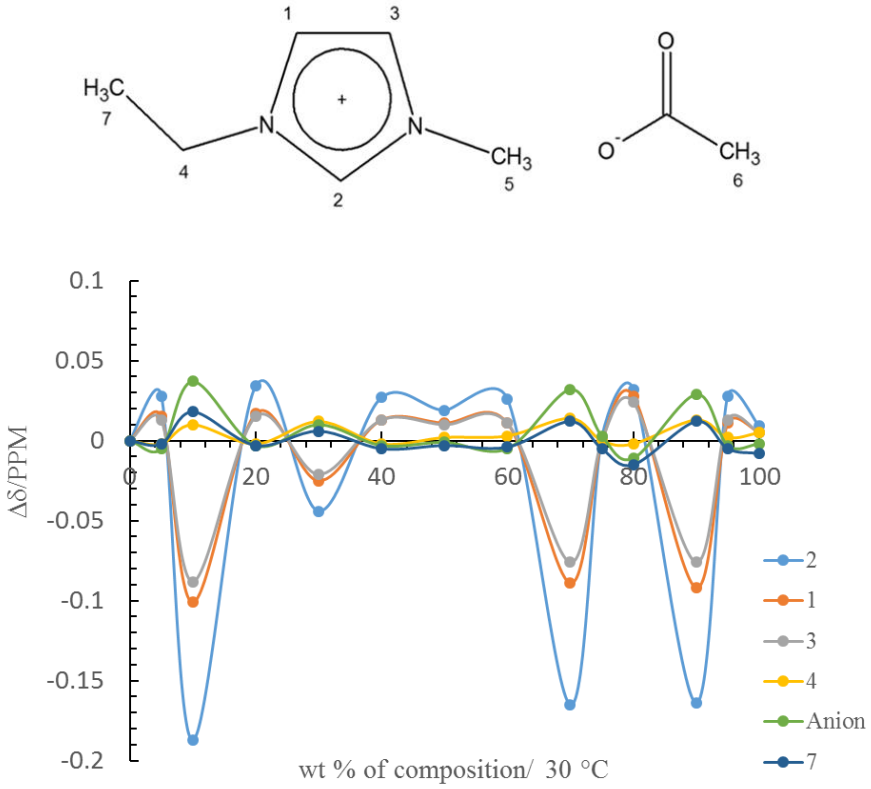

Figure 6.4: The chemical shift of protons resonances $\Delta\delta$ (ppm) plotted versus xylan-cellulose weight fractions at 30 °C. The lines provided as a visual guide. The error bars within the symbols size.

It is possible to investigate the influence of two polymers dissolved in IL [C2mim OAc] by determining the activation energies of anion and cation. The activation energies of both ions were obtained from the data in Figure 6.1, using an Arrhenius Equation 3.1. The values of activation energies of anion and cation are shown in Table 6.2. It can be observed that the activation energies, $E_{A,D}$ for anion diffusion are similar to cation in this viscous medium.

Wt%	$E_{A,D}$ /kJ mol^{-1}	
	$[C2mim]^+$	$[OAc]^-$
0	48.1± 0.1	48.3± 0.1
5	52.1± 0.1	51.1± 0.1
10	48.2± 0.1	47.7± 0.1
20	51.6± 0.1	49.9 ± 0.1
30	44.6± 0.1	45.1± 0.1
40	53.3± 0.1	50.7± 0.1
50	47.8± 0.1	47.8± 0.1
60	47.2± 0.1	45.6± 0.1
70	50.2± 0.1	51.5± 0.1
80	51.0± 0.1	51.5± 0.1
90	46.4± 0.1	45.9± 0.1
95	51.1± 0.1	48.4± 0.1
100	46.8± 0.1	47.4± 0.1

Table 6.2: The values of activation energy of anion and cations for the concentrations of blend polymers solutions with the uncertainties values.

6.3.2 Ideal Mixing Law of Diffusion coefficients

Ideal mixing law is applied to determine to quantify the interactions between the ions of IL [C2mim OAc] and molecules of the mixture of carbohydrates (cellulose and xylan) solutions. The ideal mixing rule for diffusion derives from the viscosity ideal mixing law, and it was applied for diffusion coefficients of both ions at constant temperature [59, 109].

$$lnD_i = x_1 lnD_1 + x_2 lnD_2 \tag{6.1}$$

where D_i is the of self-diffusion coefficient of ions in mixture liquid and x_1 and x_2 are the weight fraction of cellulose and xylan in solution, where x_1+x_2=1 [109-111] As well as D_1 and D_2 are diffusion coefficients of cations with cellulose and xylan solutions, respectively. We used concentrations scale from 0 to 100% with total for each concentration 10%, for ideal mixing analysis.

Figure 6.5 (a, b) shows the natural logarithm of the diffusion coefficients for the anions and cations are plotted versus the mixture of carbohydrate concentrations at 30 °C. Figure 6.5a, is displayed the linear dependence calculated according to an ideal mixing law, deviations of the diffusion values from this linear dependence indicate interactions between the polymers.

Three peaks are shown at 10:90, 70:30 and 90:10 weight fractions of xylan to cellulose. Our hypotheses are the number of available OH groups is reduced at the concentrations where these peaks are seen in Figure 6.5 (a, b) as it is the OH groups that slow down the diffusion of the ions [51].

When the weight percentages of carbohydrates were (i.e. at 30:70 and 50:50 xylan to cellulose) this lead to a minimum point. Figure 6.5b shows the same result is found for cation diffusion.

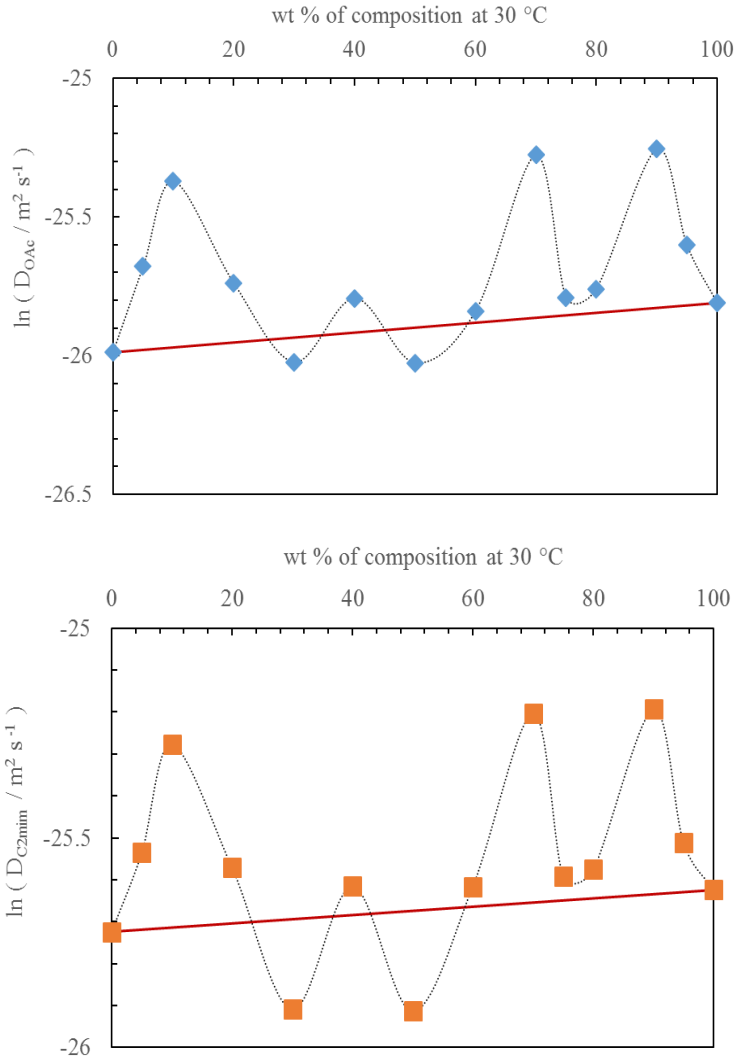

Figure 6.5: Natural logarithm of the diffusion coefficients for the anions (a) and cations (b) as a function of the mixture of carbohydrate weight fractions at 30 °C. The error bars are shown with the data. Dashed lines are provided as a visual guide.

The diffusion difference ($\Delta D\%$) between the measured values of diffusion of the cations and anions in (cellulose and xylan) solution concentrations and that predicted from ideal mixing, is given by:

$$\Delta D = \frac{D(c) - D(ideal\ mixing)}{D(ideal\ mixing)} * 100 \tag{6.2}$$

where $D(c)$ is the experimental value of diffusion and $D(ideal\ mixing)$ was calculated from ideal mixing law. Figure 6.6 (a, b) shows the difference in diffusion coefficients of anions and cations as a function of the mixture of polymers with different concentrations. The result shows that the anions diffuse faster than the cations and the difference of diffusion coefficients of anions is approximately 100% and ΔD for cations is around 80%. The difference of dissolving mechanism of cellulose and xylan in IL [C2mim OAc] has effected on the mobility of both ions.

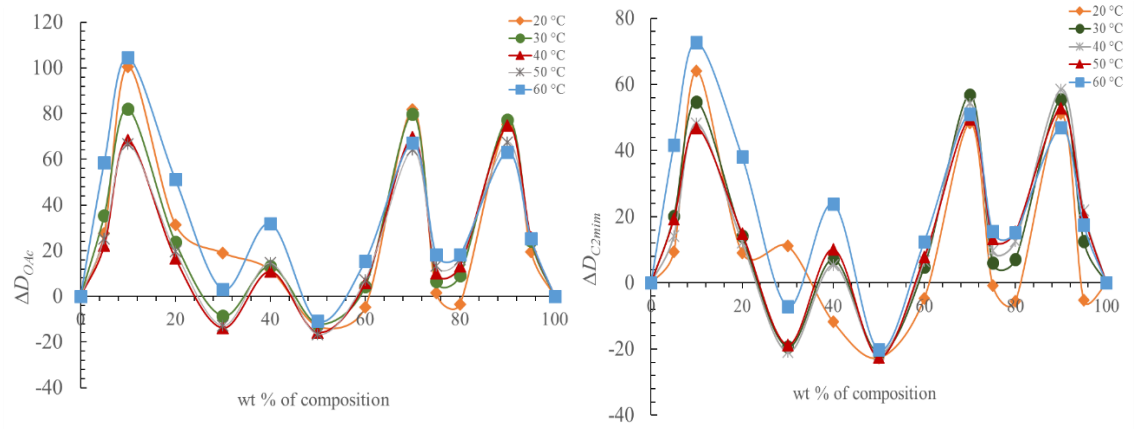

Figure 6.6: The differences in diffusion coefficients of the anions (a) and cations (b) are plotted against the mixture of polymers concentrations in solution, at various temperatures (20 ℃ - 60 ℃). The uncertainties are within the size of the symbol to avoid overlap. The solid lines provided as a visual guide.

6.3.3 Viscosity–Temperature Analysis

As discussed in section 2.3.2, the viscosity technique is used to measure the zero shear rate viscosity of composition polymers (cellulose and xylan) in IL [C2mim] [OAc] solutions with different concentrations, which are 0%, 10%, 20%, 30%, 40%, 50%, 60%, 70%, 80%, 90%, 95% and 100%, at various of temperatures from 20℃ to 60℃. Figure 6.7a shows xylan- cellulose solutions for different concentrations as a function of shear rate at 50 ℃. The data from 0 to 0.1 s^{-1} had low signal to noise ratio and thus were ignored for all composition of polymer solutions.

The concentrations 0%, 10%, 20%, and 30% are indicated to 100% of cellulose and 10:90, 20:80 and 30:70 of weight fractions of xylan to cellulose, respectively. In these concentrations, cellulose is higher weight fractions than xylan, and their viscosity values are similar at 50 ℃, as shown in Figure 6.7a.

The Cross-Viscosity Equation 2.18, was applied to experimental data, to determine the zero-viscosity η_0 of blends xylan and cellulose solution at selected temperatures. The result presents in Figure 6.7b, where the viscosity of component polymers in IL [C2mim] [OAc] solutions plotted as a function of inverse temperature. The viscosity values of all compositions of polymers solutions decrease as temperature increases, as expected. The viscosity values of solutions of varying concentrations gradually decrease with increase in weight fractions of the mixture of polymers. 100% of xylan has the lower value of viscosity, as compared to 100% of cellulose. The same results found for all temperature measured. The activation energy of viscosity is calculated using the data is shown in Figure 6.7.

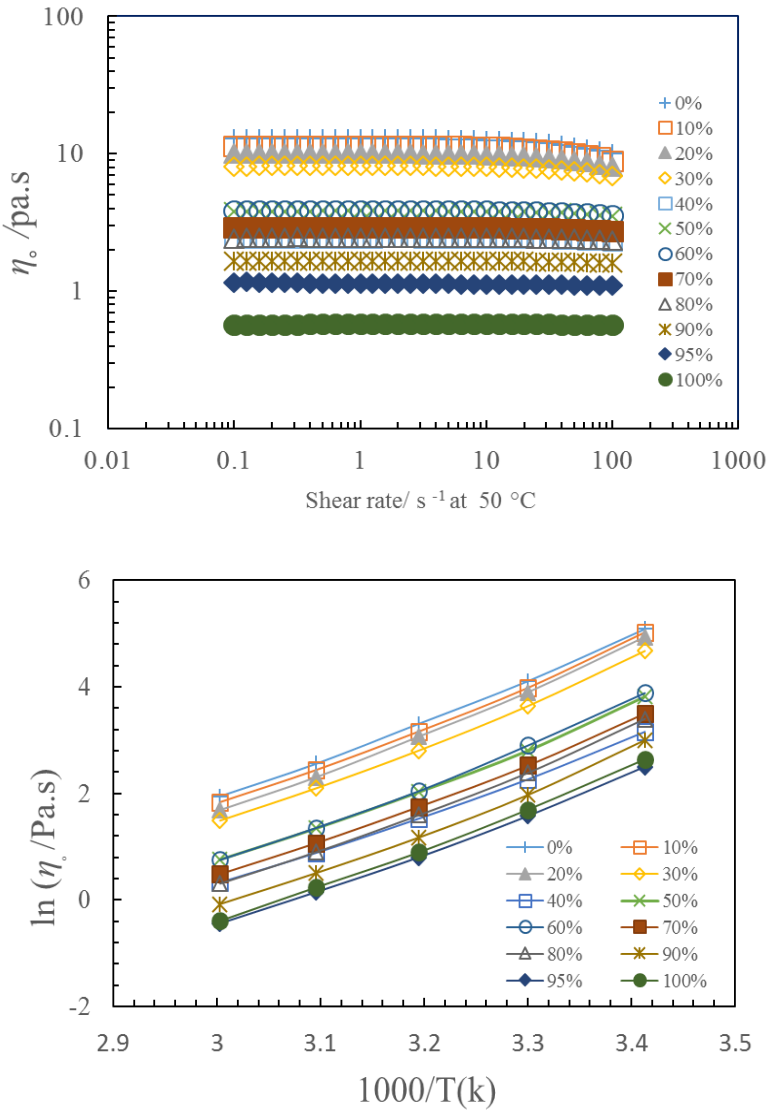

Figure 6.7: a) The zero viscosity of composition polymers (cellulose and xylan) /IL [C2mim] [OAc] solutions at different weight fractions as a function of shear rate/s. b) The logarithmic plots of the viscosity of blends polymers in IL [C2mim] [OAc] solutions versus inverse temperature. Lines are linear approximations. Error bars within the symbols size.

An Arrhenius Equation 3.3 is modelled and applied to the viscosity data to calculate the activation energy. Table 6.3 displays the values of activation energies of viscosity for the mixture of polymers. The values of $E_{A,\eta}$ are slightly varying between the compositions of polymers solutions but not in any significant way.

Wt %	$E_{A,\eta}$/kJ mol^{-1}
0	63.6 ± 0.5
10	64.4 ± 0.5
20	65.8 ± 0.5
30	64.3 ± 0.5
40	57.2 ± 0.5
50	61.7 ± 0.5
60	63.5 ± 0.5
70	60.8 ± 0.5
80	62.4 ± 0.5
90	62.0 ± 0.5
95	59.4 ± 0.5
100	61.3 ± 0.5

Table 6.3: The activation energies of viscosity for mixture of the carbohydrate polymer solutions.

6.3.3.1 Viscosity Ideal Mixing Rule

It is possible to determine to quantify the interaction between two polymers mixtures in IL [C2mim] [OAc] using the viscosity ideal mixing law at constant temperature [59, 110].

$$ln\eta_{mix} = x_1 ln\eta_1 + x_2 ln\eta_2 \quad (6.3)$$

where $\eta_{mix}$is the measured viscosity and x_1 and x_2 are the weight fraction of cellulose and xylan in solution, where x_1+x_2=1. As well as η_1 and η_2 are the viscosity of cellulose and xylan solutions, respectively [109, 110, 112]. The concentrations scale plotted for ideal mixing analysis, from 0 to 100% with the total for each concentration 10%.

Figure 6.8 presents natural logarithm of the viscosity as a function of the mixture of carbohydrate weight fractions at 40 °C. The linear dependence calculated according to an ideal mixing law deviations of polymer and solvent. The viscosity values from the straight line indicate there are interactions between the two polymers in solution. The viscosity data dropped at 40% and 90% weight fraction of xylan across temperatures 20 ℃ to 60℃.

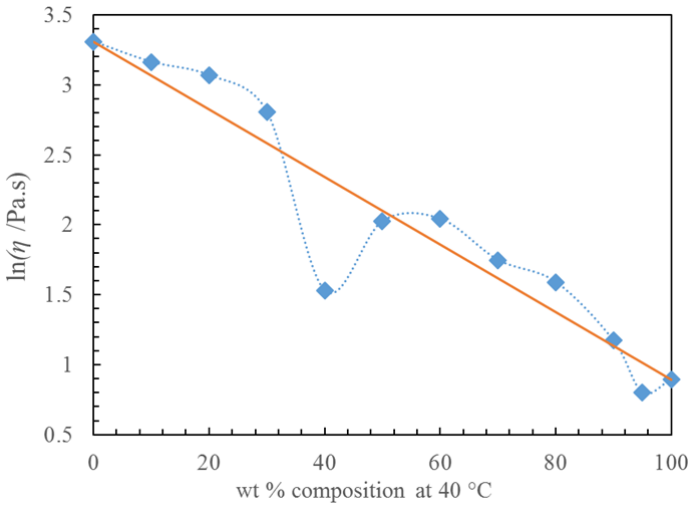

Figure 6.8: Natural logarithm of the viscosity as a function of the mixture of carbohydrate weight fractions at 40 °C. The error bars are shown with the data points. Solid is the linear fit and dashed lines are provided as a visual guide.

The viscosity difference ($\Delta\eta$ %) between the measured values viscosity in (cellulose and xylan) solution concentrations and that predicted from ideal mixing, is given by:

$$\Delta\eta = \frac{\eta(c) - \eta(ideal\ mixing)}{\eta(ideal\ mixing)} * 100 \qquad (6.4)$$

where $\eta(c)$ is experimental value of viscosity, and $\eta\ (ideal\ mixing)$ was calculated from viscosity ideal mixing law. In Figure 6.9 the result shows the difference of viscosity values of polymers mixtures in solutions at different temperatures. All viscosity data are followed the same trend during the concentrations of mixture polymers. It can be noted that the difference in viscosity $\Delta\eta$ shows there are peaks.

These three peaks in viscosity data correspond to the three peaks of diffusion measurements at the same temperatures indicate there is a real interaction between components in these solutions.

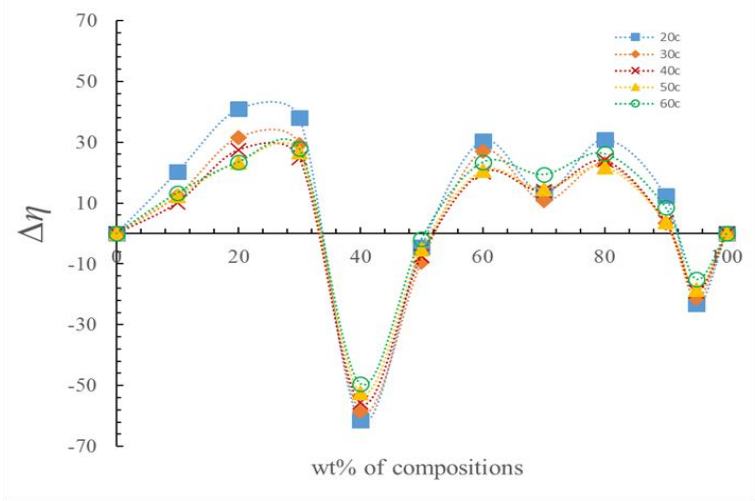

Figure 6.9: The viscosity difference against the compositions of polymers mixtures in solution across temperatures from 20 ℃ to 60 ℃. The error bars within the symbols size to avoid overlap. Dashed lines are provided as a visual guide.

6.3.4 Stokes−Einstein Analysis

Stokes-Einstein theory can also be applied on the blends of carbohydrate polymers solutions, to measure the micro-viscosity per-factor or as known the corrections term, f. Figure 6.10 (a, b) shows the correlation between the diffusion coefficients of anion and cations and the ratio of temperature (K) to the viscosity ($Pa\ s$) for all compositions of polymers solutions, with xylan weight fraction ranging from 0-100%, where 0% indicates to 100% cellulose solution. The NMR diffusion data of Figure 6.10 (a, b) was employed to investigate the influence of these compositions on the diffusing of ions in viscous solution, by determining the correction term f. The hydrodynamic radii $R_{H,i}$of ions was calculated by Hall et all using Equation 2.9, the effective radii values are for the anion 2.2 Å and the cation 2.8 Å [59]. These values of $R_{H,i}$ are employed with the gradient of the ratio of D to T/η, to calculate the correction term, f for anions and cations, using

Stokes−Einstein Equation 2.8. In Figure 6.10a the diffusion coefficients of anion increase with the increase in the ratio of temperature to the viscosity for all concentrations of the composition. Figure 6.10b is presented the same result found for diffusivity of cations. The result indicates there is a new structure (complex) occurred between 100% cellulose and 100% xylan in solution. It can see in this result the anion behaves differently than ideal mixing diffusion. The same result is found for cation diffusion.

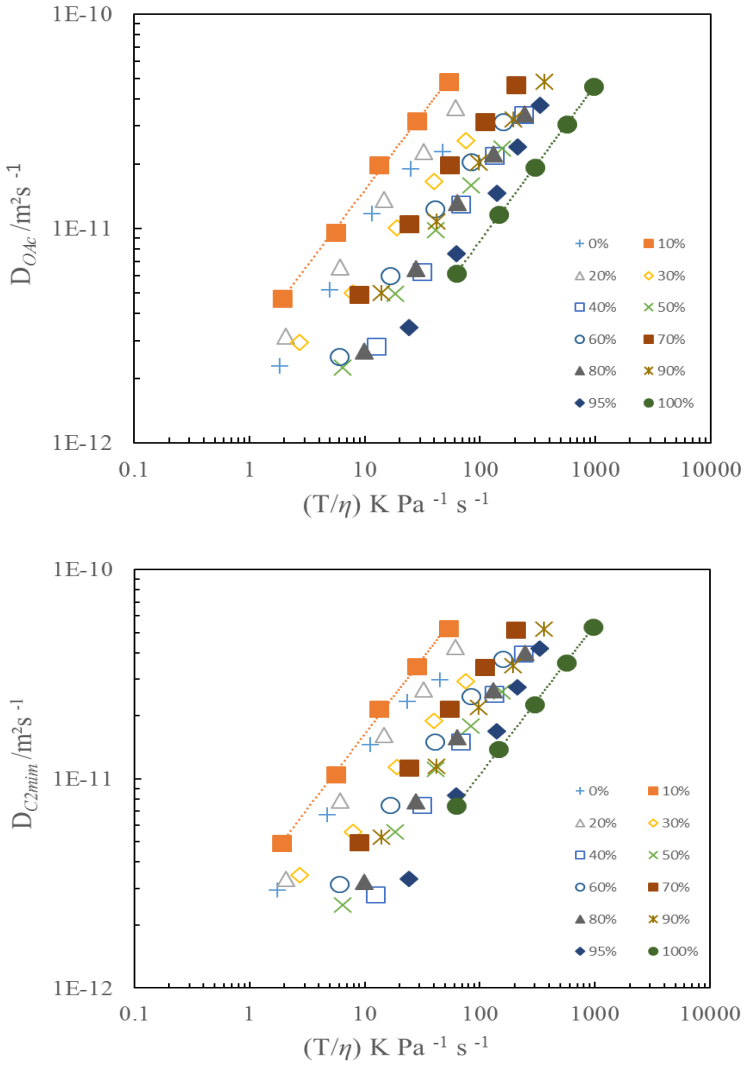

Figure 6.10: NMR diffusion coefficients of anions (a) and cations (b) against the ratio of temperature to the viscosity of pure IL [C2mim] [OAc]for the composition of carbohydrates concentrations (from 0% to 10%). Dotted lines are provided as visual guide and error bars within the symbols sizes.

Stokes-Einstein Equation 2.8 is applied to the experimental data from in Figure 6.10 (a, b) and the result presents in Figure 6.11. The correction term for anions and cations plotted against the composition of polymers. The result is shown the correction term f for anion and cation is $f < 1$. It can note that in low concentration composition, the value of correction term, f decreases, this because the microscopic viscosity is smaller than macroscopic viscosity. The value of correction term, f increases as concentrations of composition polymers in solution increase. These values of correction term indicate the new complex structure of these polymers solutions. The diffusion coefficient of anions and cations is preferentially more reduced by high concentrations of cellulose, which are 0%, 90% and 70% in these blend solution. It is interestingly to note that the result indicates the anomalous behaviour, which means the cations diffuse faster than expected.

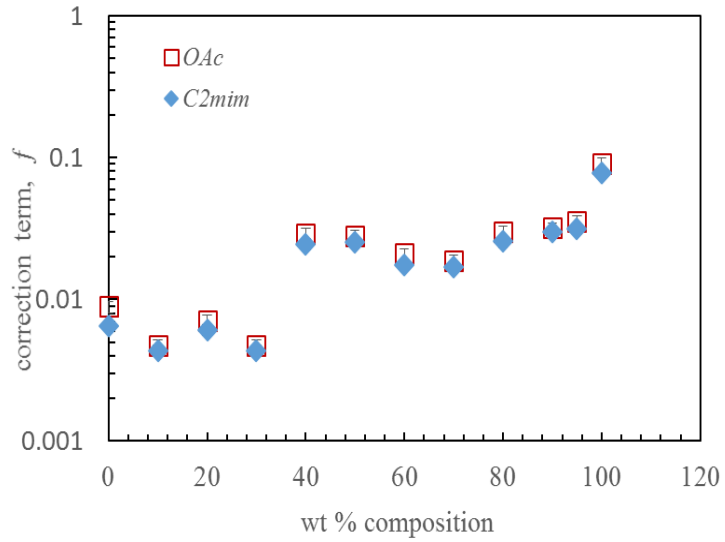

Figure 6.11: The correction term f as a function of weight fractions composition (cellulose and xylan) in solution. Error bars are within the symbols sizes.

6.3.5 Stokes−Debye–Einstein Analysis

The relaxation time T_1 was measured across arrange of temperatures (70 °C - 30 °C). These experimental data used to determine the hydrodynamic radii of averaged ions in viscous medium, using Stoke − Debye − Einstein Equation. Figure 6.12 presents the correlation between relaxation time T_1 and the ratio of the temperature (T) to the viscosity (η) for several concentrations of the blend polymers. The relaxation time T_1 for concentrations from 10% to 100% increase when the ratio of ($^T/_\eta$) increases. It can be noted that the values of T_1 is higher at 0% which is the cellulose/ [C2mim] [OAc] solution.

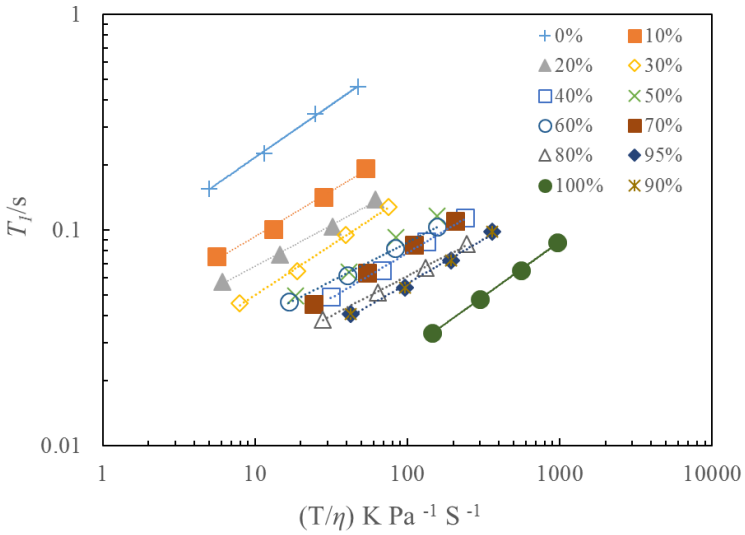

Figure 6.12: The relaxation times T_1 dependence on the ratio of temperature to viscosity for the composition of polymers concentrations. Error bars size is within data points. Dashed and solid lines are provided as a visual guide.

As discussed in section 2.2.3, Stokes− Debye – Einstein Equation 2.15 is also applied to the experimental data of blends polymer solutions, to determine the effective hydrodynamic radii, $R_{H,i}$. Figure 6.13 shows the values of the effective hydrodynamic radii, $R_{H,i}$ against the composition of polymer concentrations, with xylan weight fractions in solution. The values of $R_{H,i}$ increase with the increase in xylan weight fractions in mixture solution. A comparison between the values of correction terms from Figure 6.11 and hydrodynamic radii values in Figure 6.13, it can be noted that there are

similar results found, indicate to the complex structure of this system influences the effective size of ions IL [C2mim] [OAc]. The values of the hydrodynamic radii of ions in all the blends polymers concentrations and all the temperatures, for T_1, is almost equal to or slightly greater than T_2 experimentally.

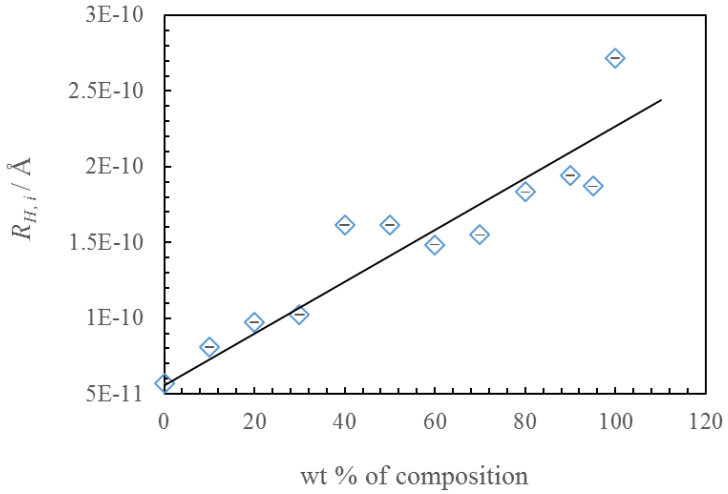

Figure 6.13: The values of hydrodynamic radii, $R_{(H,i)}$ against the polymers concentrations, with xylan weight fractions in solution and error bars are within the symbols sizes.

6.4 Conclusion

The NMR diffusion coefficients of cations and anions for a mixture of carbohydrate solution were measured and plotted against inverse temperatures, analysed using Arrhenius equation. The ratio of the anion diffusion coefficients to that of the cations as a function of the xylan-cellulose concentrations was less than 1. Cellulose preferentially more reduces the diffusion coefficient of the anion than does xylan.

It is generally agreed that the anion is more active in the dissolution of polymers than the cation. The dissolution mechanism of cellulose and xylan in [C2mim] [OAc] can be examined via the mobility of the ions. It can be proposed that the number of accessible OH groups belonging to the carbohydrate polymers be reduced at certain xylan-cellulose blend compositions, showing that at these concentrations there are significant interactions between the two biopolymers. There are peaks shown when the diffusion coefficients of ions as a function of the composition of concentration. The minimum points were at point 30:70 and 50:50 xylan to cellulose. Ideal mixing of diffusion was used for both ions to quantify the interactions between components in solution.

The chemical alteration of protons resonances displayed four peaks of proton resonance correlated with cations of imidazolium ring. The $\Delta\delta$ of anion peak is in range of 0.02 to -0.02 ppm. The chemical shift showed that the positions of ions in mixture solution were altered when compared to the chemical shift of ions in cellulose or xylan in IL [C2mim] [OAc]. These peaks matched where the diffusion differences from ideal mixing were the greatest.

The viscosity values of all compositions of polymers solutions decrease as temperature increases, as expected. The viscosity values of solutions of varying concentrations gradually decrease with increase in weight fractions of the mixture of polymers. The ideal mixing of viscosity shows there is an interaction between cellulose and xylan in the mixture solution.

Chapter 7

Conclusion and Future Works

7.1 Conclusion

This work presents an investigation into carbohydrates (glucose, cellobiose, xylose, cellulose and xylan) dissolved into the IL [C2mim] [OAc] and how they can influence the diffusivity, relaxometry time and rheological properties, as well as the chemical shift of ions. Using primarily NMR diffusion and low and high field relaxation times, as well as rheology via a dynamic stress-controlled rheometer, across arrange of temperatures 20 ℃ −70 ℃.

In chapter 3, xylose / IL [C2mim] [OAc]. The self−diffusion coefficients of anions and cations decrease with an increase in xylose weight fraction. The values of diffusion coefficients of anions and cations are increased with increase in temperature, as expected. These values showed the diffusivities of anion and cation were similar. The ratio of the diffusion coefficient of anions to cations was less than 1. This is known as ‘‘anomalous’’ diffusion because the anion is geometrically smaller than the cation and so would be expected to diffuse faster not slower than the cation. It is possible this anion is diffusing as part of an aggregation of ions. Xylose data were compared to cellobiose to compare the influence of each on ions. It was found that the values of activation energies of ions indicated an insignificant difference between xylose and cellobiose systems for diffusion, relaxation times and viscosity measurements.

The changes in ^{1}H chemical resonance frequencies $\Delta\delta$ for protons in the presence of xylose is almost identical to the chemical shift movements of cellobiose, which indicates that these carbohydrates have a similar dissolving mechanism. The correction term, f was extracted from the Stokes-Einstein relationship. It is interestingly to note that cations diffuse faster than expected. At low field relaxation (20MHz) xylose found to be in the liquid regime across all temperatures (70 °C−30 °C). The viscosity measurements and relaxation time data were used to measure the effective hydrodynamic radii, using the Stokes-Debye-Einstein relationship. The value of the hydrodynamic radii of averaged ions was between 3.5 Å to 5 Å in xylose solutions. The values of the hydrodynamic radii of ions in all the xylose concentrations and all the temperatures, for T_1, is almost equal to or slightly greater than T_2 experimentally.

The viscosity dependence increases with adding xylose through an increase in temperature. The viscosity-shear rate was used to determine the intrinsic viscosity of xylose/IL [C2mim] [OAc] solution. All data of the intrinsic viscosities of xylose solutions are combined for different temperatures into a single master curve. The values of xylose intrinsic viscosity [η] are greater than the corresponding cellobiose values at the lower temperature. The intrinsic viscosity of cellobiose was influenced slightly by temperature. The intrinsic viscosity [η] of both carbohydrates reach the same point of 10 ml/g at 60 ℃.

In chapter 4, the dissolution of xylan in IL [C2mim] [OAc] was determined. The mobility of ions in xylan solutions decreased, this due to the viscosity is increased by the presence of xylan and decreased by increasing temperature. The diffusivity of the anion is similar to that the cation, this indicates an anion is joined with other diffusing particles [101]. The ratio of the diffusion coefficient of anion to cation is less than 1. The results of the chemical shift of proton resonances in xylan system compared to cellulose / IL [C2mim] [OAc], this indicated that in both systems the dissolution mechanism is similar. The influence of xylan on the ions of IL[C2mim] [OAc] is found to be similar to that as found for cellulose; in the case of xylan dissolution, the cation and anion are though more equally affected by the addition of this carbohydrate than they were by the addition of cellulose.

At high field, the relaxation times for all the proton resonances in xylan solutions move between two regimes (solid and liquid) and so have a minimum in T_1. At 20MHz low field, xylan is also found to be in the liquid regime across all temperatures (70 °C−30 °C). Activation energies of cation and anions of xylan system were measured and compared to cellulose, and it found that both ions have similar activation energies in diffusion, relaxation time and viscosity measurements.

The viscosity data was used with diffusion to measure the correction term, and with relaxation time to calculate hydrodynamic radii, as well as being utilised to determine the intrinsic viscosity. The Stokes–Einstein relations used to determine the micro-viscosity per-factor or as known the correction term.

In xylan system, it was found that the correction term f dropped off with addition xylan in solution, this is because of the decoupling between the macroscopic and microscopic viscosities.

The values of hydrodynamic radii of ions were calculated from the correlation between the viscosity and the relaxation times using Stokes-Debye-Einstein Equation. These values found between 3Å and 2Å in xylan solutions. In fact, the size of the hydrodynamic radius of ions are not changed, but due to the structure and the size of molecular weight of carbohydrate polymer, it can influence on the effective size of ions, during their movement in solution. The values of the hydrodynamic radii of ions in all the xylan concentrations and all the temperatures, for T_1, is almost equal to or slightly greater than T_2 experimentally.

The intrinsic viscosities of all xylan solutions and for all temperatures were calculated using Wolf approach, and all samples data were fitted into a master curve by Huggins Equation. The values of intrinsic viscosity $[\eta]$ of cellulose solutions are higher compared to xylan. The intrinsic viscosity data was used to determine the overlap concentrations of xylan and cellulose. It found that xylan system has overlap concentration at 3%, whereas overlap concentration of cellulose system at 1%.

In chapter 5, the influence of carbohydrates (glucose, cellobiose, xylose, cellulose and xylan) on the diffusivity of ions was investigated by using the associated fraction α of ‘‘glucose unit’’ per molecule of IL [C2mim] [OAc]. The ratio of OH group to the molecule of IL [C2mim] [OAc] was key to determining the diffusion of ions in these carbohydrates systems.

The diffusion coefficients of anions and cations for all carbohydrate- IL [C2mim] [OAc] systems collapsed onto a single master for all temperatures measured. The numerical values of diffusion coefficients were affected by the number of OH groups of each carbohydrate. The chemical shift of protons resonances $\Delta\delta$ in these carbohydrate systems shown that the ratio of OH group to the molecule of IL [C2mim] [OAc] disrupt the associated ions in the pure IL [C2mim] [OAc]. The anions in all carbohydrate solutions followed the same trend.

The correction terms were calculated from the correlation between the diffusion and the ratio of the temperature to the viscosity for all carbohydrate system. It found that in glucose, cellobiose and xylose, the correction term of anions is $f\sim1$, so they diffuse as expected, but the cations are less than one, this indicates the cations diffuse faster than expected. In carbohydrate polymers (xylan and cellulose) systems, the correction term dropped off; this is because of the decoupling between the microscopic and macroscopic viscosities.

From the ratio of the temperature to the viscosity and relaxations times, the effective hydrodynamic radius of ion was determined using Stokes-Debye-Einstein Equation. The values of hydrodynamic radii $R_{H,i}$, gradually decreased at high concentrations. This is possible due to the size of molecular weight of carbohydrates and the decoupling between macroscopic and microscopic viscosity. The equations of BPP theory were applied to data of the relaxation time T_1 to calculate the value of correlation time, τ. Arrhenius Equation was used to determine the activation energy for all carbohydrates systems.

It was found the data of these carbohydrates fell on the straight line in α, except data of xylan / [C2mim] [OAc], this system works differently. The values of the activation energy of ions in all the carbohydrate- IL [C2mim] [OAc] systems and all the temperatures, for T_1, is almost equal to or slightly higher than T_2 experimentally.

The intrinsic viscosity of glucose is similar to the intrinsic viscosity of cellobiose, and xylose is very close to them, whereas cellulose obtained the highest values of intrinsic viscosity and then xylan.

In chapter 6 the dissolution of mixed xylan and cellulose in solvent solution was determined by the interaction between the ions of IL [C2mim] [OAc]. It found there are three peaks at particular concentrations, where interesting effects were at around 10:90, 70:30 and 90:10 weight fractions of xylan to cellulose. Ideal mixing law is applied to determine and quantify the interactions between the mixtures of carbohydrates in solutions. We suggest that the number of available OH groups was reduced at the concentrations where these peaks take place.

The difference of diffusivity of ions was measured. The result has shown that the difference of diffusion coefficients of anions was approximately 100% and ΔD for cations was around 80%. The ratio of the anion diffusion coefficients to that of the cations as is less than 1. The chemical shift, Δδ of anions and cations for composition solutions is independent evidence of interactions between cellulose and xylan, complementing the diffusion data. The activation energies for anions and cations are very similar.

The zero shear rate viscosity of solutions with different compositions were measured. The viscosity values from the straight line of ideal mixing law indicated there are interactions between the two polymers in solution. These interactions appeared in three peaks of viscosity data correspond to the three peaks of diffusion measurements at the same temperatures. This indicates there is a real interaction between components in these solutions. The correction term and the effective hydrodynamic radii of ions were determined, using Stokes-Debye-Einstein Equations.

The value of correction term, f increases as composition concentrations in solution increase. This indicates an exchange between the ions. The values of $R_{H,i}$ increase with the increase in xylan weight fractions in mixture solution. From the values of correction terms and hydrodynamic radii values, there are similar results found and indicate to the complex structure of this system.

7.2 Future Work

Recently, there is much research and interest to study cellulose blends. Therefore, chapter 6 which is an investigation of the effect of xylan and cellulose blends on the ions of IL [C2mim] [OAc] at different temperatures, was a first step and a novel approach, using diffusivity of ions in these highly viscous solutions as a probe.

We found the influence of OH group on the diffusion of ions in mixed xylan and cellulose solution needs more investigation, to understand how the ions of IL [C2mim] [OAc] interact with these carbohydrates. Other ionic liquids such as 1-ethyl-3-methylimidazolium octanoate [C_2MIM][OOct], 1-butyl-3-methylimidazolium chloride [BMIM] [Cl] and N-methylpyridinium chloride could also be used to dissolve these polymers (cellulose and xylan), to study the interactions. The results from that can be compared to see whether there peaks as happened with IL[C2mim] [OAc] are more general.

There is a plan to make films from the mixed xylan and cellulose in IL [C2mim] [OAc] with different concentrations (from 0% to 100%). These films will need an investigation to measure their mechanical, thermal and barrier properties. Some techniques can be used such as differential scanning calorimetry, confocal microscopy, FTIR spectroscopy to determine the chemical shift of the components and atomic force microscopic (AFM) to measure the elastic moduli, tensile and stiffness. One can also use scanning electronic microscopic (SEM) to characterise the films and X-ray diffraction and NMR spectroscopy to measure their crystallinity.

References

1. Wasserscheid, P. and W. Keim, *Ionic liquids—new "solutions" for transition metal catalysis.* Angewandte Chemie International Edition, 2000. **39**(21): p. 3772-3789.
2. Walden, P., *Molecular weights and electrical conductivity of several fused salts.* Bull. Acad. Imper. Sci.(St. Petersburg), 1914. **1800**.
3. Tokuda, H., et al., *Physicochemical properties and structures of room temperature ionic liquids. 1. Variation of anionic species.* The Journal of Physical Chemistry B, 2004. **108**(42): p. 16593-16600.
4. Huddleston, J.G., et al., *Characterization and comparison of hydrophilic and hydrophobic room temperature ionic liquids incorporating the imidazolium cation.* Green chemistry, 2001. **3**(4): p. 156-164.
5. Rabideau, B.D., A. Agarwal, and A.E. Ismail, *The role of the cation in the solvation of cellulose by imidazolium-based ionic liquids.* The Journal of Physical Chemistry B, 2014. **118**(6): p. 1621-1629.
6. Zhang, J., et al., *NMR spectroscopic studies of cellobiose solvation in EmimAc aimed to understand the dissolution mechanism of cellulose in ionic liquids.* Physical Chemistry Chemical Physics, 2010. **12**(8): p. 1941-1947.
7. Heinze, T., et al. *Interactions of ionic liquids with polysaccharides–2: Cellulose*. in *Macromolecular Symposia*. 2008. Wiley Online Library.
8. Olsson, C., et al., *Effect of methylimidazole on cellulose/ionic liquid solutions and regenerated material therefrom.* Journal of Materials Science, 2014. **49**(9): p. 3423-3433.
9. Graenacher, C., *Cellulose solution.* US Patent, No. 1943176, 1934.
10. Swatloski, R.P., et al., *Dissolution of cellose with ionic liquids.* Journal of the American chemical society, 2002. **124**(18): p. 4974-4975.
11. Rogers, R.D. and K.R. Seddon, *Ionic liquids--solvents of the future?* Science, 2003. **302**(5646): p. 792-793.
12. Kilpeläinen, I., et al., *Dissolution of wood in ionic liquids.* Journal of agricultural and food chemistry, 2007. **55**(22): p. 9142-9148.
13. Bylin, S., et al., *Solvation Behavior of Cellulose and Xylan in the MIM/EMIMAc Ionic Liquid Solvent System: Parameters for Small-Scale Solvation.* BioResources, 2014. **9**(1).
14. Sun, N., et al., *Complete dissolution and partial delignification of wood in the ionic liquid 1-ethyl-3-methylimidazolium acetate.* Green Chemistry, 2009. **11**(5): p. 646-655.

15. Shiflett, M.B. and A. Yokozeki, *Phase behavior of carbon dioxide in ionic liquids:[emim][acetate],[emim][trifluoroacetate], and [emim][acetate]+[emim][trifluoroacetate] mixtures.* Journal of Chemical & Engineering Data, 2008. **54**(1): p. 108-114.

16. Vitz, J., et al., *Extended dissolution studies of cellulose in imidazolium based ionic liquids.* Green chemistry, 2009. **11**(3): p. 417-424.

17. Wang, H., G. Gurau, and R.D. Rogers, *Ionic liquid processing of cellulose.* Chemical Society Reviews, 2012. **41**(4): p. 1519-1537.

18. Bowron, D., et al., *Structure and dynamics of 1-ethyl-3-methylimidazolium acetate via molecular dynamics and neutron diffraction.* The Journal of Physical Chemistry B, 2010. **114**(23): p. 7760-7768.

19. Wertz, J.-L., J.P. Mercier, and O. Bédué, *Cellulose science and technology*. 2010: EPFL press.

20. Sundarraj, A.A. and T.V. Ranganathan, *A review on cellulose and its utilization from agroindustrial waste.* Drug Invention Today, 2018. **10**(1).

21. Gyurcsik, B. and L. Nagy, *Carbohydrates as ligands: coordination equilibria and structure of the metal complexes.* Coordination chemistry reviews, 2000. **203**(1): p. 81-149.

22. Sonnenburg, E.D., et al., *Specificity of polysaccharide use in intestinal bacteroides species determines diet-induced microbiota alterations.* Cell, 2010. **141**(7): p. 1241-1252.

23. Titirici, M.-M., M. Antonietti, and N. Baccile, *Hydrothermal carbon from biomass: a comparison of the local structure from poly-to monosaccharides and pentoses/hexoses.* Green Chemistry, 2008. **10**(11): p. 1204-1212.

24. Scheller, H.V. and P. Ulvskov, *Hemicelluloses.* Annual review of plant biology, 2010. **61**.

25. Payen, A., *Mémoire sur la composition du tissu propre des plantes et du ligneux.* Comptes rendus, 1838. **7**: p. 1052-1056.

26. Siró, I. and D. Plackett, *Microfibrillated cellulose and new nanocomposite materials: a review.* Cellulose, 2010. **17**(3): p. 459-494.

27. O'sullivan, A.C., *Cellulose: the structure slowly unravels.* Cellulose, 1997. **4**(3): p. 173-207.

28. Klemm, D., et al., *Cellulose: fascinating biopolymer and sustainable raw material.* Angewandte Chemie International Edition, 2005. **44**(22): p. 3358-3393.

29. Atalla, R.H. and D.L. Vanderhart, *Native cellulose: a composite of two distinct crystalline forms.* Science, 1984. **223**(4633): p. 283-285.

30. Gross, A.S. and J.-W. Chu, *On the molecular origins of biomass recalcitrance: the interaction network and solvation structures of cellulose microfibrils.* The Journal of Physical Chemistry B, 2010. **114**(42): p. 13333-13341.

31. Luo, M., A.N. Neogi, and H. West, *Dissolution of cellulose in mixed solvent systems*. 2010, Google Patents.

32. Finkenstadt, V. and R. Millane, *Crystal structure of Valonia cellulose Iβ.* Macromolecules, 1998. **31**(22): p. 7776-7783.

33. Day, L. and I. McNeil, *Biographical dictionary of the history of technology*. 2002: Routledge.

34. Rebouillat, S. and F. Pla, *State of the art manufacturing and engineering of nanocellulose: a review of available data and industrial applications.* Journal of Biomaterials and Nanobiotechnology, 2013. **4**(02): p. 165.

35. Sundberg, J., G. Toriz, and P. Gatenholm, *Effect of xylan content on mechanical properties in regenerated cellulose/xylan blend films from ionic liquid.* Cellulose, 2015. **22**(3): p. 1943-1953.

36. da Silva, A.E., et al., *Xylan, a promising hemicellulose for pharmaceutical use*, in *Products and Applications of Biopolymers*. 2012, InTech.

37. Petzold-Welcke, K., et al., *Xylan derivatives and their application potential–Mini-review of own results.* Carbohydrate polymers, 2014. **100**: p. 80-88.

38. Daus, S. and T. Heinze, *Xylan-Based Nanoparticles: Prodrugs for Ibuprofen Release.* Macromolecular Bioscience, 2010. **10**(2): p. 211-220.

39. Ha, S.-J., et al., *Engineered Saccharomyces cerevisiae capable of simultaneous cellobiose and xylose fermentation.* Proceedings of the National Academy of Sciences, 2011. **108**(2): p. 504-509.

40. Xie, H., et al., *Capturing CO 2 for cellulose dissolution.* Green Chemistry, 2014. **16**(5): p. 2422-2427.

41. Ries, M.E., et al., *Diffusion of 1-ethyl-3-methyl-imidazolium acetate in glucose, cellobiose, and cellulose solutions.* Biomacromolecules, 2014. **15**(2): p. 609-617.

42. Sgmaaldrich.com, *https://www.sigmaaldrich.com/catalog/product*. Accessed 30/01/2018.

43. Peng, X., et al., *Hydrolysis of cellobiose to monosaccharide catalyzed by functional Lanthanum (III) metallomicelle.* RSC Advances, 2015. **5**(13): p. 9348-9353.

44. Sescousse, R., R. Gavillon, and T. Budtova, *Aerocellulose from cellulose–ionic liquid solutions: preparation, properties and comparison with cellulose–NaOH and cellulose–NMMO routes.* Carbohydrate Polymers, 2011. **83**(4): p. 1766-1774.

45. Ohira, K., et al., *Design of cellulose dissolving ionic liquids inspired by nature.* ChemSusChem, 2012. **5**(2): p. 388-391.

46. Wendler, F., et al., *Polysaccharide blend fibres formed from NaOH, N-methylmorpholine-N-oxide and 1-ethyl-3-methylimidazolium acetate.* Fibres and Textiles in Eastern Europe, 2010. **18**(2): p. Pages 21-30.

47. Kadokawa, J.-i., et al., *Preparation of cellulose–starch composite gel and fibrous material from a mixture of the polysaccharides in ionic liquid.* Carbohydrate Polymers, 2009. **75**(1): p. 180-183.

48. Kuroda, K., et al., *1H NMR evaluation of polar and nondeuterated ionic liquids for selective extraction of cellulose and xylan from wheat bran.* ACS Sustainable Chemistry & Engineering, 2014. **2**(9): p. 2204-2210.

49. Linder, Å., et al., *Mechanism of assembly of xylan onto cellulose surfaces.* Langmuir, 2003. **19**(12): p. 5072-5077.

50. Taylor, J. and C. Haigler, *Patterned secondary cell-wall assembly in tracheary elements occurs in a self-perpetuating cascade.* Plant Biology, 1993. **42**(2): p. 153-163.

51. Jin, L., K. Liu, and Y. Aoki, *Interaction of OH− with xylan and its hydrated complexes: structures and molecular dynamics study using elongation method.* Journal of molecular modeling, 2015. **21**(5): p. 117.

52. Yu, J., et al., *Cellulose, xylan and lignin interactions during pyrolysis of lignocellulosic biomass.* Fuel, 2017. **191**: p. 140-149.

53. Stevanic, J.S., et al., *Bacterial nanocellulose-reinforced arabinoxylan films.* Journal of Applied polymer science, 2011. **122**(2): p. 1030-1039.

54. Aspinall, G., E. Hirst, and R. Mahomed, *Hemicellulose A of beechwood (Fagus sylvatica).* Journal of the Chemical Society (Resumed), 1954: p. 1734-1738.

55. Larsson, M., et al., *Effect of ethanol on the water permeability of controlled release films composed of ethyl cellulose and hydroxypropyl cellulose.* Eur J Pharm Biopharm, 2010. **76**(3): p. 428-32.

56. Gordobil, O., et al., *Xylan–cellulose films: Improvement of hydrophobicity, thermal and mechanical properties.* Carbohydrate polymers, 2014. **112**: p. 56-62.

57. Paananen, A., et al., *Interaction between cellulose and xylan: An atomic force microscope and quartz crystal microbalance study*. 2004, ACS Publications.

58. Kabel, M.A., et al., *Structural differences of xylans affect their interaction with cellulose.* Carbohydrate Polymers, 2007. **69**(1): p. 94-105.

59. Hall, C.A., et al., *Macroscopic and microscopic study of 1-ethyl-3-methyl-imidazolium acetate–water mixtures.* The Journal of Physical Chemistry B, 2012. **116**(42): p. 12810-12818.

60. Hall, L., *Nuclear magnetic resonance*, in *Advances in carbohydrate chemistry*. 1964, Elsevier. p. 51-93.

61. Hore, P.J., *Nuclear magnetic resonance*. 2015: Oxford University Press, USA.

62. Simmons, T.J., et al., *Folding of xylan onto cellulose fibrils in plant cell walls revealed by solid-state NMR.* Nature communications, 2016. **7**: p. 13902.

63. Cory, D.G., Price, Mark D, and Havel, Timothy F, *Nuclear magnetic resonance spectroscopy: An experimentally accessible paradigm for quantum computing.* Physica D: Nonlinear Phenomena, 1998. **120**(1-2): p. 82-101.

64. Levitt, M.H., *Spin Dynamic, Basic of Nuclear Magnetic Resonance.* John Wiley & sons, Ltd, 2008(2nd): p. 6-565.

65. Blümich, B., *NMR Imaging of Materials. Newgen Imaging Systems (P).* Ltd. Oxford University Press Inc., New York., 2000.

66. Abragam, A., *Principles of Nuclear Magantism* Oxford Unversity Press, 1961: p. 13-71.

67. Webb, G., *Annual Reports on NMR Spectroscopy.* Academic Press, 1999. **38**.

68. Le Bihan, D. and P.J. Basser, *Molecular diffusion and nuclear magnetic resonance.* Diffusion and perfusion magnetic resonance imaging, 1995: p. 5-17.

69. Carr, H.Y. and E.M. Purcell, *Effects of diffusion on free precession in nuclear magnetic resonance experiments.* Physical review, 1954. **94**(3): p. 630-638.

70. Macchioni, A., et al., *Determining accurate molecular sizes in solution through NMR diffusion spectroscopy.* Chemical Society Reviews, 2008. **37**(3): p. 479-489.

71. Price, W.S., *Applications of pulsed gradient spin-echo NMR diffusion measurements to solution dynamics and organization.* Diffusion fundamentals, 2005. **2**(112): p. 1-19.

72. Boeré, R.T. and R.G. Kidd, *Rotational correlation times in nuclear magnetic relaxation*, in *Annual reports on NMR spectroscopy*. 1983, Elsevier. p. 319-385.

73. Callaghan, P.T., *Principles of nuclear magnetic resonance microscopy*. 1993: Oxford University Press on Demand.

74. Kimmich, R., *NMR: tomography, diffusometry, relaxometry*. 2012: Springer Science & Business Media.

75. McLaughlin, E., *Viscosity and self-diffusion in liquids.* Transactions of the Faraday Society, 1959. **55**: p. 28-38.

76. Li, J.C. and P. Chang, *Self-Diffusion Coefficient and Viscosity in Liquids.* The Journal of Chemical Physics, 1955. **23**(3): p. 518-520.

77. Bloembergen, N., E.M. Purcell, and R.V. Pound, *Relaxation effects in nuclear magnetic resonance absorption.* Physical review, 1948. **73**(7): p. 679.

78. Blicharska, B., H. Peemoeller, and M. Witek, *Hydration water dynamics in biopolymers from NMR relaxation in the rotating frame.* Journal of Magnetic Resonance, 2010. **207**(2): p. 287-293.

79. Hore, P.J., Jones, J. A., Wimperis, S.,, *NMR: The toolkit.*: p. 3-6.

80. Tanner, J.E., *Use of the stimulated echo in NMR diffusion studies.* The Journal of Chemical Physics, 1970. **52**(5): p. 2523-2526.

81. Merboldt, K.-D., W. Hanicke, and J. Frahm, *Self-diffusion NMR imaging using stimulated echoes.* Journal of Magnetic Resonance (1969), 1985. **64**(3): p. 479-486.

82. Cotts, R., et al., *Pulsed field gradient stimulated echo methods for improved NMR diffusion measurements in heterogeneous systems.* Journal of Magnetic Resonance (1969), 1989. **83**(2): p. 252-266.

83. Stejskal, E.O. and J.E. Tanner, *Spin diffusion measurements: spin echoes in the presence of a time-dependent field gradient.* The journal of chemical physics, 1965. **42**(1): p. 288-292.

84. Haase, A. and J. Frahm, *Multiple chemical-shift-selective NMR imaging using stimulated echoes.* Journal of Magnetic Resonance (1969), 1985. **64**(1): p. 94-102.

85. Frahm, J., et al., *Stimulated echo imaging.* Journal of Magnetic Resonance (1969), 1985. **64**(1): p. 81-93.

86. Green, S.M., et al., *NMR and Rheological Study of Anion Size Influence on the Properties of Two Imidazolium-based Ionic Liquids.* Scientific Reports, 2017. **7**(1): p. 8968.

87. Price, W.S., *Pulsed-field gradient nuclear magnetic resonance as a tool for studying translational diffusion: Part 1. Basic theory.* Concepts in Magnetic Resonance Part A, 1997. **9**(5): p. 299-336.

88. Cory, D.G., M.D. Price, and T.F. Havel, *Nuclear magnetic resonance spectroscopy: An experimentally accessible paradigm for quantum computing.* Physica D: Nonlinear Phenomena, 1998. **120**(1-2): p. 82-101.

89. Iggo, J., A, *NMR Spectroscopy in Inorganic Chemistry* Oxford University Press Inc., New York, 1999: p. 2-30.

90. Freude, D., *Nuclear Magnetic Resonance* Spectroscopy, 2006. **1-29**.

91. Xie, J. and Y.-C. Jin, *Parameter determination for the Cross rheology equation and its application to modeling non-Newtonian flows using the WC-MPS method.* Engineering Applications of Computational Fluid Mechanics, 2016. **10**(1): p. 111-129.

92. Rebert, J.Y.a.L., P., A.,, *Introduction to Polymers.* Taylar &Francis Group, LLC, 2011(3th): p. 299-304.

93. Eckelt, J., Knopf, Anja, Röder, Thomas, Weber, Hedda K Sixta, Herbert, and Wolf, Bernhard A, *Viscosity-molecular weight relationship for cellulose solutions in either NMMO monohydrate or cuen.* Journal of Applied Polymer Science, 2011. **119**(2): p. 670-676.

94. Wolf, B.A., *Polyelectrolytes revisited: reliable determination of intrinsic viscosities.* Macromolecular rapid communications, 2007. **28**(2): p. 164-170.

95. Rudaz, C. and T. Budtova, *Rheological and hydrodynamic properties of cellulose acetate/ionic liquid solutions.* Carbohydrate polymers, 2013. **92**(2): p. 1966-1971.

96. Zhang, J., et al., *Understanding cellulose dissolution: effect of the cation and anion structure of ionic liquids on the solubility of cellulose.* Science China Chemistry, 2016. **59**(11): p. 1421-1429.

97. Youngs, T.G., et al., *Neutron diffraction, NMR and molecular dynamics study of glucose dissolved in the ionic liquid 1-ethyl-3-methylimidazolium acetate.* Chemical Science, 2011. **2**(8): p. 1594-1605.

98. Pregosin, P.S., *Applications of NMR diffusion methods with emphasis on ion pairing in inorganic chemistry: a mini-review.* Magnetic Resonance in Chemistry, 2017. **55**(5): p. 405-413.

99. Leal, J.P., et al., *The nature of ionic liquids in the gas phase.* The Journal of Physical Chemistry A, 2007. **111**(28): p. 6176-6182.

100. MacFarlane, D.R., et al., *On the concept of ionicity in ionic liquids.* Physical Chemistry Chemical Physics, 2009. **11**(25): p. 4962-4967.

101. D'Agostino, C., et al., *Diffusion, Ion Pairing and Aggregation in 1-Ethyl-3-Methylimidazolium-Based Ionic Liquids Studied by 1H and 19F PFG NMR: Effect of Temperature, Anion and Glucose Dissolution.* ChemPhysChem, 2018. **19**(9): p. 1081-1088.

102. Burrell, G.L., et al., *NMR relaxation and self-diffusion study at high and low magnetic fields of ionic association in protic ionic liquids.* The Journal of Physical Chemistry B, 2010. **114**(35): p. 11436-11443.

103. Annat, G., D.R. MacFarlane, and M. Forsyth, *Transport properties in ionic liquids and ionic liquid mixtures: the challenges of NMR pulsed field gradient diffusion measurements.* The Journal of Physical Chemistry B, 2007. **111**(30): p. 9018-9024.

104. Gericke, M., et al., *Rheological properties of cellulose/ionic liquid solutions: from dilute to concentrated states.* Biomacromolecules, 2009. **10**(5): p. 1188-1194.

105. Sescousse, R., et al., *Viscosity of cellulose− imidazolium-based ionic liquid solutions.* The Journal of Physical Chemistry B, 2010. **114**(21): p. 7222-7228.

106. Burchard, W. and M. Eisele, *Cooperative motion and self-diffusion in dilute and semidilute poly-vinylpyrrolidone solution.* Pure and applied chemistry, 1984. **56**(10): p. 1379-1390.

107. Ying, Q. and B. Chu, *Overlap concentration of macromolecules in solution.* Macromolecules, 1987. **20**(2): p. 362-366.

108. Remsing, R.C., et al., *Mechanism of cellulose dissolution in the ionic liquid 1-n-butyl-3-methylimidazolium chloride: a 13 C and 35/37 Cl NMR relaxation study on model systems.* Chemical Communications, 2006(12): p. 1271-1273.

109. Machefer, S. and K. Schnitzlein, *Ideal Mixing Rules for the Viscosity of Complex Polymer− Solvent Mixtures: Assessment of Segment-Fraction Approximations.* Industrial & engineering chemistry research, 2006. **45**(21): p. 7293-7300.

110. Liu, W. and T. Budtova, *Ionic liquid: a powerful solvent for homogeneous starch–cellulose mixing and making films with tuned morphology.* Polymer, 2012. **53**(25): p. 5779-5787.

111. Machefer, S. and K. Schnitzlein, *Simple Determination of Segment Numbers for Complex Polymer-Solvent Systems.* Chemical engineering & technology, 2007. **30**(2): p. 193-201.

112. Bloomfield, V.A. and R. Dewan, *Viscosity of liquid mixtures.* The Journal of Physical Chemistry, 1971. **75**(20): p. 3113-3119.